NATIONAL ENERGY TECHNOLOGY LABORATORY

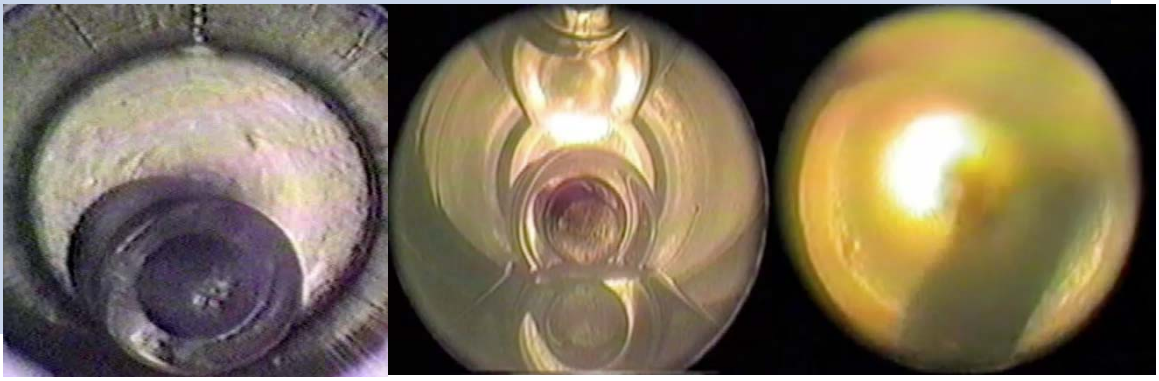

High Temperature, High Pressure Equation of State Density Correlations and Viscosity Correlations

31 July 2012

U.S. DEPARTMENT OF ENERGY

Office of Fossil Energy

NETL-TRS-1-2012

Disclaimer

The National Energy Technology Laboratory (NETL) conducts cutting-edge energy research and technology development and analyzes energy systems and international energy issues for the U.S. Department of Energy. The NETL-Regional University Alliance (NETL-RUA) is an applied research collaboration that combines NETL's energy research expertise with the broad capabilities of five nationally recognized, regional universities: Carnegie Mellon University (CMU), The Pennsylvania State University (PSU), the University of Pittsburgh (Pitt), Virginia Tech, and West Virginia University (WVU), and the engineering and construction expertise of an industry partner (URS). The NETL-RUA leverages its expertise with current fossil energy sources to discover and develop sustainable energy systems of the future, introduce new technology, and boost economic development and national security.

Cover Illustration: The image provides an inside view of the density cell, which is capable of getting density data at 500°F and 35,000 psi. The left side image shows the bubble point of the gas. The tiny bubbles can be seen at the top center of the cell. The middle image shows the liquid-liquid-gas equilibrium phase exhibiting two liquid phases at the bottom and in the middle sections as well as a gas phase at the top. The right side image shows the solid formation as the pressure is increased.

Suggested Citation:

Tapriyal, D.; Enick, R.; McHugh, M.; Gamwo, I. K.; Morreale, B. *High Temperature, High Pressure Equation of State Density Correlations and Viscosity Correlations*; NETL-TRS-1-2012; National Energy Technology Laboratory: 2012; p 114.

HIGH TEMPERATURE, HIGH PRESSURE EQUATION OF STATE DENSITY CORRELATIONS AND VISCOSITY CORRELATIONS

NETL-RUA Ultra-deepwater and Frontier Regions Research Program Equation of State Team

Deepak Tapriyal[1], Robert Enick[2], Mark McHugh[3], Isaac K. Gamwo[4], Bryan Morreale[4]

[1]URS Corporation, [2]University of Pittsburgh, [3]Virginia Commonwealth University, [4]National Energy Technology Laboratory

---

NETL-TRS-1-2012

31 July 2012

NETL Contacts:
Isaac K. Gamwo and Bryan Morreale, Principal Investigators
Kelly Rose, Technical Coordinator
George Guthrie, Focus Area Lead

www.netl.doe.gov

This page intentionally left blank

Table of Contents

Table of Figures

This page intentionally left blank

List of Tables

List of Notations

Latin letters

A	parameter for the new proposed equations of state
$\tilde{a}$	reduced Helmholtz free energy
a	energy parameter of the cubic equations of state
B	parameter for the new proposed equations of state
B	unitless pure-component parameter for free volume theory
B_0, B_1	parameters in predictive correlation for B
b	co-volume parameter of the cubic equations of state
C	compressibility term
c	volume correction
c_0-c_2	parameters of Magoulas and Tassios correlation
CLS	Chung-Lee-Starling
C_p	heat capacity at constant pressure, J/mol*K
d	temperature-dependent segment diameter, Å
EoS	equation of state
f-theory, or FT	frictional theory
FV theory, or FVT	free volume theory
g_{ii}^{hs}	hard sphere radial distribution function for component i
HTHP	high-temperature, high-pressure
HTHP-VT-PR	volume-translated PR equation designed for use at HTHP conditions
HTHP-VT-SRK	volume-translated SRK equation designed for use at HTHP conditions
I_1, I_2	abbreviations defined in reference 15
k_0-k_6	constants of the new proposed equations of state
kij	binary interaction parameter
L	length parameter in free volume theory
L_0, L_1	parameters in predictive correlation for L
m	segment number
M	molecular weight
MAPD	mean absolute percentage deviation (%)
Mol wt, or MW	molecular weight
n	number of data points
P	pressure
PC-SAFT	perturbed-chain statistically associated fluid theory
PR	Peng-Robinson
R	gas constant
SAFT	statistically associated fluid theory
SRK	Soave-Redlich-Kwong
SD	standard deviation
STDEV	standard deviation, %
T	absolute temperature
u	parameter for the general form of a two –parameter cubic EoS
u	speed of sound
VT	volume-translated
v	molar volume

w	parameter for the general form of a two –parameter cubic EoS
x_i, x_j	mole fractions of components i and j
Z	compressibility factor
Z_{RA}	Rackett compressibility factor

Greek letters

α	energy parameter in free volume theory
α_0, α_1	parameters in predictive correlation for α
α	temperature-dependent function of the energy
ω	acentric factor
δ	relative deviation (%)
ε/k_B	depth of square well potential
η	reduced molecular density
π	constant, 3.1415927
ξ_k	abbreviation (k = 0,1,2,3) defined in Eq. 6, $Å^{k-3}$
σ	temperature-independent segment diameter, Å
ρ	mass density, g/ml
ρ_{num}	number density of molecules, $Å^{-3}$

Subscripts

c	critical
r	reduced
exp	experimental
m	melting point at ambient pressure
ref	reference

Superscripts

assoc	association
chain	chain
disp	dispersion
hc	hard chain
hs	hard sphere
res	residual

Acknowledgments

The authors wish to acknowledge the excellent guidance, contributions, and cooperation of the NETL staff, particularly: Roy Long, NETL Technology Manager for providing technical guidance, continued coordination support for this project with industry, and the financial support of this project; George Guthrie, NETL-ORD Focus Area Lead who has been instrumental in leading various aspects from the initial level of the development of this project to the preparation of this report; and Jamie Brown, NETL-ORD Federal Project Manager for continuous encouragement and support of this project.

This page intentionally left blank

1. EXECUTIVE SUMMARY

Global increase in oil demand and depleting reserves has derived a need to find new oil resources. To find these untapped reservoirs, oil companies are exploring various remote and harsh locations such as deep waters in Gulf of Mexico, remote arctic regions, unexplored deep deserts, etc. Further, the depth of new oil/gas wells being drilled has increased considerably to tap these new resources. With the increase in the well depth, the bottomhole temperature and pressure are also increasing to extreme values (i.e. up to 500°F and 35,000 psi).

The density and viscosity of natural gas and crude oil at reservoir conditions are critical fundamental properties required for accurate assessment of the amount of recoverable petroleum within a reservoir and the modeling of the flow of these fluids within the porous media. These properties are also used to design appropriate drilling and production equipment such as blow out preventers, risers, etc. With the present state of art, there is no accurate database for these fluid properties at extreme conditions. As we have begun to expand this experimental database it has become apparent that there are neither equations of state for density or transport models for viscosity that can be used to predict these fundamental properties of multi-component hydrocarbon mixtures over a wide range of temperature and pressure. Presently, oil companies are using correlations based on lower temperature and pressure databases that exhibit an unsatisfactory predictive capability at extreme conditions (e.g. as great as ± 50%). From the perspective of these oil companies that are committed to safely producing these resources, accurately predicting flow rates, and assuring the integrity of the flow, the absence of an extensive experimental database at extreme conditions and models capable of predicting these properties over an extremely wide range of temperature and pressure (including extreme conditions) makes their task even more daunting.

Solution

The five-year goal of this project is to develop the thermodynamic equations of state or transport property correlations that can be used to predict the physical properties (e.g. density, ρ, and viscosity, μ), the thermal properties (e.g. constant pressure heat capacity, Cp, and thermal conductivity, k) and the equilibrium phase behavior (e.g. the number of phases and composition of phases at a specified T and P) for systems composed of hydrocarbons, water, carbon dioxide, or mixtures at high temperature and high pressure conditions.

This research project is the first step towards reaching this goal. An extensive database of literature density and viscosity of hydrocarbons was compiled, new experimental data was obtained especially at extreme temperature and pressure conditions (i.e. up to 500°F and 35,000 psi) representative of ultradeep formations, and new correlations for the density and viscosity of individual hydrocarbon compounds or multiple-component mixtures. The research team, composed of the National Energy Technology Laboratory, the University of Pittsburgh and Virginia Commonwealth University, proposes utilizing a systematic experimental and modeling approach in an effort to develop a pressure-specific volume-temperature-viscosity P-V-T-μ database, density (1/specific volume) models and viscosity models for hydrocarbons and hydrocarbon mixtures (the current work), water-hydrocarbon systems, and carbon dioxide-water mixtures at P-T conditions consistent with those for the exploration and characterization of ultradeep reservoirs at extreme operating depths.

The accomplishments during the first phase of the project are provided below:

1) Thermodynamic and Transport Property Database Development

- Detailed and thorough reviews of literature density and viscosity data were done to develop a comprehensive P-V-T-μ database. Components of interest include propane, pentane, n-octane, n-decane, n-hexcadecane, n-octadecane, n-eicosane, 2,2,4 trimethyl pentane, methyl cyclohexane, ethylcyclohexane and toluene at pressures and temperatures ranging from 2,000 to 35,000 psi and 40 to 500°F, respectively. The P-V-T-μ database also includes pure component and mixture data relating temperature, pressure, and density information. This database clearly illustrated regions where there were significant gaps in the data.
- **We have designed and built a new windowed HTHP densimeter at NETL.** It is capable of measuring fluid density of a single phase while enabling the visual verification that only a single phase exists in the cell; small amounts of a second phase (whether solid, liquid, or gas) that begin to appear can readily be detected. The device is rated to 500°F and 40,000 psi. These devices are robust instruments capable of providing accurate and reproducible density values at extreme conditions.
- We have begun the measurement of hydrocarbon density values at extreme conditions to fill in the large gaps in density data. For the first time, NETL has provided experimental density data for hydrocarbons in the table below, ranging for temperatures up to of 500°F (260°C) and pressures up to 40,000 psi. Various linear alkanes, branched alkanes, cyclic compounds, and aromatics were selected.

n-alkanes	Iso-alkanes	Cyclic	Aromatics
Propane	2-Methyl pentane	Methyl cyclohexane	Toluene
n-Pentane	2,2,4-Trimethyl pentane	Ethyl cyclopentane*	p-Xylene*
n-Octane		cyclooctane	m-Xylenes*
n-Decane		Ethylcyclohexane	o-Xylenes*
n-Hexadecane		cis-1,2-Dimethyl cyclohexane,*	2-Methyl naphthalene*
n-Octadecane		trans-1,4-Dimethyl cyclohexane*	
n-Eiocsane		cis-1,4-Dimethyl cyclohexane*	
		Cyclohexane	

***Have obtained the density data at 50°C and 150°C**

- **Based on the proven capabilities and sleek design of the windowed densimeter, we have designed and constructed a windowed rolling ball viscometer that is rated to 500°F and 40,000 psi**. In essence, it functions by placing an incredibly precise Inconel ball within the windowed Inconel vessel that has a smooth hole drilled through its center. The cell is tilted and the liquid viscosity is determined by measuring the terminal velocity of the rolling ball as it passes by small sets of opposing sapphire windows. A large sapphire window at the end of the vessel permits direct verification that only a single phase is present and that the ball is rolling, rather than skidding or stopping intermittently. This is the first windowed rolling ball viscometer built for measuring the viscosity of hydrocarbons or hydrocarbon mixtures at extreme conditions up to 500°F and 40,000 psi. This viscometer is currently being calibrated with various size balls in order for it to be used for fluids exhibiting a very wide range of viscosity values.

2) EOS Model Assessment & Development

- **NETL has developed the most accurate "cubic" equations of state for predicting the density of hydrocarbons in the table above at extreme conditions.** Further, using correlations based on correlations for the parameters associated with these compounds, we are able to accurately predict the density of any hydrocarbons, or hydrocarbon mixtures, at a specified pressure and temperature as a function of the same three physical properties (Tc, Pc and ω) that are required for all cubic equations of state. These cubic equations of state include a HTHP volume-translated Peng-Robinson equation of state, and a HTHP volume-translated Soave-Redlich-Kwong equation of state. They also provide density values within 1% of experimental values over the 70–500°F and 1,000–40,000 psi range. Because cubic equations of state are provided as an option in virtually every reservoir simulator, our new cubic formulations allow users to quickly incorporate these results into powerful reservoir simulation tools.
- **NETL has developed the most accurate "SAFT-based" equations of state for predicting the density of hydrocarbon at extreme conditions.** SAFT models are complex three-parameter models, but they provide a more accurate description of molecules' interactions than the cubic equations of state. New HTHP PCSAFT parameters were developed that can predict the density with ± 1% at HTHP conditions, but were not suitable for low pressure region and conditions near critical point. We developed a new thermodynamic model that combines the predictive power of the G-S PC-SAFT method at low pressures for phase equilibria and the vapor pressure curve with the superior densities provided by the HTHP PC-SAFT method at pressures above ~ 55 MPa. This model gives accurate phase equilibrium predictions at pressures up to ~ 35 MPa while retaining the superior ability of HTHP PC-SAFT to predict density values within better than ±1% in the HTHP region. SAFT-type equations are becoming more frequently employed in simulators.

- The two types of viscosity models capable of predicting the viscosity of multi-component mixtures over a broad range of temperature and pressure include the friction theory (FT) model and the free volume theory (FVT) model. Both models must be used in conjunction with a density model to yield viscosity predictions. **We have determined that when the PC-SAFT density model is used in conjunction with the free volume theory viscosity model, the resultant PC-SAFT-FVT model consistently gives the lowest mean absolute percent deviations (MAPDs) of ±3% from reference value for the compounds examined in this work.** Notably, it can be employed to successfully predict viscosities for normal and branched alkanes, aromatics, and cycloalkanes.

3) Deepwater Viscosity Standard: 20cP at 500°F and 35,000 psi

- **We are the first research group to successfully suggest a fluid that can satisfy the requirements of a desired "Deepwater Viscosity Standard," and to experimentally verify that it exhibits the desired viscosity at extreme conditions.** In the past few years scientists and engineers in industry, academia, and government have reached a consensus that it would be useful to identify a safe, thermally-stable liquid that exhibits a viscosity of roughly 20 cP at 500°F and 35,000 psi. This would enable researchers in viscosity studies of petroleum fluids found in ultradeep formations to have a fluid that can reliably calibrate their viscometer at the relevant conditions. We have determined, using both the rolling ball viscometer and NETL's HTHP Couette viscometer that the perfluorpolyether oils known as DuPont Krytox 101 and 102 are excellent candidates. **Krytox 101 has a viscosity of ~16 cP at 500°F and 35,000 psi, while Krytox 102 (a higher molecular weight version of the same polymer) has a viscosity of about 26 cP. Both are close to 20 cP that either could be chosen as the Deepwater Viscosity Standard.** We were the first group in the world to suggest a viable chemical to serve as the standard and to provide viscosity data at the Deepwater Standard conditions and have presented these results to the rheology community.

In summary, NETL is in the lead for providing accurate density data and viscosity data, along with modeling tools suitable for incorporation into reservoir simulators, to the scientific community. The ability to accurately characterize the density and viscosity of petroleum over an extremely wide range of temperature and pressure, including conditions found in ultradeep formations, will foster safer drilling and production operations and more accurate predictions of the recoverable reserves and rates of petroleum production from these prolific and critically important reservoirs.

2. INTRODUCTION

The Macondo oil well blowout, one mile deep in the Gulf of Mexico, was the largest accidental oil release in an ocean. The amount is estimated to be 4.9 million barrels of oil before accounting for containment [1]. This incident has highlighted various problems and areas that need considerable attention to improve the safety and production in such demanding environments. Looking at the history of well depth in the Gulf of Mexico, we have to drill deeper to find new oil to meet growing demands for oil. Figure 1 shows the depth of wells in the Gulf of Mexico as a function of the year when they were drilled [2]. With the increase in well depth, there has been steady increase in the bottomhole temperatures and pressures shown in Figure 2.

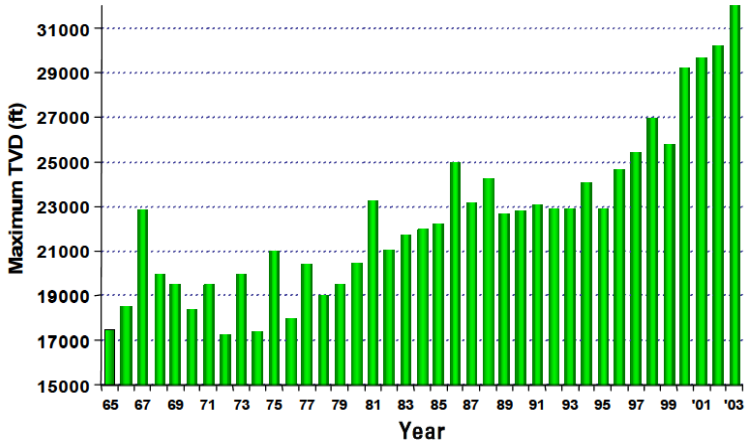

Figure 1: Well depth in Gulf of Mexico [2].

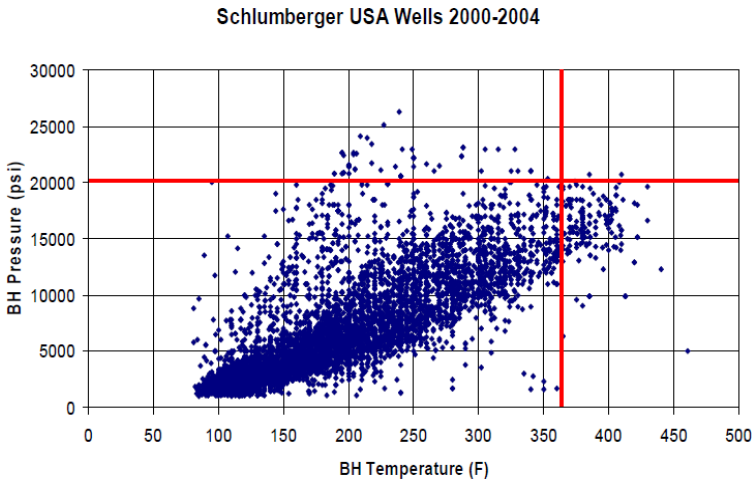

Figure 2: HTHP Drilling trend in U.S. market [2].

Figures 1 and 2 correspond to wells drilled no later than 2004; more extreme conditions have been encountered in more recent wells. For example, McMoRan has recently drilled an exploratory well, Davy Jones [3], in 20 feet of water and about 10 miles south of the Louisiana coast on South Marsh Island. It is expected to have 2-6 trillion cubic feet of natural gas reserves. Notable characteristics of this well are:

- Bottomhole Temp = 440 deg. F. = 227 deg. C.
- Bottomhole Press = 27,000 PSI
- 135 ft. of pay @ 20% porosity
- Possibility that fluid contains CO_2

Figure 3 [4] shows formations associated with Davy Jones and other onshore and offshore deep oil/gas wells. Davy Jones extends into the upper Wilcox Sandstone. According to McMoRan, drilling might be continued for another thousand feet into the Cretaceous Tuscaloosa Sandstone to evaluate the complete potential of reservoir.

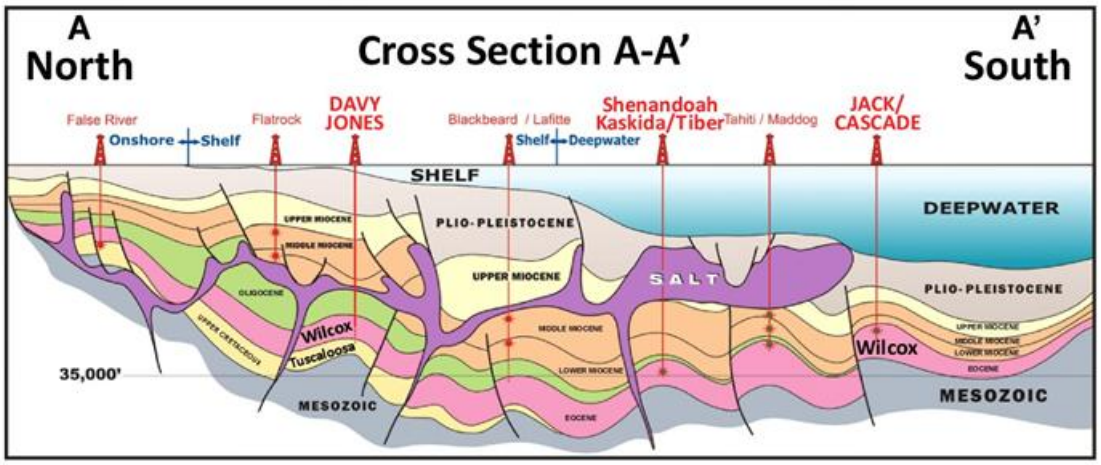

Figure 3: Idealized structural cross section showing prospects: McMoRan Exploration Company [4].

The precision of all the simulators that are used to predict the reserves retained within a gas/oil reservoir and the performance of oil/gas production wells depends on numerous aspects related to the description of the formation itself and the fluids retained therein. **In this project, the focus is on providing an accurate description of the reservoir fluid.** An equation of state (EOS) is used to predict the number of phases, phase density, vapor/liquid equilibrium (composition of two phases that are in equilibrium), and heat capacity of a multiple-component gas/crude oil at reservoir conditions in a particular location in the reservoir. Transport equations are used in conjunction with equations of state to determine the viscosity of each phase.

2.1 PROBLEM STATEMENT I: ACCURATE ESTIMATION OF PETROLEUM PROPERTIES WITHIN THE RESERVOIR

Density of gas/oil at reservoir conditions is one of the very important properties required for accurate assessment of the amount of recoverable petroleum within a reservoir and the flow of fluids within the porous media. There is a great deal of density data for crude oil hydrocarbons at lower pressures (up to 10,000 psi) and lower temperatures (up to 300°F or 149°C). However with the increase in well depth the borehole temperature and pressure are increasing beyond these bounds. There are very little data for crude oil hydrocarbons at high pressure (up to 35,000 psi) and high temperature (up to 500°F or 260°C). For example, the amount of n-pentane literature density data decreases as temperature and pressure are increased, shown in Figure 4.

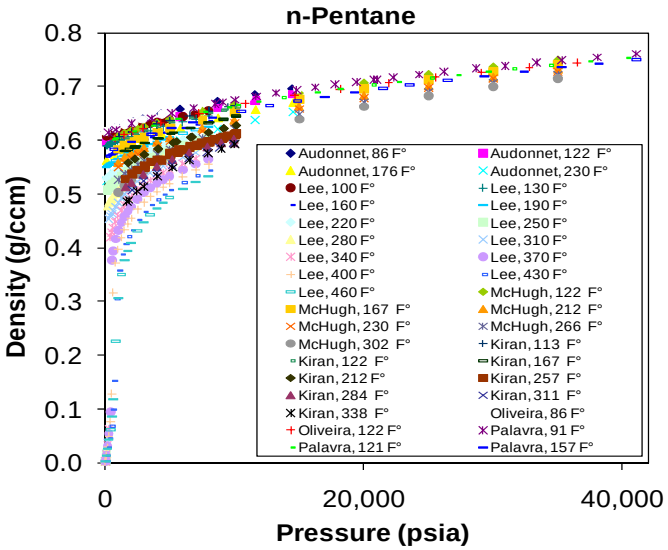

Figure 4: Pentane density over extended temperature and pressure range.

All major oil companies use cubic equations of state, such as Peng-Robinson (PR) or Soave-Redlich-Kwong (SRK), for the prediction of gas/crude oil properties. Figure 5 shows the density prediction of n-pentane using PR and SRK. At high pressure and temperature density can be significantly over-estimated by the PR EOS, while the SRK EOS underestimates the density. The error is even more substantial when the PR or SRK EOS is used to calculate the derivative fluid properties that are based on the derivatives of theses curves, such as compressibility.

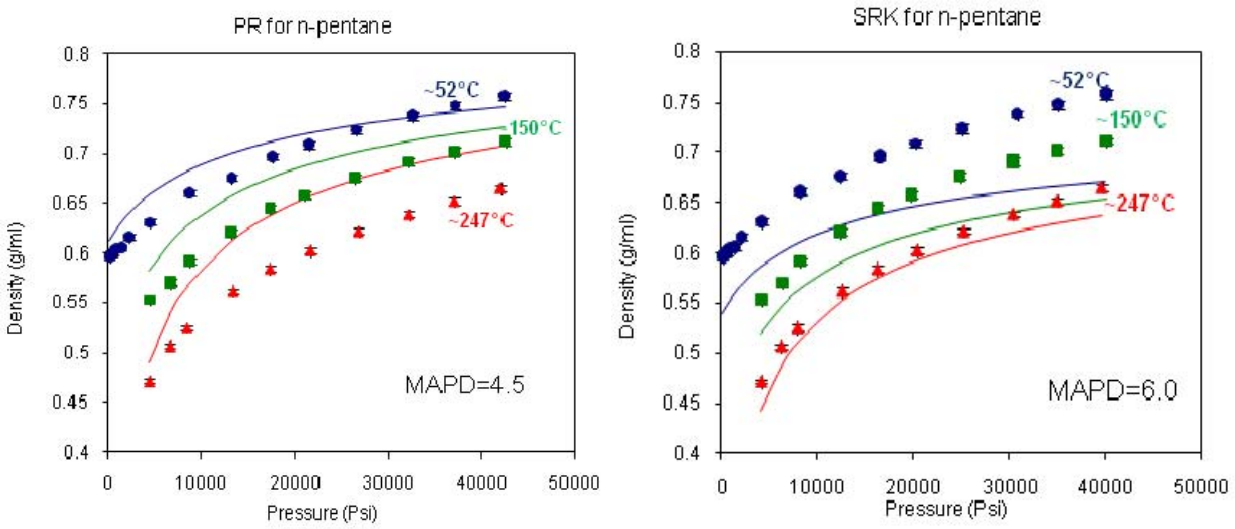

Figure 5: Density prediction using PR and SRK EOS.

There are similar gaps in the database for the hydrocarbons that constitute petroleum at these extreme conditions.

2.2 PROBLEM STATEMENT II: FLOW OF PETROLEUM FROM RESERVOIR TO SURFACE

Density and viscosity are the two most important fluid properties that influence the magnitude of flow not only in porous media, but also through wells and pipelines. This information is critical to the design of the production equipment used to transport the gas/crude from the reservoir to the surface and subsequently through the production and processing facilities. The ability to calculate the number and composition of each phase and the density, and viscosity of each phase during its transport through the pores of the ultradeep formation into and up the wellbore and through the production and processing facilities is critical for achieving flow assurance, precisely modeling the magnitude of the petroleum flow at any location during its transport, calculating the pressure drops associated with this flow, and assessing the magnitude and nature of the flow that would be predicted if unexpected pressure drops associated with failures in the wells or the equipment should occur.

3. OBJECTIVE

The overall objective of this work is to develop the capability for predicting phase equilibrium properties (e.g. the number of phases and composition of phases at a specified T and P), physical properties (e.g. density/ ρ, and viscosity/μ), and the thermal properties (e.g. constant pressure heat capacity/Cp, and thermal conductivity/k) for systems composed of hydrocarbons, water, carbon dioxide, or mixtures at high temperature and high pressure conditions. This research addresses the development of predictive models and the measurements of fluid properties at the harsh ranges of pressure and temperature representative of the conditions anticipated with future geological explorations. For example, extremely high temperatures and pressures associated with CO_2 sequestration in deep saline aquifers and the production of natural gas from ultra-deep wells are of particular interest. Temperatures as high as 500°F (260°C) and pressures up to 35,000 psia can be encountered for mixtures composed of water, CO_2, methane, and alkanes in these situations. Components of interest include propane, pentane, octane, n-decane, n-hexcadecane, n-octadecane, n-eicosane, 2,2,4 trimethel pentane, methel cyclohexane, ethylcyclohexane, and toluene. This component list is growing based on industry input and modeling support input.

Accurate EOS models at extreme conditions will provide a means for improved characterization of reservoir fluids and the dynamics of these fluids as they are extracted, thus decreasing the uncertainty associated when modeling or predicting fluid flow. For example, having a better estimate of the hydrocarbon viscosity and density within the formation at high pressure will allow for improved estimates of the pressure at any point in a well. This will enable drilling engineers to better determine the amount of hydrostatic pressure that must be supplied by drilling muds to control the flow of petroleum into the well during drilling operations, thereby mitigating some of the risks associated with drilling.

4. OUTCOME

4.1 SAFETY IMPROVEMENT

The biggest outcome of this project will be increased safety while drilling of ultra-deep wells and long-term production of petroleum from these wells. Further, this improved understanding of fluid phase behavior and properties will enable engineers to design safer flow systems and to better understand the physics of what is occurring during unexpected events. This research has a potential to improve the understanding of incidents like BP's blowout in the Gulf of Mexico. A better understanding of the nature of the fluids in wells, pipes and production equipment can help engineers to prevent such events in the future, determine the appropriate response to accidents if they occur, and accurately estimate the magnitude of spills should they occur.

4.2 BETTER RESERVOIR EVALUATIONS

After discovery, initial development of the field is dependent on volumetric estimation. Accurate density, viscosity and phase composition prediction from accurate EOS models and transport equations will lead to better understanding of the amount of recoverable petroleum and the economic potential of the reservoir.

5. APPROACH

One objective of this project is to use literature sources and data obtained from an in-house, focused experimental program to create comprehensive pressure-volume-temperature (P-V-T) and viscosity (μ) databases for pure hydrocarbons and mixtures at high temperatures and high pressure (HTHP) that are representative of the conditions anticipated with future geological explorations. A second objective is to utilize the P-V-T database to develop new equation of state correlations that accurately predict and characterize the number of phases, composition of phases, phase densities, and the phase boundaries (e.g. dew and bubble points, solidification boundaries, etc.) for pure components or mixtures at extreme pressure and temperature conditions. A third objective is to utilize the μ database to develop viscosity correlations for pure components and mixtures at extreme HTHP conditions. As mentioned, these correlations are being designed to be accurate at HTHP conditions associated with those found with emerging deep aquifer sequestration and ultra-deep gas production technologies.

This project is divided into three major tasks:

1. Thermodynamic and Transport Property Database Development: Density and Viscosity Database Development
2. EOS Model Assessment & Development: Assessment & Development of EOS Models for Density and Transport Models for Viscosity
3. Viscosity Standard: Identification of a Deepwater Viscosity Standard target of 20cP at 35,000 psi and 500°F

6. THERMODYNAMIC AND TRANSPORT PROPERTY DATABASE DEVELOPMENT

Literature Thermodynamic Property Database Development: This task includes detailed and thorough reviews of the literature in an effort to develop a comprehensive P-V-T database. Components of interest include H_2O, CO_2, and hydrocarbons associated with crude oil at pressures and temperatures ranging from 2,000 to 35,000 psi and 40 to 500°F (4 to 260°C), respectively. The P-V-T database will include pure component and mixture data relating temperature, pressure, and density (1/specific volume) information. In a parallel effort, a viscosity database is being developed to include viscosity data of these components and their mixtures at pressures and temperatures ranging from 2,000 to 35,000 psi and 40 to 500°F (4 to 260°C), respectively. A third HTHP database is also planned for heat capacity and thermal conductivity information for these compounds of interest.

6.1 EXPERIMENTAL DENSITY AND VISCOSITY

This task aims at determining density and viscosity data at HTHP conditions where literature data are not available. A major focus of this task is the design, procurement, and operation of a reliable density cell and a viscosity cell capable of measuring fluid properties, phase behavior, and viscosity behavior at HTHP conditions. This task undertakes the development of high pressure high temperature density and viscosity cells capable of operating at 500°F (260°C) and 35,000 psi.

6.2 DENSITY CELL

The initial stages of this project focused on the design of a versatile HTHP cell capable of measuring fluid density as well as measuring mixture phase boundaries including vapor-liquid, liquid-liquid, and solid-liquid transitions. This HTHP cell is now housed at NETL and design details can be found in internal NETL reports. The cell design is based on the cells currently in operation in McHugh's lab at Virginia Commonwealth University (VCU). The initial design of the NETL cell by McHugh meets the guidelines listed in the 2007 ASME Boiler & Pressure Vessel Code, Section VIII, Division 3 manual. The final design used for fabricating the HTHP cell was performed by an outside professional engineering design firm. Reported here is a brief description of a typical HTHP cell in operation in the VCU labs. The VCU density cells are virtually identical to the cell housed at NETL.

Figure 6 shows a picture of a typical “view" cell used in the VCU labs and a schematic diagram of the entire apparatus. A general description of the operation of the cell is given here. The body of the cell (working volume of ~35 ml) is constructed of a high nickel content steel (either Nitronic 50 or Inconel 718) that maintains a high tensile strength at high temperatures. The thick sapphire window, which is fitted to one end of the cell and is sealed with an elastomeric o-ring, makes it possible to observe the contents of the cell at HTHP conditions. The contents of the cell are projected onto a video monitor using a camera coupled to a boroscope placed directly against the sapphire window. The cell contents are compressed to the desired operating pressure by displacing a piston in the cell using water pressurized with a high pressure generator. The system pressure is measured on the water side of the piston using a pressure transducer calibrated against a highly accurate Heise pressure gauge. The transducer reading is within ± 0.07 MPa of the Heise gauge to pressures of ~56.5 MPa, hence, the transducer is considered accurate to ± 0.07 MPa to pressures of 56 MPa and to ± 0.35 MPa for pressures from 56 to 275 MPa. The

reported system pressure is equal to the transducer reading plus 0.07 MPa, which is the pressure needed to move the piston as determined by measuring the pressure on each side of the piston during a calibration experiment. The Type-k thermocouple used to measure the temperature of the fluid in the view cell is calibrated against a precision immersion thermometer (Fisher Scientific, 35 to 200°C, precise to 0.1°C, accurate to better than ± 0.10°C, recalibrated by ThermoFisher Scientific Company at four different temperatures using methods traceable to NIST standards). The typical temperature variation for an isotherm is less than ± 0.20°C. A stir bar activated by a magnet located below the cell mixes the contents of the cell. Figure 7 shows a composite picture of the apparatus in operation in one of the VCU labs.

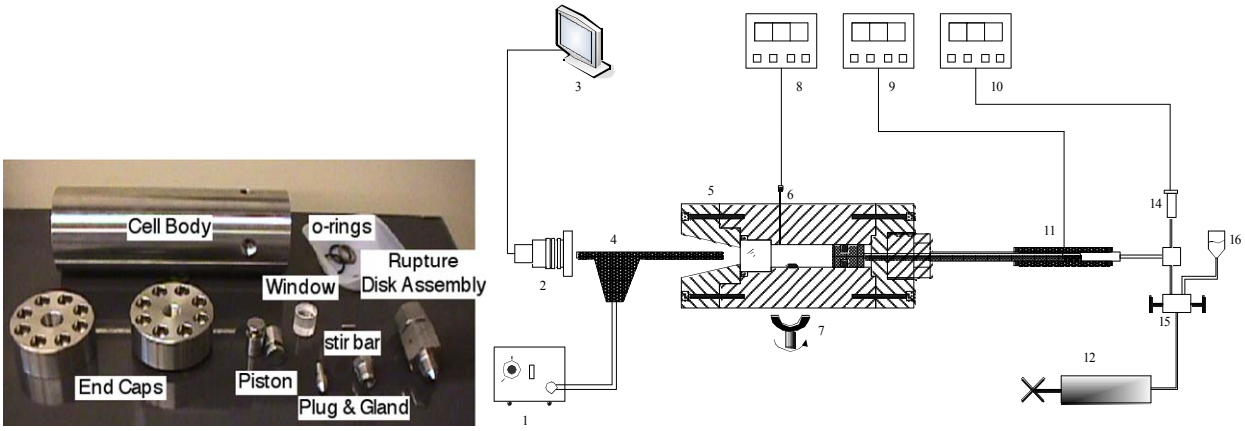

Figure 6: View cell apparatus (not to scale) and picture of the view cell parts. 1. light source 2. camera 3. monitor 4. boroscope 5. high-pressure view cell 6. thermocouple 7. magnetic stirring 8. temperature readout 9. linear variable differential transformer (LVDT) readout 10. pressure readout 11. LVDT 12. pressure generator 14. pressure transducer 15. double-stem valve 16. water reservoir.

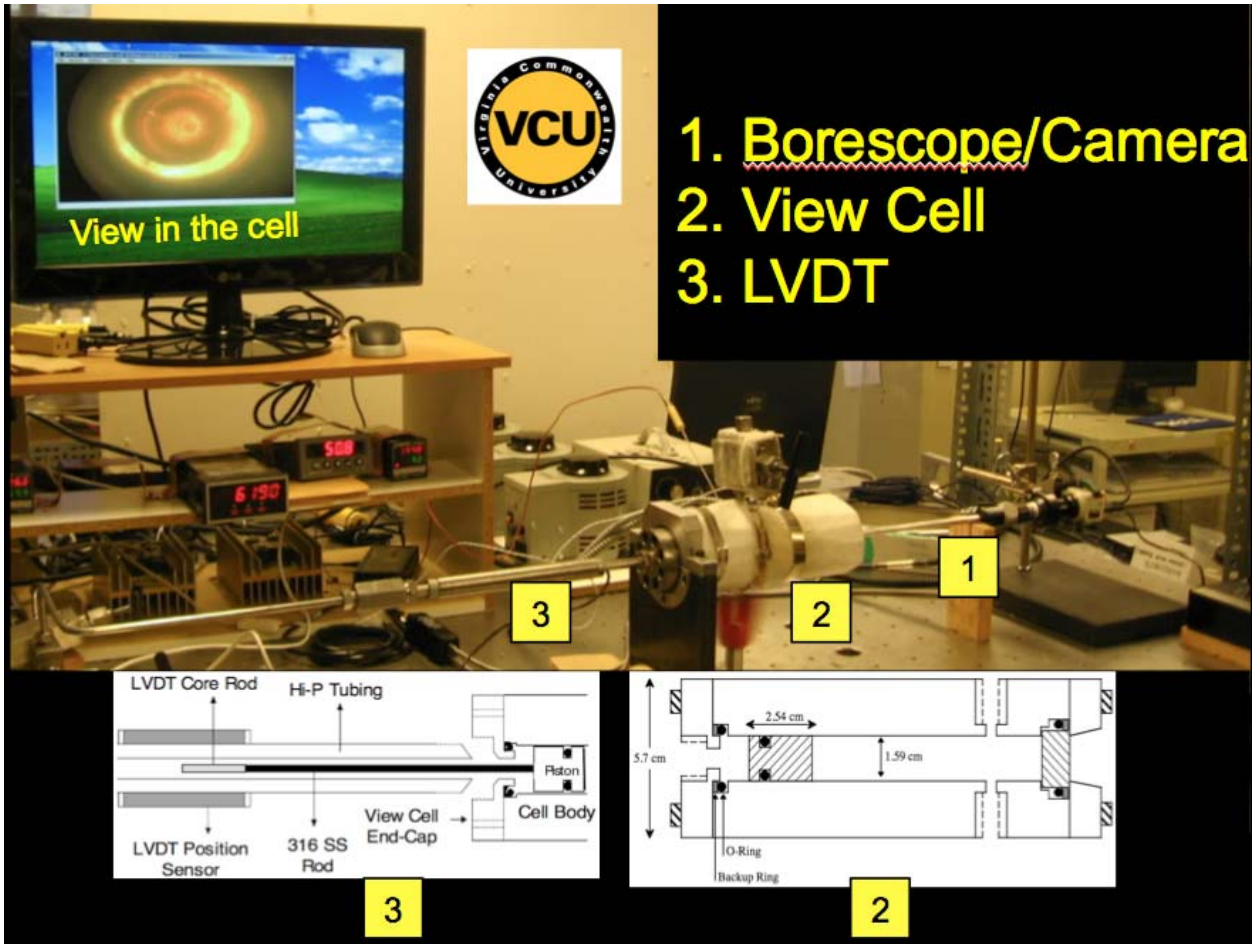

Figure 7: Composite picture of the HTHP view cell apparatus in operation at one of the VCU labs.

6.2.1 Calibration of Cell Volume for Density Measurements

The internal volume of the cell is calibrated using a linear variable differential transformer that tracks the location of the internal floating piston as shown in Figure 6. Connected to the piston is a rod with a magnetic end piece, called a core, and as the piston moves the magnetic core travels through the LVDT located outside the high-temperature air bath. The view cell volume is calibrated using highly accurate trimethylpentane at 50°C [5], n-decane at 150°C [6], and n-decane at 250°C [7] data. Typically, 7.0 to 9.0 ± 0.001 grams of the fluid of interest are charged to the view cell, which results in an uncertainty of not more than 0.20%. Since the volume is equal to the mass of fluid added to the cell divided by the calculated density, the primary error in the volume calibration curve emanates from the error in the calculated density. This is a maximum of 0.50% of the density at high pressures determined from the NIST Chemistry WebBook for trimethylpentane and n-decane[7], and much less than 0.50% for the trimethylpentane data of Malhotra [5] and the n-decane data of Caudwell [6]. The maximum estimated error of the NIST data is used to determine the accumulated error of the technique used in the present study. The accumulated error in the density at k = 2, which is closely related to a 95% confidence level, is estimated to be not more than ± 0.70% of the value of the density.

6.2.2 Calibration of Equipment

This section describes the techniques used to calibrate the thermocouples and pressure transducers used in the VCU labs. This calibration information, along with information on the volume calibration curve for the view cell, is used to determine the accumulated experimental error in the density measurements reported in this study.

Thermocouple Calibration

This section describes the typical process used to calibrate the thermocouples used in this study. A Type-k thermocouple (Omega Corporation) is used to measure the temperature of the fluid of interest in the view cell. This thermocouple was calibrated against a digital thermometer (Control Company, Model 15-077-8A, calibration traceable to NIST standard, –50 to 260°C, accurate to ± 1.0°C from 0 to 60°C and ± 2.0°C from 60 to 260°C) using a temperature-controlled silicone oil bath (Dow Company, Syltherm 800, recommended for –20°C to 200°C). The Type-k thermocouple was also calibrated against a precision immersion thermometer (Fisher Scientific, 35°C to 200°C, readable to 0.1°C, accurate to better than ±0.10°C, recalibrated by ThermoFisher Scientific Company at four different temperatures using methods traceable to NIST standards). Table 1 shows the thermocouple-digital thermometer-Hg thermometer calibration data, which are also shown in Figure 8. The thermocouple calibration equation is:

$$T_{correct}\ (°C) = 0.992 \bullet T_{Type\text{-}k}\ (°C) - 0.285 \qquad (1)$$

where $T_{correct}$ is the temperature of the mercury thermometer.

Table 1: Data obtained in this study for the calibration of the Type-k thermocouple ($T_{Type\text{-}k}$) used with the view cell against a calibrated digital thermometer ($T_{digital}$) and a calibrated mercury thermometer accurate to better than ±0.10°C.

T_{Hg} (°C)	$T_{digital}$ (°C)	$T_{Type\text{-}k}$ (°C)
50.25	49.15	50.90
101.20	100.60	102.10
124.85	124.70	126.55
150.10	149.50	151.30

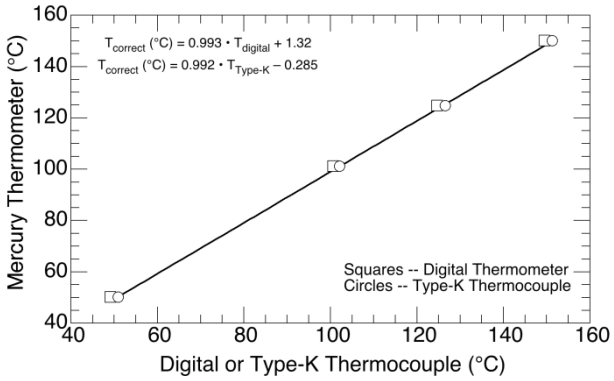

Figure 8: Results from the calibration of the Type-k thermocouple (T_{Type-k}) used to measure the temperature of the fluid in the view cell against a calibrated digital thermometer ($T_{digital}$) and a calibrated mercury thermometer (T_{Hg}). The error is less than 0.6% in the slope of the line shown in the graph, which is the fit of the T_{Type-k} data.

Pressure Transducer Calibration

This section describes the typical process used to calibrate the pressure transducers and pressure gauges used in this study. The pressure transducer used to determine the pressure in the view cell (Viatran Corporation, Model 245, 0 - 50,000 psig, accurate to ± 50 psi) was first calibrated to 30,000 psig against an identical Viatran-calibrated pressure transducer (Viatran, Model 245, 0 - 50,000 psig, accurate to ± 50 psi). The transducer was then calibrated to 10,000 psig against both the Viatran-calibrated pressure transducer and a pressure gauge (Heise Corporation, Model CC, 0 - 10,000 psig, accurate to ± 10 psi). The transducer for the view cell will be used at room temperature and therefore the two pressure calibration experiments were performed at room temperature.

Table 2 and Table 3 show the results from the two different calibration runs. It is apparent that the pressure reading from the transducer used for the view cell experiments is in good agreement with the pressure reading from the Heise gauge, accurate to ± 10 psi and to pressures of ~8,200 psig. Figure 9 shows a comparison of the performance of the transducer used for view cell experiments to the Viatran-calibrated transducer. The pressure on the view cell transducer is accurate to pressures of 8,200 psig and no correction is needed. The equation needed to correct the pressure reading of the view cell transducer at pressures greater than 8,200 psig is

$$P_{correct}\ (psig) = 0.985 \bullet P_{view\ cell\ transducer}\ (psig) + 123 \quad \text{for } P > 8{,}200\ psig \tag{2}$$

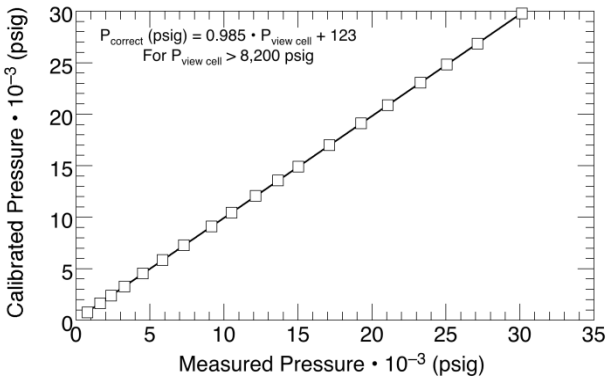

Figure 9: Comparison of the readings from the view cell pressure transducer (Measured Pressure) and the calibrated pressure transducer.

Table 2: Data obtained in this study for the calibration of the transducer used with the view cell ($P_{view\ cell}$) against the Viatran-calibrated pressure transducer ($P_{Viatran}$) at room temperature.

$P_{Viatran}$ (psig)	$P_{view\ cell}$ (psig)	$\Delta P = P_{Viatran} - P_{view\ cell}$ (psig)
770	760	10
1635	1620	15
2390	2380	10
3285	3280	5
4525	4520	5
5850	5850	0
7280	7290	-10
9110	9160	-50
10445	10500	-55
12070	12140	-70
13570	13650	-80
14915	15020	-105
16995	17120	-125
19115	19270	-155
20890	21070	-180
23050	23270	-220
24815	25070	-255
26830	27120	-290
29775	30130	-355

Table 3: Data obtained in this study for the calibration of the transducer used with the view cell ($P_{view\ cell}$) against the Viatran-calibrated pressure transducer ($P_{Viatran}$) and a Heise gauge at room temperature.

P_{Heise} (psig)	$P_{Viatran}$ (psig)	$P_{view\ cell}$ (psig)	$\Delta P_1 = P_{Heise} - P_{view\ cell}$ (psig)	$\Delta P_2 = P_{Viatran} - P_{view\ cell}$ (psig)	$\Delta P_1 = \Delta P_2$ (psig)
500	495	490	10	5	5
990	975	980	10	-5	15
1480	1470	1470	10	0	10
1980	1975	1970	10	5	5
2470	2465	2460	10	5	5
2990	2980	2980	10	0	10
3500	3505	3500	0	5	-5
4000	4005	4000	0	5	-5
4500	4495	4500	0	-5	5
4970	4965	4970	0	-5	5
6250	6240	6250	0	-10	10
7200	7195	7210	-10	-15	5
8188	8165	8200	-12	-35	23
9275	9255	9300	-25	-45	20

View Cell Calibration

As previously mentioned, the LVDT is used to determine the volume of the view cell. Shown here are the equations used to determine the accumulated experimental error in the density measurement. The density is calculated using the following equation:

$$\rho = m/V \tag{3}$$

where ρ is the density (g/ml), m is the mass (g), and V is the cell volume (ml) at a particular pressure and temperature. The estimate for the accumulated error in ρ is given as:

$$\sigma_\rho = \sqrt{\left(\frac{1}{V}\right)^2 \bullet \sigma_m^2 + \left(\frac{m}{V^2}\right)^2 \bullet \sigma_V^2} \tag{4}$$

where σ_m is the estimate of the error in the mass and σ_V is the estimate of the error in the cell volume. The calibration curve for the cell volume is:

$$V = I + S \bullet TR \tag{5}$$

where I is the intercept, S is the slope, and TR is the LVDT reading. Therefore, σ_V is calculated as:

$$\sigma_V = \sqrt{\left(\frac{\delta V}{\delta I}\right)^2 \bullet \sigma_I^2 + \left(\frac{\delta V}{\delta S}\right)^2 \bullet \sigma_S^2 + \left(\frac{\delta V}{\delta TR}\right)^2 \bullet \sigma_{TR}^2} \tag{6}$$

Where σ_I is the estimate of the error in the intercept, σ_S is the estimate of the error in the slope and σ_{TR} is the estimate of the error in the LVDT. Therefore:

$$\sigma_V = \sqrt{\sigma_I^2 + (TR)^2 \bullet \sigma_s^2 + (S)^2 \bullet \sigma_{TR}^2} \tag{7}$$

Equation (7) is combined with Equation (4) to give:

$$\sigma_\rho = \sqrt{\left(\frac{1}{V}\right)^2 \bullet \sigma_m^2 + \left(\frac{m}{V^2}\right)^2 \bullet \sigma_I^2 + \left(\frac{m}{V^2}\right)^2 \bullet (TR)^2 \bullet \sigma_s^2 + \left(\frac{m}{V^2}\right)^2 \bullet (S)^2 \bullet \sigma_{TR}^2} \tag{8}$$

One example is provided here to show how the measurements and the calibration curve affect the accumulated error of the density. In this instance decane data are presented at 250°C with m = 5.6632 g, σ_m = 0.0001, I = 4.1398, σ_I = 0.0162, S = 0.0445, σ_S = 0.0002, and σ_{TR} = 0.0025. Table 4 shows how each term in Equation (8) contributes to the estimate of the error in the density. It is apparent that a term involving the cell calibration, $\left(\frac{m}{V^2}\right)^2 \bullet (TR)^2 \bullet \sigma_s^2$, dominates the other terms in Equation (8). Further work has been done to refine the volume calibration of the view cell to reduce the error in the density measurements.

Table 4: Decane density data obtained at 250°C at VCU and estimates of the error in the density from each term in Equation (8). Only select data are shown to demonstrate the impact of each term.

Pressure (psia)	TR	V (ml)	Density (g/ml)	1st term • 10^6	2nd term • 10^6	3rd term • 10^6	4th term • 10^6	Density Error (g/ml)	Density Error (%)
3815	119.3	9.45	0.599	0.0001	1.05	1.49	0.71	0.0018	0.30
6005	111.8	9.11	0.621	0.0001	1.22	1.51	0.72	0.0019	0.30
9998	102.3	8.69	0.652	0.0001	1.47	1.53	0.73	0.0019	0.30
15799	93.6	8.30	0.682	0.0001	1.76	1.53	0.73	0.0020	0.29
24714	84.8	7.91	0.716	0.0002	2.14	1.53	0.73	0.0021	0.29
34603	77.9	7.61	0.745	0.0002	2.51	1.51	0.72	0.0022	0.29
39252	75.1	7.48	0.757	0.0002	2.68	1.50	0.71	0.0022	0.29

6.2.3 Phase Boundary Measurements

Dew, Bubble, and Critical Points

To reach thermal equilibrium, the cell remains at the temperature of interest for at least 30 minutes. The mixture in the cell is compressed to a single phase and the pressure is then slowly decreased until a second phase appears. A bubble point is obtained if small bubbles appear in the cell, while a dew point is obtained if a fine mist appears in the cell. In both cases, the composition of the predominant phase is considered equal to the overall solution composition as the amount of mass present in the second phase is negligible. Once the data point is obtained the mixture is compressed to elevated pressures and the mixture density is measured. Mixture critical points are obtained by adjusting the temperature and pressure of the mixture until critical opalescence is observed along with equal liquid and vapor volumes upon the formation of a second phase.

Solid-Liquid Transitions

The compound of interest is loaded into the cell as a solid powder or using a syringe for a liquid at ambient conditions. The temperature is adjusted as desired and the pressure is fixed so that a single liquid phase exists in the cell; the pressure is noted as P_1. The system pressure is lowered until the clear liquid phase turns opaque. Eventually the liquid becomes transparent and solid crystals are observed. If the system remains at this new condition the entire liquid phase will solidify. The pressure at this solid-liquid condition is noted as P_2. Then the pressure is increased until all of the crystals redissolve. The system pressure is again lowered past P_1 but before the liquid become opaque and now this new single-phase pressure is noted as P_1. The pressure is lowered until the liquid becomes opaque either at P_2 or at a pressure slightly higher than the previous value of P_2. The interval between a clear liquid and having crystals in the liquid is now reduced. This process is continued until $|P_2 - P_1| < 0.35$ MPa and the final P_1 is determined as the crystallization pressure at this temperature. The process is repeated at a new temperature. The maximum temperature and pressure fluctuations are maintained ± 0.2 K (0.2°C) and ± 0.2 MPa during a measurement.

6.2.4 Experimental Density Data Obtained

Experimental densities are reported for n-pentane, n-octane, cyclooctane, 2,2,4-trimethylpentane, n-decane, toluene, n-hexadecane, n-octadecane, and n-eicosane to ~280 MPa and ~250°C obtained at VCU. These densities are in agreement with available literature data that typically cover lower pressure and temperature ranges than those reported here. These data tables list the fluctuation in the temperature, as well as the mean absolute percentage deviation (MAPD) defined as:

$$\mathrm{MAPD} = \frac{1}{n}\sum_{1}^{n}\left|\frac{\rho_{i,\mathrm{experimental}} - \rho_{i,\mathrm{literature}}}{\rho_{i,\mathrm{experimental}}}\right| \bullet 100 \qquad (9)$$

Table 5: Density of n-pentane at 52.6, 149.9, and 247.3°C obtained in this study. MAPD is the average absolute percent deviation in density for n data points relative to those calculated at the NIST website to a maximum density of 0.762 g/ml or a pressure of 100 MPa [7].

52.6 ± 0.2°C MAPD = 0.5, n = 9		149.9 ± 0.1°C MAPD = 0.5, n = 4		247.3 ± 0.3°C MAPD = 0.5, n = 4	
P (MPa)	Density (g/ml)	P (MPa)	Density (g/ml)	P (MPa)	Density (g/ml)
1.8	0.595	28.6	0.553	28.5	0.472
3.6	0.598	43.7	0.570	43.1	0.507
7.0	0.603	56.8	0.592	54.9	0.526
13.8	0.613	85.5	0.621	87.1	0.562
28.9	0.630	112.8	0.645	112.7	0.584
43.3	0.643	137.0	0.658	141.2	0.603
55.3	0.653	171.9	0.676	174.7	0.622
70.9	0.664	209.4	0.692	209.6	0.639
84.1	0.672	241.0	0.702	241.1	0.652
110.2	0.686	276.6	0.712	273.5	0.665
137.8	0.700				
171.0	0.714				
206.2	0.727				
239.5	0.739				
275.5	0.750				

The pentane density shown in Figure 10 is an example of the operating features of the view cell used at VCU consider. Of the 35 n-pentane densities obtained in this study, the first nine density values at 52.6°C and the first four values at 149.9 and at 247.3°C are directly comparable to those calculated from the NIST website [7]. It is important to note that the equation of state for pentane in the NIST website is based on the work of Span [8,9] who only considered experimental data up to 100 MPa. The nine data points at 52.6°C have an MAPD of 0.1% and the four data points at 149.9 and at 247.3°C have an MAPD of 0.5%. These MAPD values are well within the estimated accumulated error of 0.7% for the experimental densities reported here. The n-pentane density data of Easteal and Woolf at 50.0°C [10] are within 0.5% of those obtained by calculation from the NIST website at pressures to 100 MPa and, therefore, the first nine density values at 52.6°C in the present study also agree with those of Easteal and Woolf within 0.5%. The n-pentane data at 52.6°C obtained in the present study are within 0.4% of the data reported by Byun, et al. [11]. However, the data reported by Byun et al. at 150°C are consistently as much as 2% greater than the present data at the same temperature. The reason for this discrepancy is not apparent although the data of the present study at 150°C are believed to be more reliable given that they are within 0.5% of the NIST data. The first four density data points at 250°C also have an MAPD of 0.5% relative to those obtained from the NIST website. Table 5 shows the density data collected for pentane.

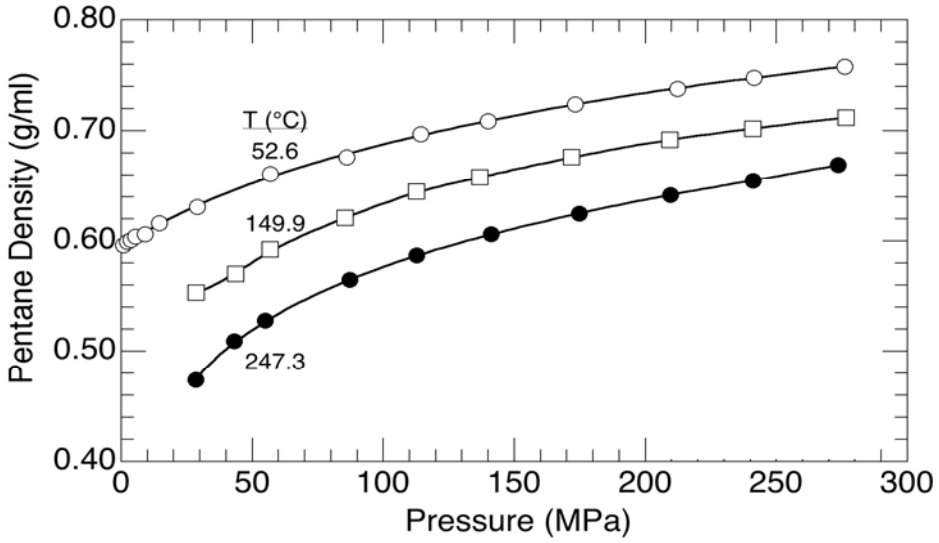

Figure 10: Pentane density data measured at VCU for this project.

Similar results are obtained for the densities of n-octane, cyclooctane, 2,2,4-trimethylpentane, n-decane, toluene, n-hexadecane, n-octadecane, and n-eicosanealso measured to ~280 MPa and ~250°C at VCU. Data sets for these hydrocarbon densities are found in Appendix A to this report. Appendix A also contains a table listing the available literature for these C5 to C20 hydrocarbons.

The VCU group also determined density data for Krytox® GPL 102, a perfluoropolyether being considered as a viscosity standard at 500°F (260°C) and 35,000 psia. The Krytox density data are listed in Appendix A of this report.

6.3 VISCOSITY CELL

To determine the viscosity of hydrocarbons at high temperature, high pressure (HTHP) conditions associated with ultradeep petroleum reservoirs, we designed a windowed, variable-volume, rolling ball viscometer rated to 500°F (260°C) and 275 MPa. The viscometer has three sets of small opposing sapphire windows for the determination of the ball velocity at three points and is mounted on a tilting table. Presently, very precisely machined Inconel balls are used as a rolling ball. Pyrex tube inserts and Pyrex balls can also be used for measurements of low viscosity gases. The large window at the end of the viscometer is used to verify that only one phase is present in the sample volume and to confirm that the ball does not slide or stop during its roll. The three sets of small opposing sapphire windows allow observation of the positions of the ball as a function of time without exposing any electronic equipment to the high temperature (this is the fundamental reason that other types of viscometers are limited to lower temperature ranges). This HTHP rolling ball viscometer will be used to measure the viscosity of hydrocarbon fluids ranging from methane to C_{40}. The viscometer has been calibrated with n-octane and dioctyl phthalate (DOP) at tilt angles ranging from of 7o to 40o using a ball with a ball diameter: tube diameter (d/D) ratio of 0.995. Calibrations with smaller balls are underway. The calibrated viscometer was then used to determine the viscosity of n-C10 and Krytox® GPL 102 (a high viscosity fluid that we have suggested for the Deepwater Viscosity Standard).

6.3.1 Viscosity Cell Design

Figure 11 shows an expanded view of the design of the rolling ball viscometer used for viscosity measurements performed in this study. The body of the cell is constructed from Inconel 718, and a working volume of 50 ml. The spheres are also made of Inconel 718 in order to match any thermal expansion that might occur when operating over a broad range of temperature and pressure. Pyrex 7740 tubes and balls can be inserted into this viscometer for the measurement of extremely low-viscosity fluids, such as methane and propane. Figure 12 shows the whole experimental setup.

Figure 11: Expanded view of the HTHP rolling ball viscometer used in this study. The front window and rolling ball are shown on the left-hand side of the viscometer body. The floating piston that separates the test fluid from the overburden fluid (water) is shown on the right-hand side of the viscometer body.

Figure 12: Experimental setup of the HTHP rolling ball viscometer.

The cell contents are compressed to the desired operating pressure by displacing the piston using water pressurized with a high pressure generator. The system pressure is measured on the water-side of the piston. A videoscope is positioned against the window at the front end of the cell to view the solution inside the cell and to watch the motion of the rolling ball.

Equation (10) shows that the viscosity, η in cP, is determined from the tilt angle of the cell, θ, the difference in the density between the ball and the fluid in units of g/cm^3, $(\rho_b - \rho_{fl})$, the terminal velocity of the rolling ball, v in cm/s, and the viscometer constant, K in units of cm^4/(m•s^2):

$$\eta = \frac{K\left(\rho_b - \rho_{fl}\right)\sin\theta}{v} \tag{10}$$

The velocity of the rolling ball through the inclined cell is determined by sensing light passing radially through three sets of opposing sapphire windows arranged radially along the length of the viscometer. The detection system is composed of a light source and three pairs of glass fiber optics attached to the small sapphire windows. This arrangement allows for six independent ball velocity measurements since the velocity can be determined from the time it takes for a ball of specified diameter to roll past each set of three opposed windows, or the time it takes the ball to roll between two windows that are separated by a known distance, or the time it takes to roll past the first and last set of opposing windows. The rolling ball viscometer is calibrated with n-octane at room temperature and pressures to 252 MPa with ball-tube-diameter ratios, d_{ball}/d_{tube}, of 0.998, 0995, 0.990, and 0.980. Figure 13 shows the velocity as a function in the tilting angle at different position. The velocity profile for the third window is very close to the one for the distance between the second and third window indicating that the ball reaches the terminal velocity after passing the second window. Figure 14 [12] shows the results for the calibration constant K determined for a diameter ratio of 0.995 at three different temperatures 293 K, 323 K, and 373 K.

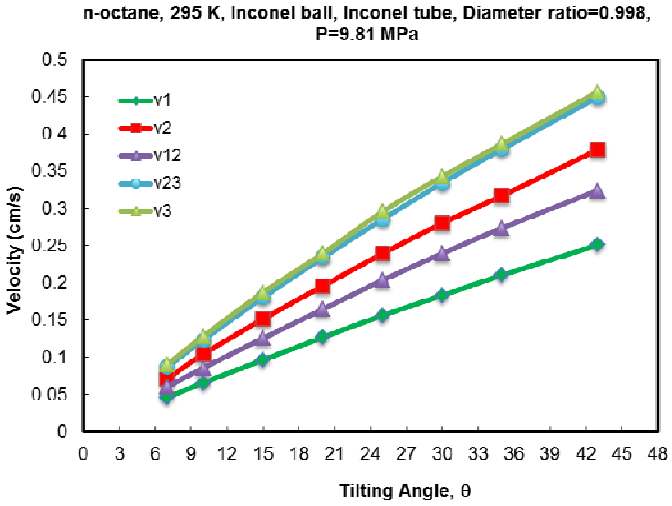

Figure 13: Velocity profiles obtained with n-octane and diameter ratio of 0.998 at 9.81 MPa.

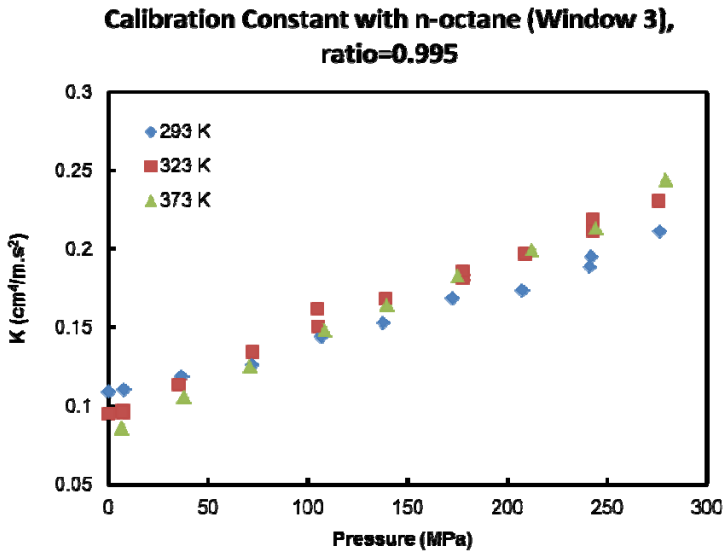

Figure 14: Viscometer constant K (see Equation (10)) as a function of pressure determined for a diameter ratio of 0.995 using viscosity literature data of n-octane [12].

Preliminary viscosity results, shown in Figure 15, for n-decane at 294 K (21°C) obtained with the viscometer constant *K* determined for a diameter ratio of 0.998 and tilting angle of 20°. The measured viscosity data at 294 K (21°C) are consistent with the literature data at a slightly higher temperature [12].

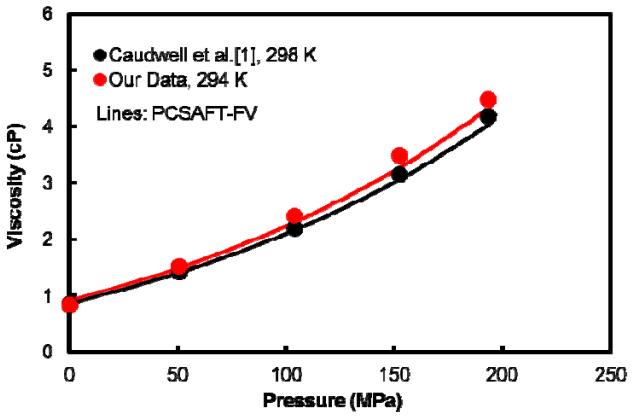

Figure 15: Comparison of measured viscosity for n-decane at 294 K (21°C) with literature data at 298 K (25°C). Solid lines are the corresponding PC-SAFT-FV theory viscosity predictions.

6.3.2 Pressure and Temperature Effects on Ball-Tube-Diameter Ratio

The pressure and temperature effects on the ball-tube diameter ratio d_{ball}/D_{tube} was studied and found that by increasing the pressure, the ratio decreases. An increase of the temperature causes a slight decrease in the ratio. Figure 16 shows P-T effect on sphere with an initial of 0.99816 at 294 K (21°C) and 0.1 MPa.

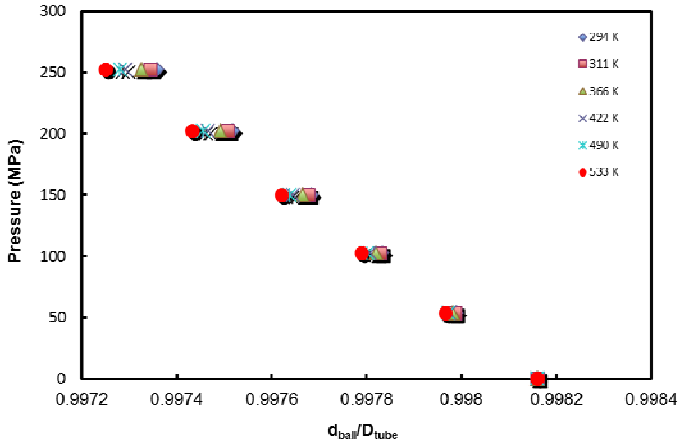

Figure 16: Pressure and temperature effect on the ball-tube diameter ratio dball/Dtube.

6.3.3 Viscosity Results

Figure 17 shows the viscosity predictions for n-octane obtained with the corrected F-theory model coupled with the HTHP-VT-PR EoS. The results are in agreement with the experimental data over the entire temperature and pressure ranges. The mean absolute percentage deviation (MAPD) of 1.68% is less than the value of 2.61% obtained with the un-translated F-theory model.

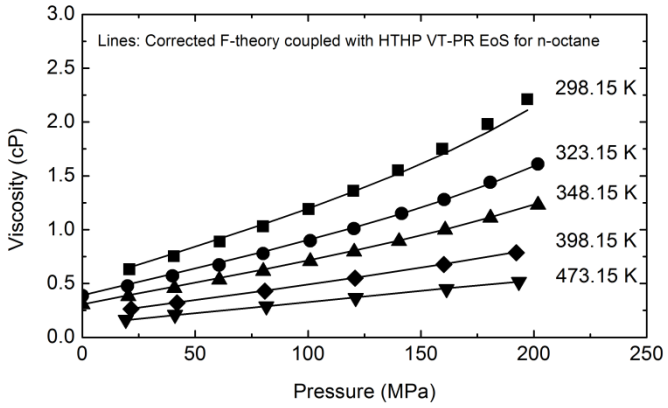

Figure 17: Comparison of experimental viscosity data [12] (symbols) of n-octane with the prediction of the F-theory model coupled with the HTHP-VT-PR EoS. (k = -5.275 x 10^{-8}cP, m = -4.908 x 10^{-10}, n = 7.776).

The free volume theory model is also assessed in combination with the equations of state mentioned earlier. The FV theory provides MAPD values of ~3% for the viscosity when coupled with the HTHP-VT-PR or HTHP- VT-SRK EOS for pressures to 276 MPa. Better results are obtained when the FV theory is combined with PC SAFT-based density predictions. As shown earlier in Figure 3, the viscosity predictions of n-decane obtained with the FV theory in conjunction with the PC-SAFT EoS are in agreement with the experimental data. The FV theory parameters used for n-decane are L = 0.6423 Å, α = 178.46 $m^5/(mol*s^2)$, and B = 0.0041173.

Figure 18 is another example of the performance of the FV theory when coupled with PC-SAFT. The MAPD is 1.57% for the viscosity predictions of n-octane presented in this figure. In general,

MAPD values of less than 2% can be obtained with the combination of the FV theory with the PC-SAFT EoS.

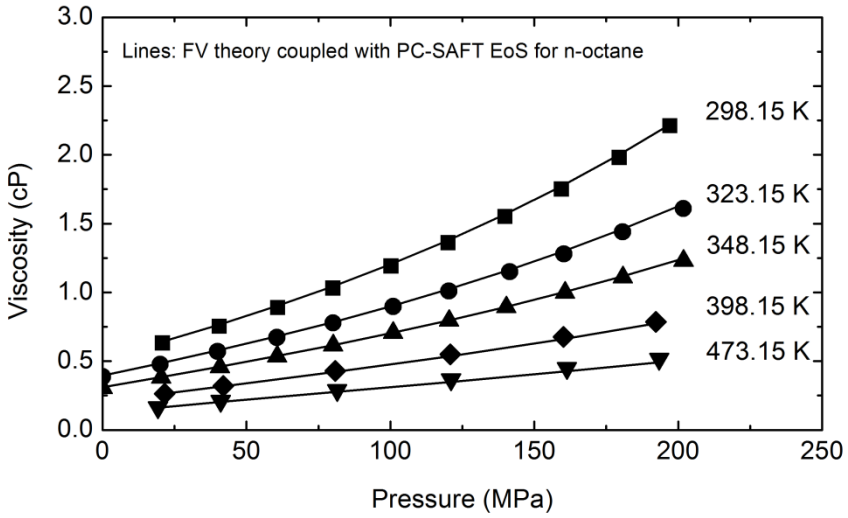

Figure 18: PCSAFT-FV theory viscosity predictions for n-octane (L = 0.6652 Å, α = 141.33 m5/(mol*s^2), B = 0.0048357).

Hydrocarbon viscosities are measured with a newly designed high temperature, high pressure, windowed, rolling ball viscometer composed of an Inconel 718 body and Inconel 718 balls. The viscometer is calibrated with n-octane and DOP. Preliminary experimental viscosity results for n-decane measured for pressures of ~ 191 MPa and 294 K (21°C) are consistent with literature data at 298 K. Viscosity values are predicted with the frictional theory (F-theory) and free volume (FV) theory models. MAPD values of ~2 to 5% for the viscosity are obtained for pressures up to 100 MPa when the PC-SAFT, HTHP-VT-PR, and HTHP-VT- SRK EOSs, are used to estimate the attractive and repulsive pressure input values for the F-theory. When pressures approach 276 MPa, F-theory under-predicts the viscosity by as much as 10% and as high as 20%. However, viscosity predictions at very high pressures obtained with the F-theory can be improved by adding a correction term. The FV theory, which requires fluid density as an input, provides MAPD values of ~3% for the viscosity when coupled with the HTHP-VT-PR or HTHP-VT-SRK EOS. Combined with PC SAFT-based density predictions, the FV theory had MAPD values of less than 2% for hydrocarbon viscosities.

7. EOS MODEL ASSESSMENT & DEVELOPMENT

Modeling fluid flow in petroleum reservoirs and production wells requires reliable predictions of the density and viscosity of the brine phase and the hydrocarbon phase(s). This study focuses on the accurate prediction of hydrocarbon density at the extreme conditions associated with ultra-deep formations—temperatures from ambient to 533 K (260°C) and pressures up to 276 MPa. Because reservoir compositional simulators typically model crude oil, condensate, and natural gas as a mixture of components, this study will focus primarily on hydrocarbons ranging between methane and tetracontane. CO_2 is also included.

There are two general classes of models with which researchers have demonstrated prior success in modeling the density of multi-component hydrocarbon mixtures. The first class is the cubic equation of state (EOS), such as Peng-Robinson (PR) and Soave-Redlich-Kwong (SRK), which is relatively compact, and is the main type of EOS presently used in reservoir simulators. PR and SRK equations of state fail to give accurate density predictions at high pressures for hydrocarbons; even volume-translated PR and SRK models that are correlated to saturated liquid density values fail to provide adequate results at extreme pressures [13,14,15]. However, our group has recently demonstrated that a high temperature, high pressure volume-translated SRK (HTHP VT-SRK) equation, which is correlated to hydrocarbon $P\rho T$ data obtained at pressures of 6.9 to 276 MPa and temperatures of 293 to 533 K (20 to 260°C), exhibits greatly improved predictive ability [14].

The other class of models is the set of EOS that are based on the Statistical Associated Fluid Theory (SAFT) EOS, put forth by Chapman, Radosz, and coworkers in the 1990s [16,17,18,19]. SAFT is generally acknowledged as superior to cubic equations of state with respect to describing the physics of the system, but it is less frequently used in reservoir simulations. The SAFT theory represents the pure component or mixture Helmholtz free energy as a sum of terms accounting for hard sphere repulsion, dispersion interactions, chain connectivity, and association between segments [20]. A modification of SAFT theory, the PC-SAFT equation, has been used to model the phase behavior for many classes of organic compounds including normal and branched alkanes, cycloalkanes, alkenes, gases, ethers, esters, benzene derivatives, halogenated hydrocarbons, and poorly defined materials such as polymers, as well as mixtures of polymers and low molecular weight hydrocarbons [20]. In addition, the PC-SAFT equation provides superior phase equilibrium predictions for mixtures with both associating and non-associating substances [20,21,22]. The PC-SAFT equation has recently been used to accurately predict the pure component densities of toluene, *n*-pentane, *n*-octane, isooctane, cyclooctane, *n*-decane, *n*-hexadecane, *n*-octadecane, and *n*-eicosane [13,23]. However, for n-alkanes, PC-SAFT has the tendency to over-predict density values at pressures greater than ~ 55 MPa. This over-prediction can be as much as 5% more than the experimental value at pressures greater than 241 MPa.

Such extreme temperatures and pressures are found throughout ultra-deep reservoirs, a relatively new petroleum and prolific resource of great importance to the oil industry. Therefore, the objective of this study was to evaluate cubics and PC-SAFT for pure component/mixture density predictions at temperatures from ambient to 500°F (260°C) and pressures from 6.9 to 276 MPa.

7.1 CUBICS EVALUATIONS

Due to the simplicity of calculation and the remarkable predictive capabilities, cubic equations of state (EoS) are widely used to predict the phase behavior and volumetric properties of pure fluids

and mixtures. Two of the most common cubic equations of state in petroleum engineering industry are the Soave-Redlich-Kwong (SRK) EoS [24] and the Peng-Robinson (PR) EoS [25]. Equation 11 shows the general form of these two-parameter cubic equations of state [26]:

$$P = \frac{RT}{v-b} - \frac{a_c\,\alpha}{v^2 + ubv + wb^2} \tag{11}$$

Here, P is the pressure, T is the absolute temperature, and v is the molar volume. For the SRK EoS, $u = 1$ and $w = 0$, and for the PR EoS, $u = 2$ and $w = -1$. The function α in the attractive term is a correlation of temperature, critical temperature, and acentric factor. The parameter b represents the effective molecular volume in the hard sphere repulsive term. The parameters a_c and b depend only on the critical properties and the equations defining these two parameters are obtained by applying the constraints shown in Equation 12 at the critical point.

$$\left(\frac{\partial P}{\partial v}\right)_{T=T_c} = 0, \qquad \left(\frac{\partial^2 P}{\partial v^2}\right)_{T=T_c} = 0 \tag{12}$$

The SRK EoS predicts a critical compressibility, $Z_C = \frac{P_C\, v_C}{RT_C}$, of 0.3333 whereas the PR EoS predicts a value of 0.3074.

The experimental values of Z_c are generally smaller than those predicted by either cubic equation of state. As a result, the predicted liquid molar volumes in the near-critical region may differ considerably from experimental values. Nonetheless, satisfactory density calculation results can be obtained for sub-critical conditions associated with many chemical and petroleum engineering applications.

Another type of equation of state is the class of equations based on the statistical associating fluid theory (SAFT) proposed by Chapman et al.[27,28]. One of the most successful modifications of SAFT EoS is the perturbed chain SAFT (PC-SAFT EoS) put forth by Gross and Sadowski[20]. The SAFT equations of state are generally more accurate than the cubic equations of state in estimating the liquid density, however some SAFT models may provide inaccurate estimation of the pure compounds critical data or saturated liquid-vapor predictions [29].

The Cubic-Plus-Association equations of state (CPA EoS) developed by Kontogeorgis et al. [30,31] combines the SRK EoS with an association term from the Wertheim theory (the same as in SAFT models) accounting for hydrogen bonding effects. When dealing with non-associating fluids, the CPA EoS reduces to the SRK EoS. The three remaining CPA parameters a_0, c_1, b are regressed simultaneously from vapor pressure and saturated liquid density data instead of using the critical constants as is done for SRK EoS. Considerable improvements in the phase equilibria and density predictions of associating fluids can be achieved with the CPA EoS [32]. Recently, the CPA has been successfully used to predict the density of the non-associating ester mixtures at pressures up to 45 MPa when the regressed CPA pure compound parameters are used instead of the parameters computed from correlations [33]. However, the density predictions for n-alkanes (non-associating) obtained with the CPA EoS are not always reliable. For instance, the density predictions for n-pentane at 520.45 K (247.3°C) obtained with the CPA EoS are inferior to the results obtained with the classical SRK EoS, as seen in Figure 19 [34].

Recently, Polishuk proposed a hybrid EoS model that combines a modified SAFT with the attractive term of cubic EoS (SAFT+Cubic) [29]. This model was developed based on the idea of gathering the strengths of both SAFT and cubic equations of state. The performance of this model has been evaluated for several fluids including n-pentane, n-hexane, cyclohexane, and toluene at extremely high pressures. Its predictions of the density and some auxiliary properties such as speed of sound and bulk moduli are impressive [35].

High accuracy for predictions on the thermodynamic properties of fluids can be obtained with the empirical multiparameter equations of state [36,37,38]. These equations of state are fluid specific and commonly expressed in terms of the reduced Helmholtz energy.

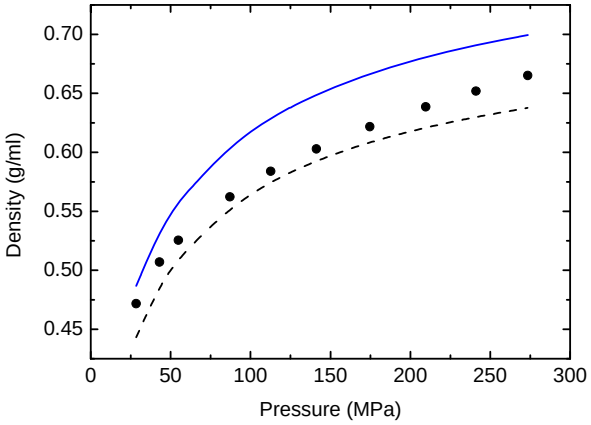

Figure 19: Density isotherm at 520.45 K (247.3°C) for n-pentane. ● Experimental data [23], - - - - SRK EoS, _____ CPA EoS (the three CPA parameters a0, c1, b were taken from [34]).

RPSEA [39] recently affirmed the need for accurate thermodynamic models for hydrocarbon fluid density at extreme conditions associated with ultra-deep reservoirs. Citing the continued prevalence of cubic equations of state (specifically the Peng-Robinson and Soave-Redlich-Kwong EoS) in modern reservoir simulation software packages and the simplicity of replacing cubic EoS with volume-translated EoS in a reservoir simulator, RPSEA stated its desire for new volume-translated PR and SRK EoS with enhanced predictive capabilities at temperatures to 500°F (260°C) and pressures between 1,000-40,000 psi (7- 276 MPa). This study addresses this specific industry need. RPSEA also noted that despite the relatively small number of petroleum reservoir simulations that include the more complex and SAFT-based models, the promising density results associated with such models at low temperature and pressure merited their consideration as an alternative to the PR and SRK EoS. Therefore, the PC-SAFT equation of state, which was found to provide more accurate density predictions than the SAFT EoS [23], was included for comparison with the volume-translated PR and SRK EoS.

7.1.1 HTHP Volume Translation

While cubic equations of state such as the SRK and PR EoS provide accurate predictions for vapor molar volumes, they fail to predict accurate liquid molar volumes over wide pressure ranges. One of the most successful ways to overcome this limitation has been to shift, or translate, the predicted liquid volume. In fact, a systematic deviation, c, is observed between the predicted liquid molar volume (v_{EoS}) and the corresponding experimental value ($v_{\exp}$).

$$c = v_{EoS} - v_{\exp} \tag{13}$$

The parameter *c* is also known as a volume translation that can be utilized to greatly improve the prediction of densities in the sub-critical region. The effect of the volume translation on the gas-phase density is insignificant due to the large value of the vapor volume compared to that of the liquid. The calculation of the pure component vapor pressure is not affected when *c* is a constant or is a function only of temperature. A wide variety of correlations for c has been proposed [40,41,42,43,44,45,46,47,48,49,50,51,52,53] but none are satisfactory for high temperature, high pressure density because all of them base the value of c on low pressure saturated liquid data and/or single fluid, liquid phase density. As stated in this work, we are interested in the fluid density of hydrocarbon fluids at high temperatures and high pressures associated with the flow of petroleum in ultra-deep reservoirs and the production wells. Therefore, rather than correlating the volume correction to saturated liquid densities, as is done in most prior volume translation methods, the volume translation term in this study is correlated to pure component, single-phase density data [13,23,54,55,56,57,58,59,60] for short- and long-chain alkanes, cycloalkanes and aromatics over a pressure range ~(7-276) MPa and a temperature range ~(278-533) K (5-260°C).

The difference between the predicted liquid molar volume, v_{EoS}, and the corresponding experimental value, $v_{exp,}$ has been averaged for each isotherm (i.e. each value of T_r indicated by data markers in Figure 20) for literature data within the HTHP range. Therefore, the density dependency of the volume correction expression is neglected, hence a component-dependent, temperature-dependent volume translation was employed. After determining the optimal value of *c* for each isotherm associated with a specified component, the volume correction was plotted against reduced temperature and expressed as a linear function of T_r:

$$c = \Delta v = v_{EoS} - v_{\exp} = A + B \cdot T_r \tag{14}$$

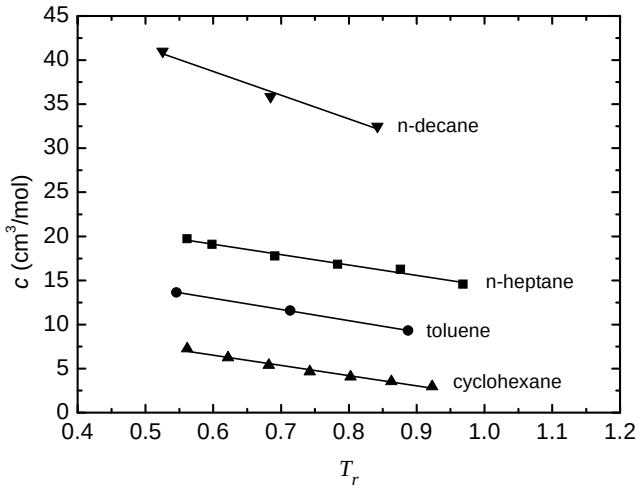

Figure 20: Volume correction, c, of the SRK EoS for cyclohexane [54] , toluene [23], n-heptane [55] and n-decane [23] as a linear function of the reduced temperature, T_r.

Figure 21 shows an example of the results of utilizing this technique for the determination of *c* for n-decane at reduced temperatures of 0.53 and 0.84. This approach was applied to the SRK EoS and PR EoS. The pure fluid parameters *A* and *B* in Equation 14 have been regressed for 17 pure components spanning the C_1 to C_{40} range and their values for both the SRK EoS and PR EoS are listed in Table 6.

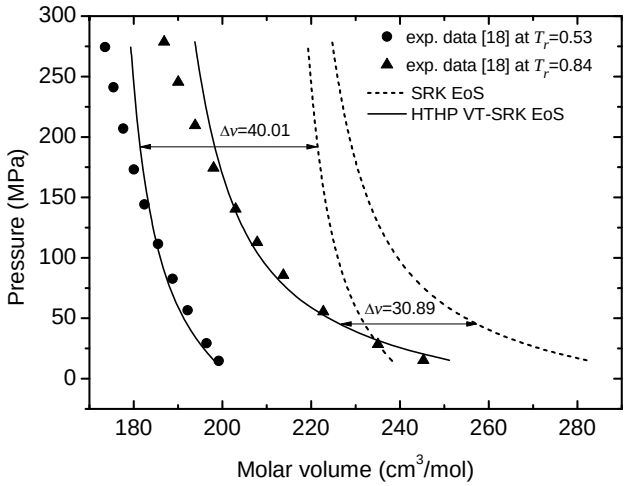

Figure 21: Volume translation results based on average volume differences between SRK EoS predicted molar volumes and their corresponding experimental values for n-decane at the isotherms T_r = 0.53 and 0.84.

Table 6: Optimized values of the volume translation parameters A and B based on literature data in the ~ (7-276) MPa and ~(278-533) K (5-260°C) ranges.

Compound	Ref.	M (g/mol)	ω	T_c (K)	P_c (bar)	$(M\omega)^{-1}$ (mol/g)	HTHP VT-SRK EoS		HTHP VT-PR EoS	
							A (cm^3/mol)	B (cm^3/mol)	A (cm^3/mol)	B (cm^3/mol)
methane	[56,57]	16.04	0.012	190.56	45.99	5.420	0.233	-0.420	-3.047	-0.610
propane	[58]	44.10	0.152	369.83	42.48	0.149	2.977	-1.225	-3.328	-3.189
n-pentane	[23]	72.15	0.251	469.70	33.70	0.055	17.95	-12.39	7.181	-13.89
cyclohexane	[54]	84.16	0.208	553.80	40.80	0.057	13.52	-11.65	3.864	-15.02
n-heptane	[55]	100.20	0.349	540.20	27.40	0.029	26.21	-11.82	11.24	-14.57
n-octane	[23]	114.23	0.399	568.70	24.90	0.022	36.80	-20.15	20.70	-23.73
isooctane	[23]	114.23	0.303	543.90	25.70	0.029	23.92	-17.46	7.824	-19.51
cyclooctane	[23]	112.21	0.236	647.20	35.60	0.038	23.48	-19.22	9.066	-20.72
n-decane	[23]	142.29	0.492	617.70	21.10	0.014	54.85	-26.90	33.71	-30.91
n-tridecane	[55]	184.36	0.617	675.00	16.80	0.009	90.21	-38.01	62.23	-45.39
n-hexadecane	[13]	226.45	0.717	723.00	14.00	0.006	127.5	-52.69	88.55	-55.34
n-octadecane	[13]	254.50	0.811	747.00	12.70	0.005	155.1	-73.00	109.0	-72.80
n-eicosane	[13,55]	282.55	0.907	768.00	11.60	0.004	169.4	-62.91	116.5	-60.70
n-C_{30}	[55]	422.83	1.307	844.00	8.00	0.002	325.8	-146.7	250.3	-150.6
n-C_{40}	[55]	563.08	1.500	887.00	4.40	0.001	881.2	-201.1	750.5	-246.9
benzene	[59,60]	78.11	0.210	562.05	48.95	0.061	11.51	-6.490	2.074	-8.227
toluene	[23]	92.14	0.264	591.75	41.08	0.041	20.57	-12.66	12.17	-15.37

7.1.2 General Correlation Development

In order to provide a generalized method for determining A and B for compounds not included in the database, correlations for A and B were developed as functions of molecular weight (M) and acentric factor (ω). Although correlations for A and B based on either M or ω were generated, but not shown here, the correlations in this study based on $(M\omega)^{-1}$ provided significantly better fits of the optimized A and B values. Figure 22-Figure 25 show the correlations developed in this study.

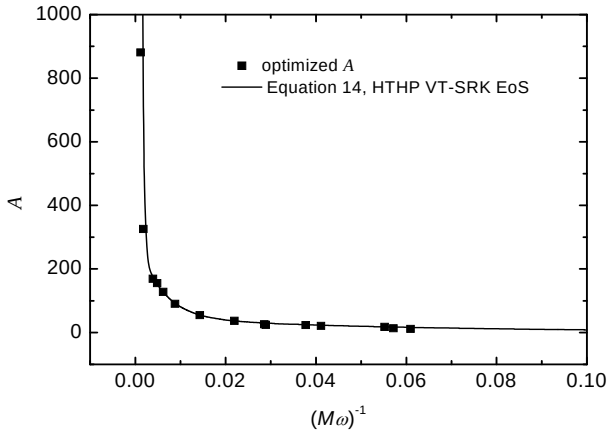

Figure 22: Parameter A of Equation 10 and its correlation, Equation 14, for HTHP VT-SRK EoS. Only the markers for components between and including n-C_{40} and n-pentane are shown; methane and propane values of $(M\omega)^{-1}$ are off-scale to the right.

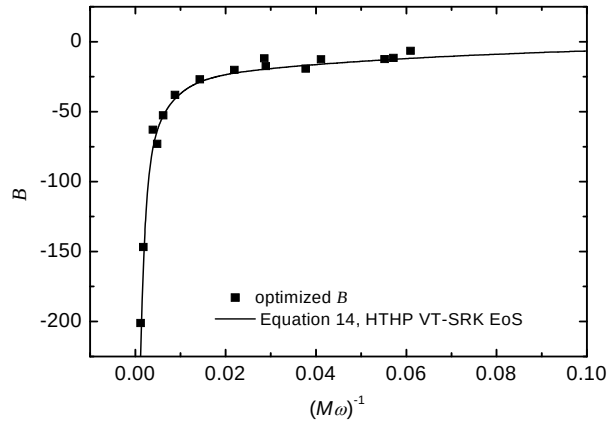

Figure 23: Parameter B of Equation 10 and its correlation, Equation 14, for HTHP VT-SRK EoS. Only the markers for components between and including n-C_{40} and n-pentane are shown; methane and propane values of $(M\omega)^{-1}$ are off-scale to the right.

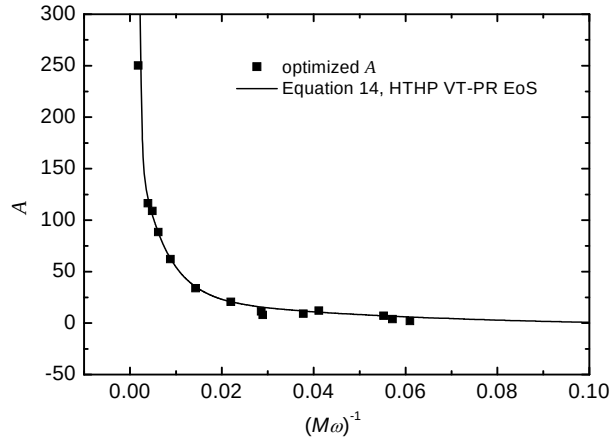

Figure 24: Parameter A of Equation 10 and its correlation, Equation 14, for HTHP VT-PR EoS. Only the markers for components between and including n-C_{40} and n-pentane are shown; methane and propane values of (M are off-scale to the right).

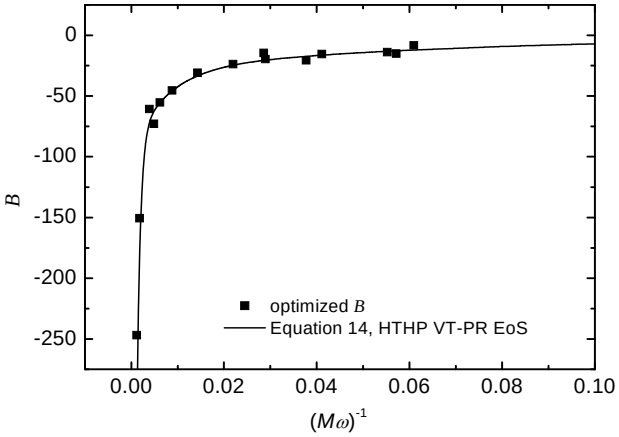

Figure 25: Parameter B of Equation 10 and its correlation, Equation 14, for HTHP VT-PR EoS. Only the markers for components between and including n-C_{40} and n-pentane are shown; methane and propane values of $(M\omega)^{-1}$ are off-scale to the right.

The high temperature, high pressure volume translated forms of the SRK EoS and PR EoS, referred as HTHP VT-SRK and HTHP VT-PR EoS, are presented here:

HTHP VT-SRK EoS:

$$P = \frac{RT}{v+c-b} - \frac{a_c\,\alpha}{(v+c)(v+c+b)} \tag{15}$$

HTHP VT-PR EoS:

$$P = \frac{RT}{v+c-b} - \frac{a_c\,\alpha}{(v+c)(v+c+b)+b(v+c-b)} \tag{16}$$

where:

$$c = A + B \cdot T_r \tag{17}$$

$$A, B = f(M, \omega) = k_0 + k_1 \exp\left(\frac{-1}{k_2 M \omega}\right) + k_3 \exp\left(\frac{-1}{k_4 M \omega}\right) + k_5 \exp\left(\frac{-1}{k_6 M \omega}\right) \tag{18}$$

Values for the parameters of Equation 18 are listed for both equations of state in Table 7. The correlations of parameters *A* and *B* (rather than the optimized values) have been used for subsequent density calculations reported in this study.

Table 7: Parameters of Equation 14.

Constants		HTHP VT-SRK EoS	HTHP VT-PR EoS
A (cm^3/mol)	k_0	0.2300	-4.1034
	k_1	46.843	31.723
	k_2	0.0571	0.0531
	k_3	23161	188.68
	k_4	0.0003	0.0057
	k_5	267.40	20196
	k_6	0.0053	0.0003
B (cm^3/mol)	k_0	-0.3471	-0.3489
	k_1	-29.748	-28.547
	k_2	0.0644	0.0687
	k_3	-347.04	-817.73
	k_4	0.0010	0.0007
	k_5	-88.547	-65.067
	k_6	0.0048	0.0076

7.1.3 HTHP Volume Translation Predictions

The performance of the new volume translated equations of state, the HTHP VT-SRK EoS and the HTHP VT-PR EoS, is compared to the performance of standard Soave-Redlich-Kwong (SRK EoS) [24] and Peng-Robinson (PR EoS). The accuracy of the predictions of each equation of state is represented by the mean absolute percentage deviation (MAPD) for the *n* data points:

$$MAPD = \frac{1}{n}\sum_{1}^{n}\left|\frac{\rho_{i,experimental} - \rho_{i,calculated}}{\rho_{i,experimental}}\right| \times 100 \tag{19}$$

and the standard deviation (SD) associated with the value of the MAPD. Figure 26 shows the calculated results of the different methods for n-pentane as an example. Figure 26a shows that the SRK EoS provides a reasonably small under-estimation of density at 520.45 K (247.3°C), but yields a more significant under-estimation of the n-pentane density at 325.85 K (52.7°C) and 423.05 K (149.9°C) over the entire pressure range of interest. Figure 26b shows that the PR EoS provides a reasonable fit of n-pentane density data at 325.85 K, a slight over-estimation at 423.05 K, and a significant over-estimation of density at 520.45 K. The MAPD for the PR EoS is 4.68%, while the MAPD for the SRK EoS is 5.63%. Given that the goal is to attain density values within ~1% of experimental values, both EoS are considered unsatisfactory.

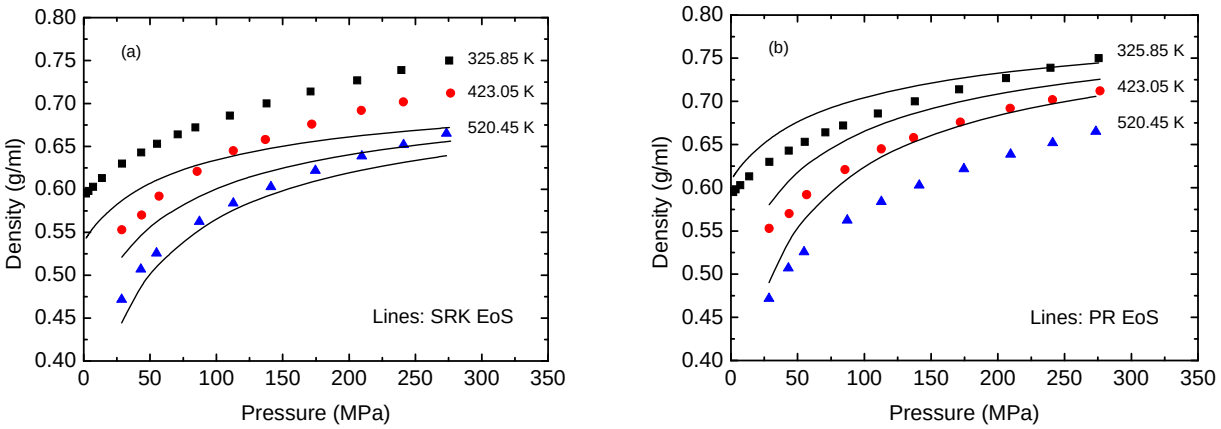

Figure 26: (a) Comparison of the SRK EoS with n-pentane density data[23], (b) Comparison of the PR EoS with n-pentane density data [23].

Figure 27 shows that the performance of the HTHP VT-SRK EoS and HTHP VT-PR EoS models developed in this study are superior to the performance of the other models. Both HTHP models provide very good results for pressures up to 200 MPa for all isotherms and underestimate the density at 325.85 and 423.05 K as the pressure increases. The HTHP VT-SRK EoS has an MAPD of 1.11%, which is slightly better than the 1.54% calculated for the predictions of the HTHP VT-PR EoS.

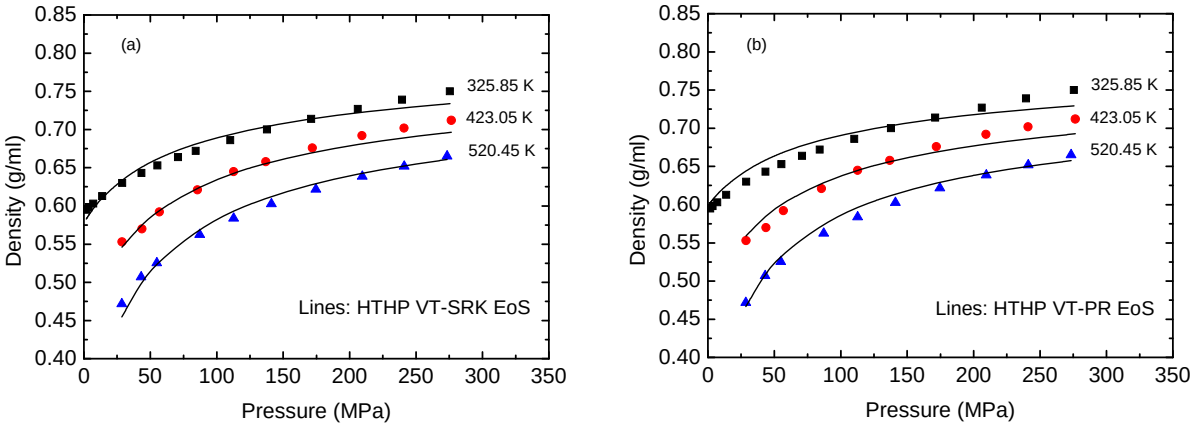

Figure 27: (a) Comparison of the new HTHP VT-SRK EoS with n-pentane density data [16], (b) Comparison of the new HTHP VT-PR EoS with n-pentane density data [16].

Table 8 presents the MAPD and SD values for the high pressure, high temperature densities for the 17 fluids considered in this study. The overall MAPD values were 1.47 % and 2.01 % for the HTHP VT-SRK and HTHP VT-PR EoS, which are considered low. The HTHP region demonstrates the benefits of utilizing a volume translation approach for a cubic EoS. It should be noted that these values of the MAPD are obtained when utilizing an HTHP data base to determine the volume translation equation rather than using sub-critical saturated liquid phase density values. The volume translation correlations presented here provide a method for accurate EoS calculations for the ~(7 - 276) MPa pressure range and ~(278 - 533) K (5-260°C) temperature range related to ultradeep reservoir and well conditions. Volume translated cubic equations of state can provide more accurate HTHP density predictions than untranslated models and other translated models only when the volume correction is based on an HTHP data base (e.g. HTHP VT-SRK EoS and HTHP VT-PR EoS).

Table 8: Mean absolute percentage deviation (MAPD) and standard deviation (SD) for all compounds and equations of state studied in this work.

Compound	SRK		PR		HTHP VT-SRK		HTHP VT-PR	
	MAPD	SD	MAPD	SD	MAPD	SD	MAPD	SD
methane	1.27	0.64	8.62	3.28	0.81	0.80	0.66	0.35
propane	2.00	1.29	8.79	1.36	1.54	1.30	1.16	0.63
n-pentane	5.63	2.45	4.68	2.44	1.11	0.74	1.54	0.81
cyclohexane	5.47	1.35	5.95	1.29	2.15	1.17	3.60	1.15
n-heptane	10.22	1.81	1.58	1.18	1.30	1.52	1.33	0.73
n-octane	11.89	2.60	2.75	2.13	1.36	1.31	1.56	1.07
isooctane	6.27	2.43	4.77	2.13	2.63	1.39	4.34	2.01
cyclooctane	6.77	2.05	3.88	2.19	1.91	1.07	3.65	1.36
n-decane	15.67	2.59	6.13	2.93	1.19	0.95	1.59	1.02
n-tridecane	20.95	2.49	11.87	2.87	1.14	0.61	1.55	0.76
n-hexadecane	31.79	4.30	18.40	3.91	1.24	1.05	1.62	1.23
n-octadecane	33.31	4.70	19.75	4.25	1.55	1.03	1.90	1.20
n-eicosane	35.88	4.69	22.05	4.27	1.60	1.65	2.02	1.66
n-C30	30.69	2.53	22.88	2.84	1.98	0.81	2.45	1.11
n-C40	50.63	2.05	45.10	2.26	1.27	1.00	1.58	0.96
benzene	7.33	1.38	4.00	1.42	1.57	1.20	1.53	0.85
toluene	9.73	2.11	2.12	1.51	0.70	0.52	2.07	1.28
Overall	**16.79**	**2.44**	**11.37**	**2.49**	**1.47**	**1.07**	**2.01**	**1.07**

7.1.4 Mixture Density Prediction

The HTHP VT-SRK EoS and HTHP VT-PR EoS can be extended to mixtures using the following mixing rule proposed in other volume-translated cubic EoS models [41,42,47]:

$$c_m = \sum_i x_i \, c_i \tag{21}$$

Here, x_i and c_i are the mole fraction and the volume translation term of pure component i in the mixture, respectively. Both new models have been tested on binary mixtures using the conventional van der Waals mixing rules for the parameters of the original cubic equations:

$$a_m = \sum_i \sum_j x_i \, x_j \left(a_i a_j\right)^{0.5} \left(1 - k_{ij}\right) \tag{22}$$

$$b_m = \sum_i x_i b_i \tag{23}$$

Here, k_{ij} is the binary interaction parameter between molecules i and j. The use of one interaction parameter is sufficient, even at high pressures, but near the critical region the use of two parameters (k_{ij} , l_{ij}) provides more accurate predictions[61]. k_{ij} values are typically obtained by fitting sub-critical VLE data. For alkane-alkane pairs, k_{ij} can be approximately set to zero if experimental VLE data are unavailable. For other pairs, especially those including non-hydrocarbons, k_{ij} should be different from zero and must be determined [62]. Figure 28 [63] shows the density predictions for the binary system methane n-decane ($x_{methane}$= 0.3124) at 293.15, 333.15, and 373.15 K (20, 60, and 100°C) obtained with the HTHP VT-SRK EoS (k_{ij} = 0.062). The binary interaction parameters, which were determined by modeling after experimental VLE data taken from [64], were used in both the translated and untranslated estimates. The prediction results of both HTHP VT equations of state are in agreement with the experimental data throughout the entire pressure range. The total MAPD values obtained with the HTHP VT-SRK EoS and the HTHP VT-PR EoS for these density isotherms are 0.70 % and 0.42 %, respectively.

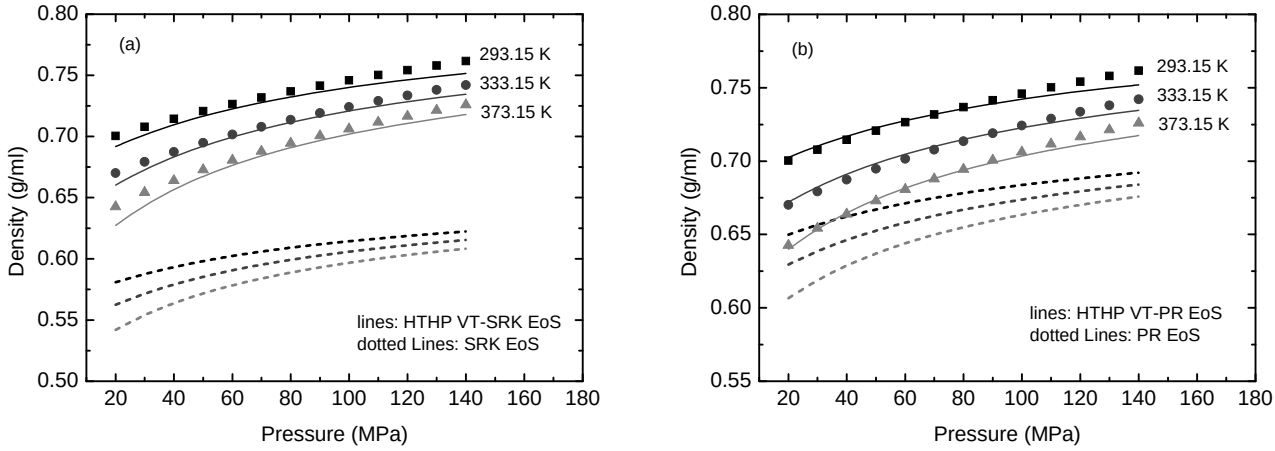

Figure 28: Comparison of density experimental data [64](symbols) of the binary mixture methane/n-decane (xmethane= 0.3124) at 293.15, 333.15, and 373.15 K (20, 60, and 100°C) with (a) predicted densities using SRK EoS (dotted lines) and HTHP VT-SRK EoS (lines) with kij = 0.062. (b) predicted densities using PR EoS (dotted lines) and HTHP VT-PR EoS (lines) with kij = 0.065.

In an attempt to improve the performance of cubic equations of state for predicting molar volumes at extremely high temperature, high pressure (HTHP) conditions associated with ultra-deep petroleum formations, a temperature-dependent volume-translation (VT) term is employed in the SRK and PR equations of state. Rather than correlating the volume-correction to saturated liquid densities, as is done in most prior volume translation methods, the volume-translation term in the HTHP VT-SRK EoS and HTHP VT-PR EoS is correlated to pure component, single-phase density literature data at pressures between 7 and 276 MPa and temperatures between 278 and 533 K (5 and 260°C). The VT parameters were determined for 17 compounds, including short- and long-chain alkanes ranging from CH_4 to n-$C_{40}H_{82}$, several cycloalkanes, and several aromatics. Our recent HTHP density data for several hydrocarbons have been included in this HTHP density data base to enhance the accuracy of these models. The volume correction parameters were correlated to the inverse of the product of the molecular weight and acentric factor, $(M\omega)^{-1}$, allowing these models to be used for compounds not included in the data base. The mean absolute percentage deviation (MAPD) values of (1-2%) and (1-4%) (an overall MAPD of 1.47% and 2.01%, respectively) obtained with the HTHP VT-SRK EoS and HTHP VT-PR EoS, respectively, are substantially better than those calculated with other models. The proposed models have been successfully extended to mixtures. The new HTHP VT-EoS do not exhibit any thermodynamic inconsistency that other volume translated models might have at HTHP conditions.

8. HTHP PCSAFT

For most of the n-alkanes and other compounds studied by Gross and Sadowski [20], the three pure-component PC-SAFT parameters (m, the number of hard spheres in a molecule; σ, the temperature-independent hard core diameter of a sphere; ε/k_B, the attractive energy of dispersion divided by the Boltzmann constant) were obtained by fitting sub-critical $P\rho T$ data, although occasionally both sub-critical and supercritical density data were used. In this project we derive a new set of pure-component PC-SAFT parameters by fitting the equation to high temperature, high pressure (HTHP) density data present in the literature [13,23,55,65,66] that covers almost the entire pressure and temperature ranges of interest for deep reservoirs. Sub-critical density data are not used to obtain these new parameters. For each set of density data, the pressure ranged between ~ 6.9 and ~ 300 MPa, while the temperature was usually ~ 423 K (150°C). A downhill simplex method is used to determine the best values for the three pure-component PC-SAFT parameters by minimizing the value of the mean absolute percent deviation (MAPD) between the experimental density and the PC-SAFT prediction.

8.1 NEW HTHP PC-SAFT PARAMETERS

New HTHP PC-SAFT parameters were obtained by fitting them to new high temperature high pressure density data. A downhill simplex method was used to determine the optimum values of the pure-component HTHP PC-SAFT parameters σ, ε/k_B, and m, which are given in Table 9.

PC-SAFT equation was fit to density values covering both the sub-critical and supercritical regions for the compounds of interest, but preliminary results indicated that the PC-SAFT density predictions at high pressures were not greatly improved over those made with the PC-SAFT parameters derived by Gross and Sadowski [20]. Thus, the PC-SAFT equation was only fit to density values found in a range of pressures between approximately 6.9 and 300 MPa. Typically, the PC-SAFT density values were fit to HTHP density data obtained at a single temperature and covering the full range of pressures The PC-SAFT parameters for all compounds in Table 9 are determined from a fit of experimental data at or near 423 K (150°C) except for *n*-tetracontane (C_{40}) at 473 K (200°C), cyclooctane and *n*-dodecane at or near 523 K (250°C), and *n*-nonane at 373 K (100°C). This was done for the latter two compounds because experimental data was not available over the full range of pressures for the 423 K (150°C) isotherm, while the cyclooctane and tetracontane density predictions are more reliable when the fit is made to the experimental data collected at the higher temperatures.

The MAPD values are shown in Table 9 and plotted in Figure 29 for results from both the PC-SAFT parameters obtained by Gross and Sadowski (G-S) and the parameters from fitting a single high temperature, high pressure (HTHP) density isotherm. The MAPD values given in Figure 29 indicate that the density predictions made using the HTHP PC-SAFT parameters at temperatures from ambient to 533 K and pressures from 6.9 to 276 MPa are typically an order of magnitude better than those obtained from the PC-SAFT predictions using parameters recommended by Gross and Sadowski (G-S). When using carbon dioxide the G-S PC-SAFT model yields better results.

Table 9: Values of the PC-SAFT pure-component parameters m, σ, and ε/k_B obtained from fitting a single, high temperature density isotherm (HTHP data). MAPD values are determined with PC-SAFT using parameters fit to HTHP data at or near 423 K and also from parameters recommended by Gross and Sadowski (G-S) for all of the isotherms available for each hydrocarbon (typically at or around 323, 423, and 523 K (50, 150, and 250°C) and at pressures ranging from 4.2 to 300 MPa).

Compound	Mol Wt	*M*	σ	ε/k_B	MAPD		P range	Ref
	g/mol		Å	K	HTHP	G-S	MPa	
Methane	16.043	1.0944	3.6129	144.54	0.34	1.81	5-290	66
Propane	44.096	2.1994	3.5381	204.81	0.38	2.15	6-269	[67]
n-pentane	72.146	3.8898	3.3149	204.20	0.82	1.68	7-277	23
n-heptane	100.20	4.7159	3.4364	221.04	0.49	1.36	5-300	55
n-octane	114.23	5.0291	3.5167	229.30	0.55	2.81	14-277	23
Isooctane	114.23	5.2063	3.4530	213.06	0.59	N/A	4-281	23
n-nonane	128.25	6.0513	3.4110	229.37	0.54	1.52	5-300	55
n-decane	142.29	6.9000	3.3665	226.86	0.26	2.22	14-279	23
n-undecane	156.31	7.2945	3.4005	229.34	0.46	1.43	5-300	55
n-dodecane	170.34	7.9338	3.3945	229.01	0.28	1.92	5-260	65,66
n-tridecane	184.37	8.4830	3.4089	235.18	0.50	1.31	5-300	55
n-hexadecane	226.45	9.3485	3.5424	255.06	0.16	1.93	14-262	13
n-heptadecane	240.47	11.019	3.3962	238.56	0.58	1.23	5-300	55
n-octadecane	254.50	12.496	3.3091	233.30	0.29	2.67	7-256	13
n-eicosane	282.55	10.888	3.6193	263.86	0.31	2.10	7-260	13
n-triacontane C30	422.83	15.976	3.6337	275.49	0.44	N/A	5-300	55
n-tetracontane C40	563.08	21.032	3.6387	276.19	0.32	N/A	5-300	55
CO_2	44.01	2.4639	2.6126	158.17	0.72	0.70	10-270	66
Toluene	92.14	4.234	3.2193	246.54	0.35	0.94	28-275	23
cyclooctane	112.21	5.9785	3.1395	250.05	0.76	N/A	14-276	23

[a] Correlated to data obtained at 373 K (100°C),[b] Correlated to data obtained at 523 K (250°C).
[c] Correlated to data obtained at 473 K (200°C),[d] Correlated to data obtained at 523.7 K (250.7°C).

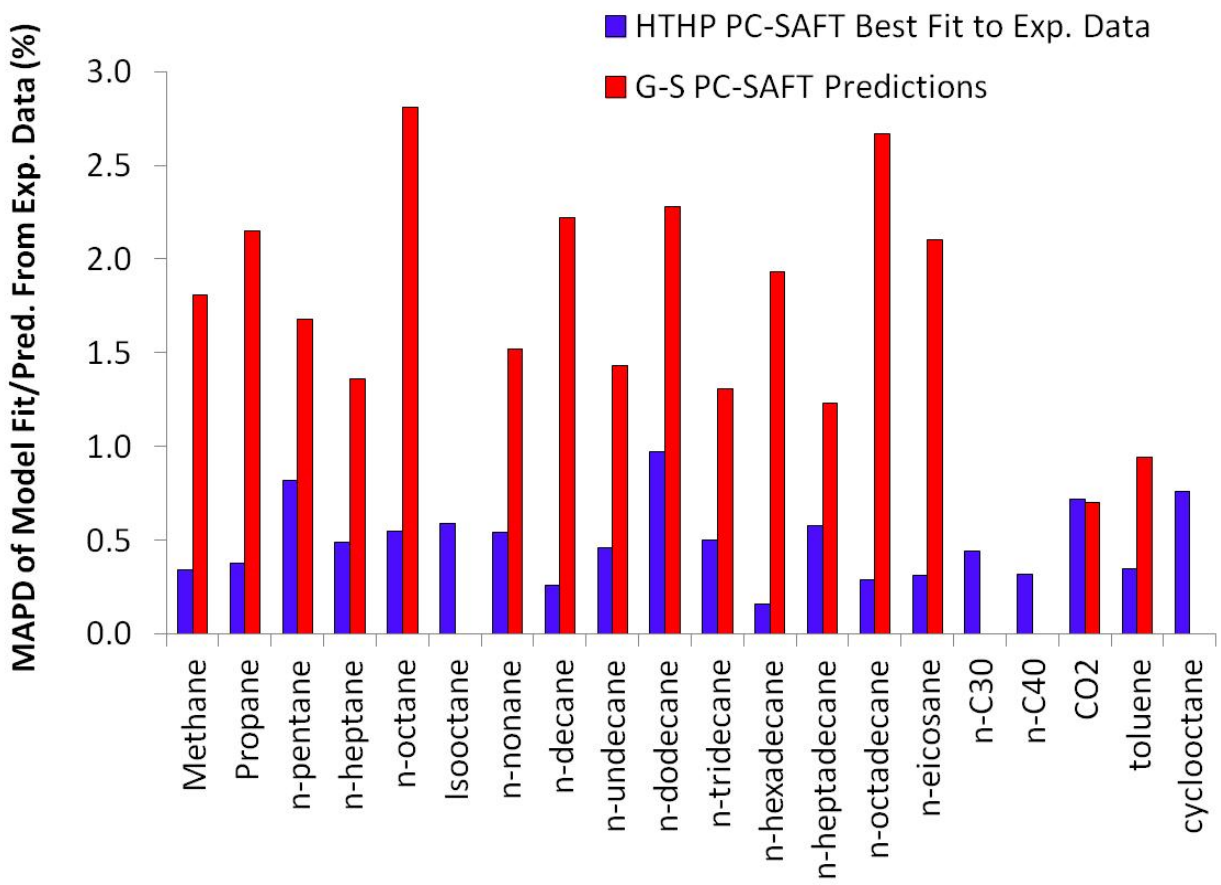

Figure 29: Plot of MAPDs given in Table 1. HTHP PC-SAFT predictions at pressures from 4.2 to 300 MPa and near 323, 423, and 523 K (50, 150, and 250°C) are significantly better than those from the G-S PC-SAFT equation of state.

8.1.1 HTHP Density Predictions

The overall performance of the HTHP PC-SAFT parameters was evaluated by comparing the predicted density data to the experimental data available in the literature in the range of 6.9 to 276 MPa. Density predictions were made for *n*-pentane (a small n-alkane chain with a normal boiling point of just 309 K, or 36°C), *n*-decane (an alkane chain containing ten carbon atoms, with a boiling point of 447 K, or 174°C), *n*-dodecane (a longer n-alkane chain that has a normal boiling point of 490 K), and toluene (an aromatic compound with a normal boiling point of 384 K, or 111°C). The MAPDs between PC-SAFT prediction and experimental values [23,65,66,68,69,70,71] and HTHP PC-SAFT predictions are summarized in Table 10, while the individual absolute percent deviations are plotted for each compound in Figure 30. HTHP PC-SAFT gives excellent density predictions for *n*-pentane at 325.9 K (52.7°C) and 423.2 K (150.1°C), but density predictions at 520.5 K (247.3°C) are only a moderate improvement on those given by the G-S PC-SAFT parameters (see Figure 31). Almost all of the MAPDs for the toluene, *n*-decane, and *n*-dodecane density values fall within 0±1%.

Table 10: MAPD and standard deviation (STDEV) of HTHP PC-SAFT and G-S PC-SAFT density predictions from selected experimental data collected at pressures 6.9 to 276 MPa.

		HP PC-SAFT		G-S PC-SAFT	
Component	Boiling point K	MAPD	STDEV	MAPD	STDEV
n-pentane	309	0.78	0.60	1.33	1.19
Toluene	384	0.28	0.19	0.98	0.62
n-decane	447	0.24	0.21	1.97	1.31
n-dodecane	490	0.23	0.20	1.44	0.82

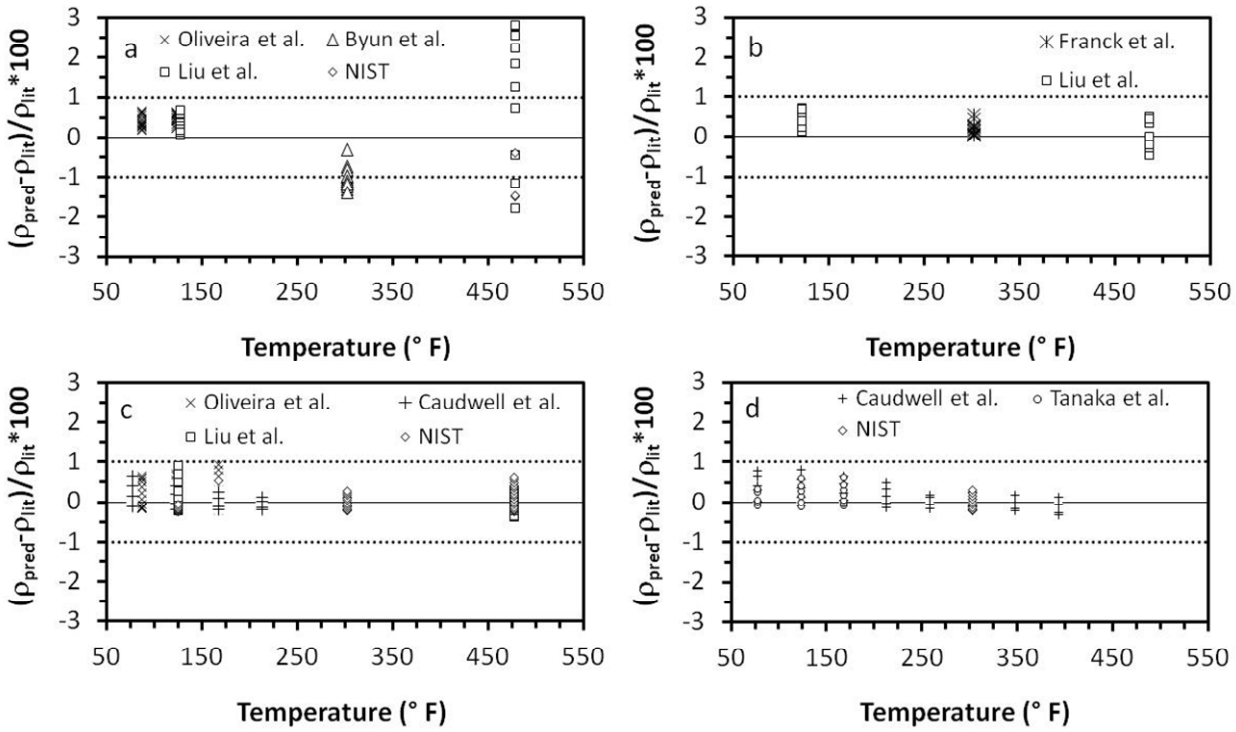

Figure 30: Percent deviation of HTHP PC-SAFT predictions from experimental values for the density values of (a) n-pentane, (b) toluene, (c) n-decane, and (d) n-dodecane. Data to which the fit was made in Table 1 are excluded from these plots.

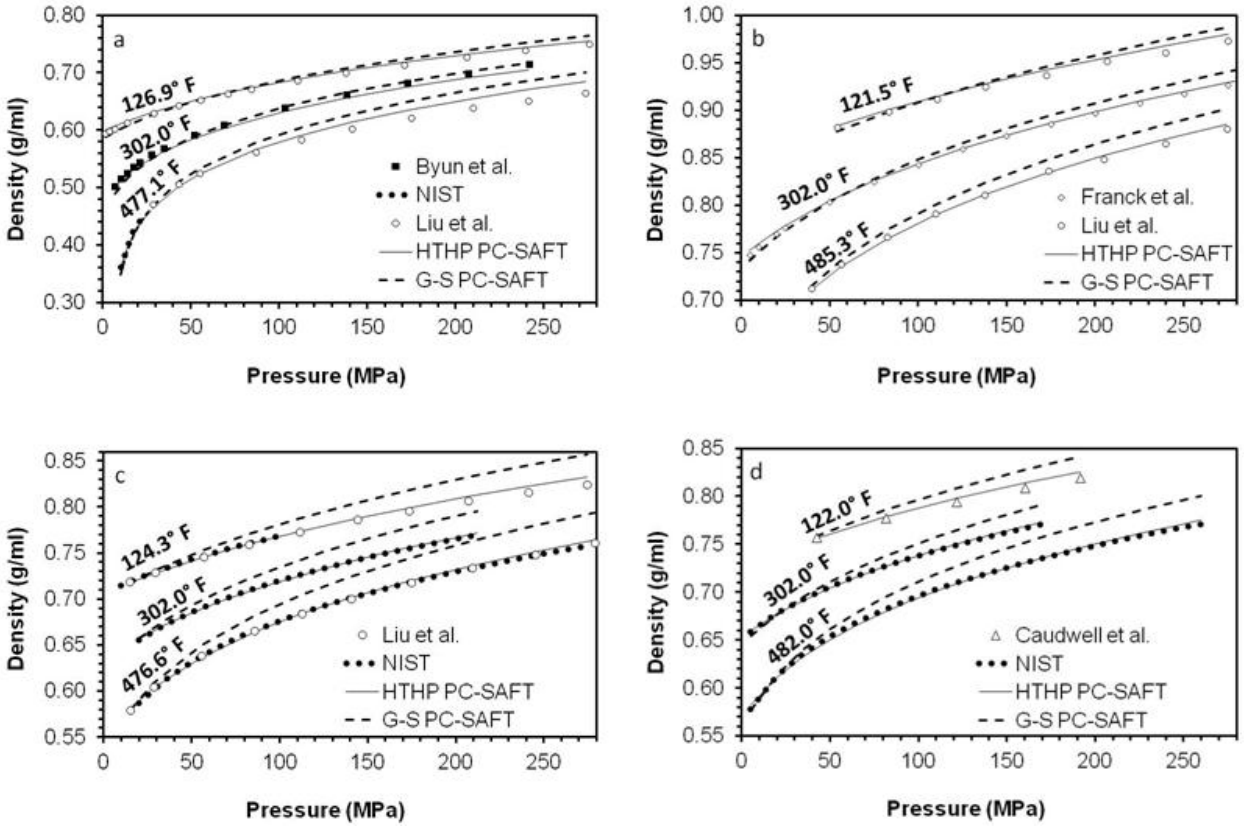

Figure 31: Using the HTHP PC-SAFT parameters greatly reduces the density over-prediction at high pressures for (a) n-pentane, (b) toluene, (c) n-decane, and (d) n-dodecane that are observed when utilizing the G-S PC-SAFT parameters.

8.1.2 General Correlation Development

For the compounds where density data was not available, correlations were developed to predict the HTHP PC-SAFT parameters. These correlations were obtained by plotting HTHP PC-SAFT parameters (listed in Table 1) m, σ, and ε/k_B as a function of molecular weight shown in Figure 32a-c. These equations were used to predict the HTHP PC-SAFT parameters listed in Table 11 along with the MAPD values for density predictions obtained using these parameter sets. HTHP PC-SAFT with predicted parameters provides a very good representation of the density of alkanes and isooctane, a branched alkane. However, as expected, for cyclooctane, carbon dioxide, and toluene the MAPD for density predictions were ranged from 14.2% to 42.5%. As shown in Table 11, the density MAPD values obtained using predicted HTHP parameters are 0.97% or less and are similar in value to those obtained with parameters fit directly to experimental data, with the exception of methane.

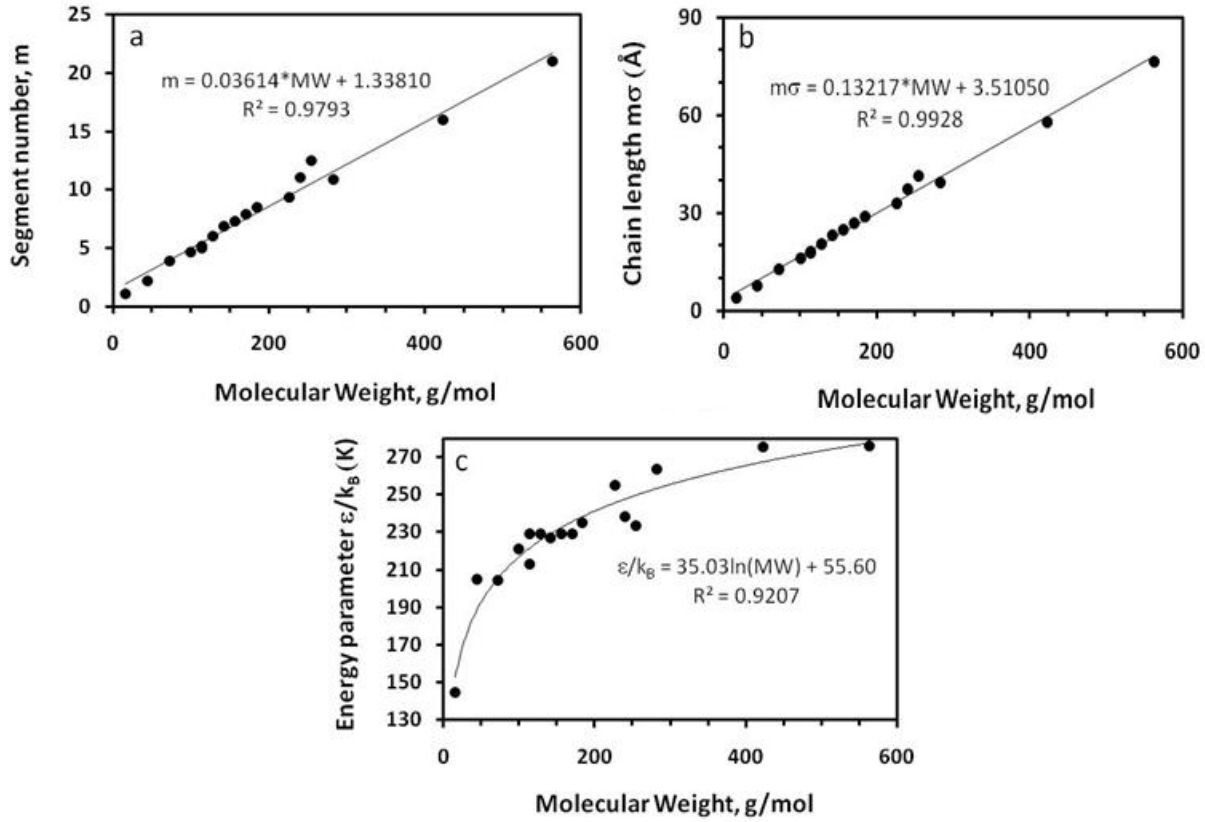

Figure 32: Effect of molecular weight on the HTHP PC-SAFT pure-component parameters m (a), σ (b), and ε/k_B (c) for the alkanes listed in Table 9. The filled circles represent the value of the parameters obtained by fitting experimental data, and the curves are the best fit of the parameters to a correlation equation shown in each figure.

Table 11: Performance comparison for the correlated and predicted HTHP PC-SAFT parameters.

		HTHP PC-SAFT Parameters			4.2-300 MPa	
		Predicted			MAPD	
Compound	Mol Wt (g/mol)	m	σ(Å)	ε/k_B (K)	Best Fit	Pred.
methane	16.043	1.9179	2.9360	152.82	0.34	5.49
propane	44.096	2.9317	3.1854	188.24	0.38	0.97
n-pentane	72.146	3.9455	3.3066	205.48	0.82	0.68
n-heptane	100.203	4.9594	3.3783	216.99	0.49	0.63
n-octane	114.231	5.4664	3.4041	221.58	0.55	0.65
isooctane	114.231	5.4664	3.4041	221.58	0.59	0.47
n-nonane	128.250	5.9731	3.4256	225.64	0.54	0.67
n-decane	142.285	6.4803	3.4437	229.28	0.26	0.37
n-undecane	156.312	6.9872	3.4592	232.57	0.46	0.63
n-dodecane	170.338	7.4941	3.4726	235.58	0.28	0.32
n-tridecane	184.365	8.0011	3.4843	238.35	0.5	0.6
n-hexadecane	226.446	9.5219	3.5119	245.55	0.16	0.29
n-heptadecane	240.473	10.0288	3.5192	247.66	0.58	0.59
n-octadecane	254.500	10.5357	3.5259	249.64	0.29	0.44
n-eicosane	282.553	11.5496	3.5374	253.31	0.31	0.3
n-C30	422.830	16.6192	3.5739	267.43	0.44	0.48
n-C40	563.079	21.6878	3.5934	277.46	0.32	0.65
CO_2	44.010	2.9286	3.1849	188.17	0.72	41.48
toluene	92.141	4.6681	3.3609	214.05	0.35	20.77
cyclooctane	112.210	5.3934	3.4007	220.96	0.76	14.19

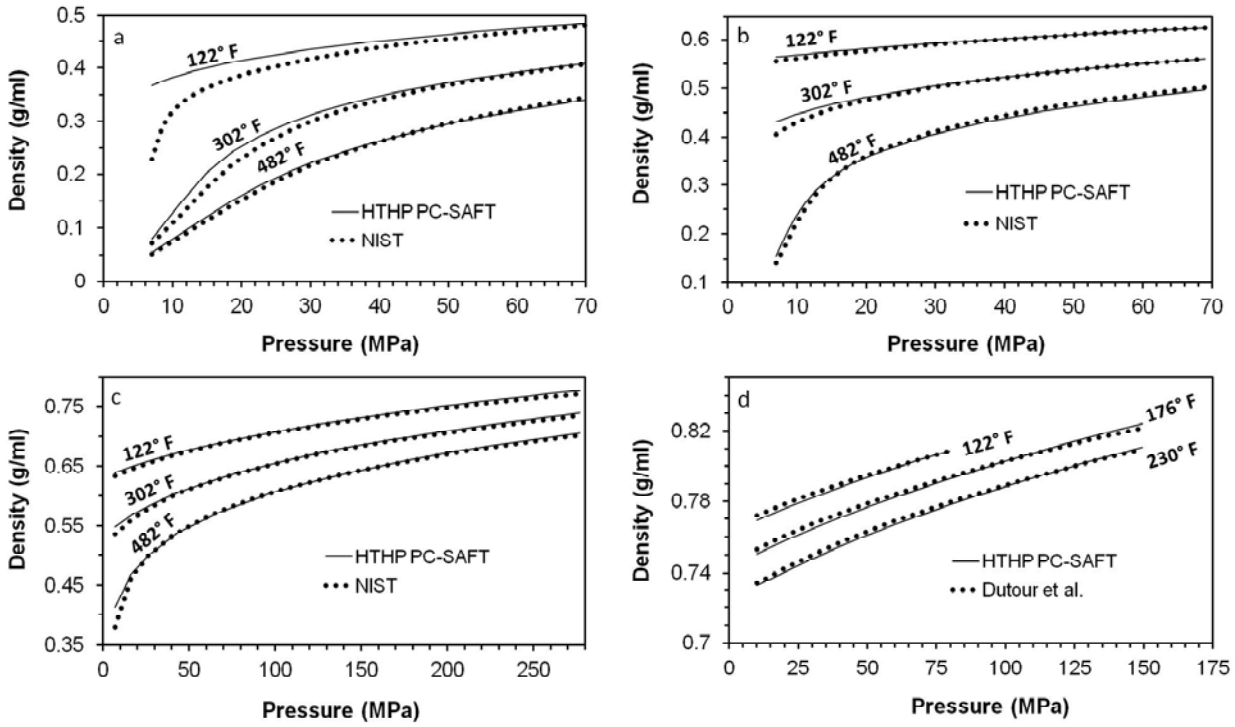

Figure 33: Density predictions for (a) ethane, (b) n-butane, (c) 2-methylpentane, and (d) n-nonadecane obtained using the PC-SAFT equation with HTHP parameters calculated with predictive correlations. The data points are from "NIST" [72]. The n-nonadecane densities are from Dutour, et al. [73].

Table 12: Predicted HTHP PC-SAFT parameters used to obtain density predictions in Figs. 6a-d, along with the MAPDs between the predicted and experimental data sets shown therein.

		Pred. HTHP PC-SAFT Parameters			
Compound	**Mol Wt**	**m**	**σ**	**ε/k_B**	**MAPD**
	g/mol		**Å**	**K**	**%**
ethane	30.069	2.4248	3.0867	174.83	6.38
n-butane	58.123	3.4387	3.2549	197.91	1.82
2-methylpentane	86.177	4.4525	3.3465	211.71	0.49
n-nonadecane	268.527	11.0427	3.5319	251.52	0.19

HTHP PC-SAFT correlations were used to predict the HTHP parameters, shown in Table 12, for ethane, n-butane, 2-methylpentane, and n-nonadecane. Density predictions using these parameters are shown in Figure 33 a-d. The density predictions for *n*-butane, 2-methylpentane, and *n*-nonadecane are in excellent agreement with experimental data. For ethane the density predictions are in good agreement at 523K (250°C). The density predictions using HTHP PC-SAFT are not good near critical point regions.

The new HTHP PC-SAFT parameters presented in Table 9 are derived using HTHP PρT data at pressures greater than 6.9 MPa, while the PC-SAFT parameters reported by Gross and Sadowski [20] are based almost exclusively on lower pressure sub-critical data. Preliminary calculations using the new set of parameters to predict PρT values for pure n-alkanes in this range indicated two interesting trends: (1) over-prediction of the density by HTHP PC-SAFT is largest within at least 55 K of the critical temperature, and (2) the model predictions begin to exhibit deviations

greater than ~ 5% from experimental data at the point where the vapor pressure is equal to approximately one half of the critical pressure of the compound in question.

8.2 DEVELOPMENT OF HYBRID PC-SAFT PARAMETERS

The GS PC-SAFT parameters were good at low pressure. Less than 6 MPa and HTHP PC-SAFT parameters gave good density prediction above 6 MPa. A continuum of parameter sets may exist at intervals between the values of the G-S and HTHP PC-SAFT parameters for a given species that provide accurate reproduction of experimental data. We investigated various arithmetic relationships and a final correlation was defined as:

$$m = m_{G-S} + \left(m_{HTHP} - m_{G-S}\right) e^{-\left(\frac{P}{100}\right)^2} \tag{24}$$

$$\sigma_0 = \sigma_{G-S} + \left(\sigma_{HTHP} - \sigma_{G-S}\right) e^{-\left(\frac{P}{100}\right)^2} \tag{25}$$

$$\sigma = \sigma_0 \left(1 - 0.12 \left(\sigma_{HTHP} - \sigma_0\right)\left(\sigma_{G-S} - \sigma_0\right)\right) \tag{26}$$

$$\frac{\varepsilon}{k} = \left(\frac{\varepsilon}{k}\right)_{G-S} + \left[\left(\frac{\varepsilon}{k}\right)_{HTHP} - \left(\frac{\varepsilon}{k}\right)_{G-S}\right] e^{-\left(\frac{P}{100}\right)^2} \tag{27}$$

8.2.1 Hybrid PC-SAFT Density Predictions

Table 13 shows the MAPD of density predictions using hybrid PC-SAFT along with MAPD form G-S PC-SAFT and HTHP PC-SAFT parameter sets. The results in Table 13 indicate that the hybrid PC-SAFT gives density predictions accurate to better than ±1% in this region, and can be used with only a small penalty relative to the HTHP PC-SAFT density values, and sometimes even results in more accurate density predictions overall.

Table 13: Comparison of the predictive capabilities of the G-S, HTHP, and hybrid PC-SAFT parameters at pressures to 276 MPa and temperatures to 533 K (260°C).

	MAPD of Exp. Density Value and				
Compound	**G-S PC-SAFT**	**HTHP PC-SAFT**	**Hybrid PC-SAFT**	**P range (MPa)**	**Ref.**
methane	1.81	0.34	0.37	5-290	74
propane	2.15	0.38	0.74	6.8-269	75
n-pentane	1.68	0.82	0.87	1.8-277	23
n-heptane	1.36	0.49	0.44	5-300	76
n-octane	2.81	0.55	0.55	14.3-277	23
n-nonane	1.52	0.54	0.30	5-300	76
n-decane	2.22	0.26	0.33	14.6-279	23
n-undecane	1.43	0.46	0.37	5-300	76
n-dodecane	1.91	0.28	0.31	5-260	74,77
n-tridecane	1.31	0.50	0.85	5-300	76
n-hexadecane	1.93	0.16	0.32	14.1-262	13
n-heptadecane	1.55	0.48	0.45	5-300	76
n-octadecane	2.67	0.29	0.57	7-256	13
n-eicosane	2.10	0.31	0.52	7.3-260	13
CO2	0.70	0.72	0.59	10.1-270	74
Toluene	0.94	0.35	0.34	28.6-275	23

The percent deviations with respect to pressures up to 276 MPa were plotted for toluene (aromatic), n-pentane (short n-alkane chain), and n-decane (longer n-alkane chain) at temperatures of approximately 323, 423, and 523 K (50, 150, and 250°C). Figure 34 shows that there is some difference in density prediction using hybrid parameters and HTHP PC-SAFT parameters below 140MPa but overall is still under ±1%. At pressure above then 140 MPa, hybrid parameter density predictions are in agreement with HTHP PC-SAFT density predictions.

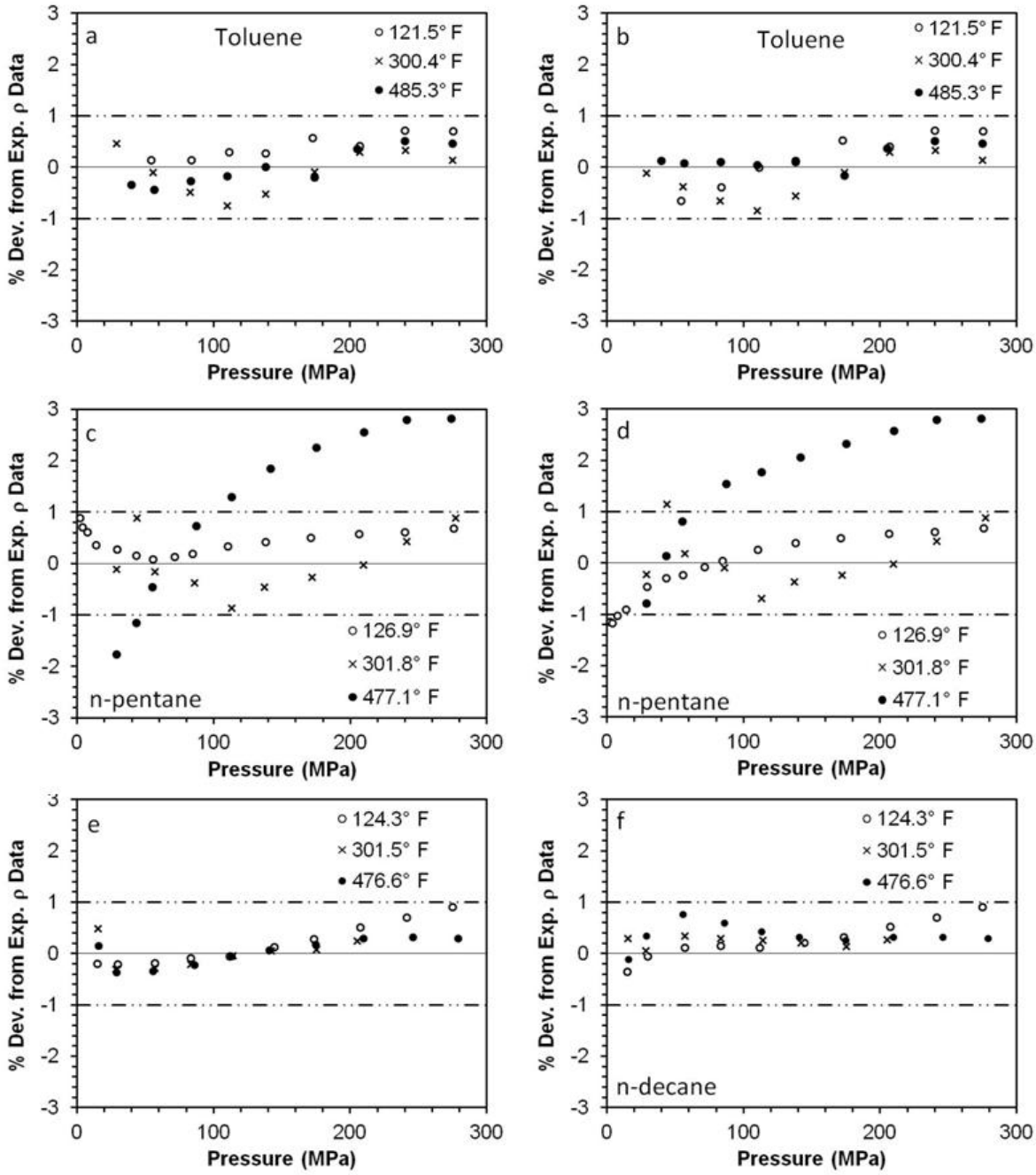

Figure 34: HTHP PC-SAFT density predictions for (a) toluene, (c) n-pentane, and (e) n-decane deviate only slightly from the respective hybrid PC-SAFT predictions for these compounds (b, d, f), indicating that the hybrid PC-SAFT density predictions increase smoothly with respect to pressure. Experimental data were obtained from reference [23].

Hybrid PC-SAFT was analyzed for the density prediction at pressure less than 6.9 MPa. The HTHP PC-SAFT predictions were not ideal at low pressures and around critical region for hydrocarbon. The density predictions were made using the hybrid PC-SAFT parameters to evaluate its ability to predict the sub-critical, near-critical, and super-critical density values for

toluene, n-pentane, and n-decane. The saturation curve PρT predictions by hybrid PC-SAFT (see Figure 35 a-c) are in agreement with experimental data.

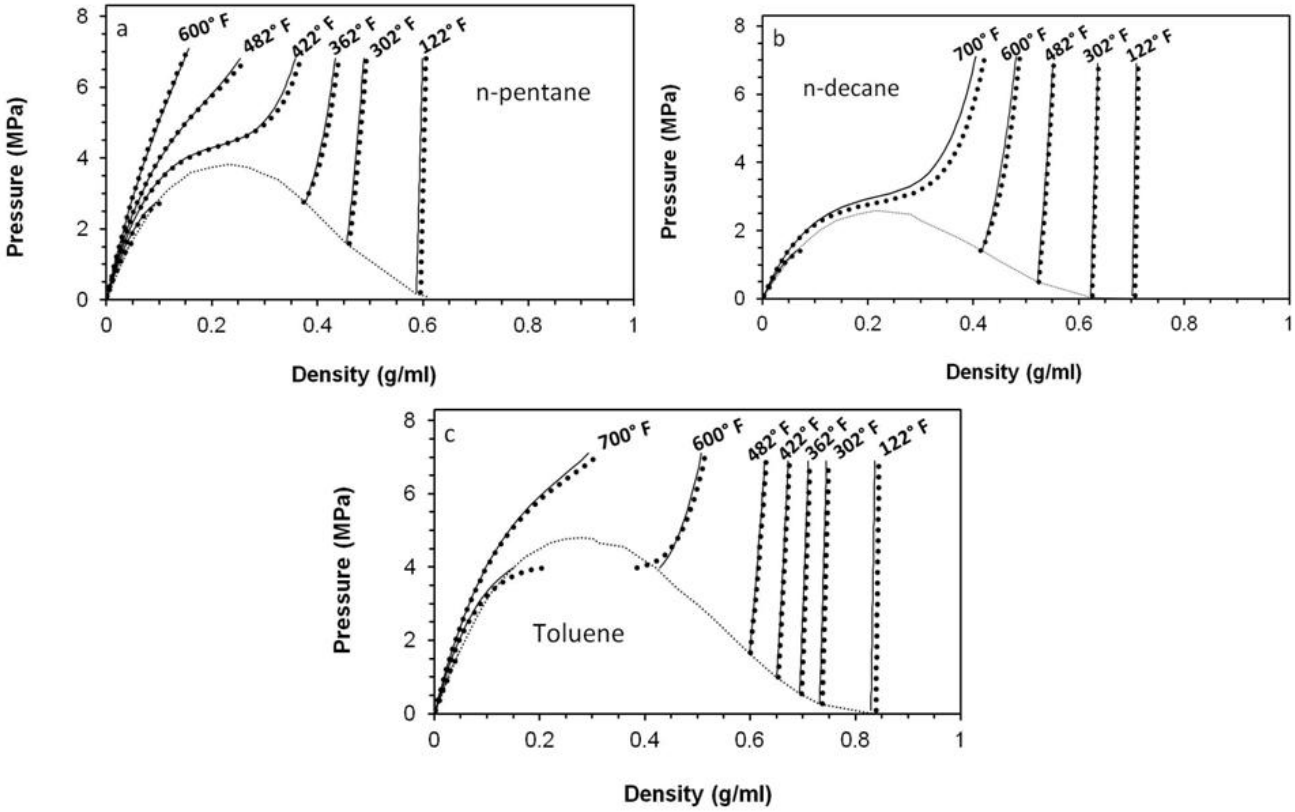

Figure 35: The hybrid PC-SAFT model gives reliable pure-component density predictions in the near-critical region for (a) n-pentane, (b) n-decane, and (c) toluene. (–) Two-phase boundary (Hybrid PC-SAFT) (–) Hybrid PC-SAFT density predictions ••••• Density values given by NIST [74].

8.2.2 Hybrid PC-SAFT Predictions for Mixtures

There is limited experimental data that exists for mixture density values for the entire range of HTHP conditions. However, there is data for *n*-hexane (C6) + *n*-hexadecane (C16) and propane (C3) + *n*-decane (C10) mixtures at the temperatures and pressures of interest. Density predictions for these mixtures were made using hybrid PC-SAFT over much of the HTHP region. The binary interaction parameter (k_{12}) was set to zero for all hydrocarbon mixtures.

For propane and n-decane mixtures shown is Figure 36 [78], the HTHP PC-SAFT over predicts the density at low pressure (less than 20MPa). The over prediction can be about 15-20% depending on mixture critical points. Hybrid PC-SAFT greatly reduces the density over prediction and gives accurate density predictions over the full composition range for propane-n-decane mixtures. Notably, the transition from G-S to HTHP parameters with respect to increasing pressure is smooth and gradual.

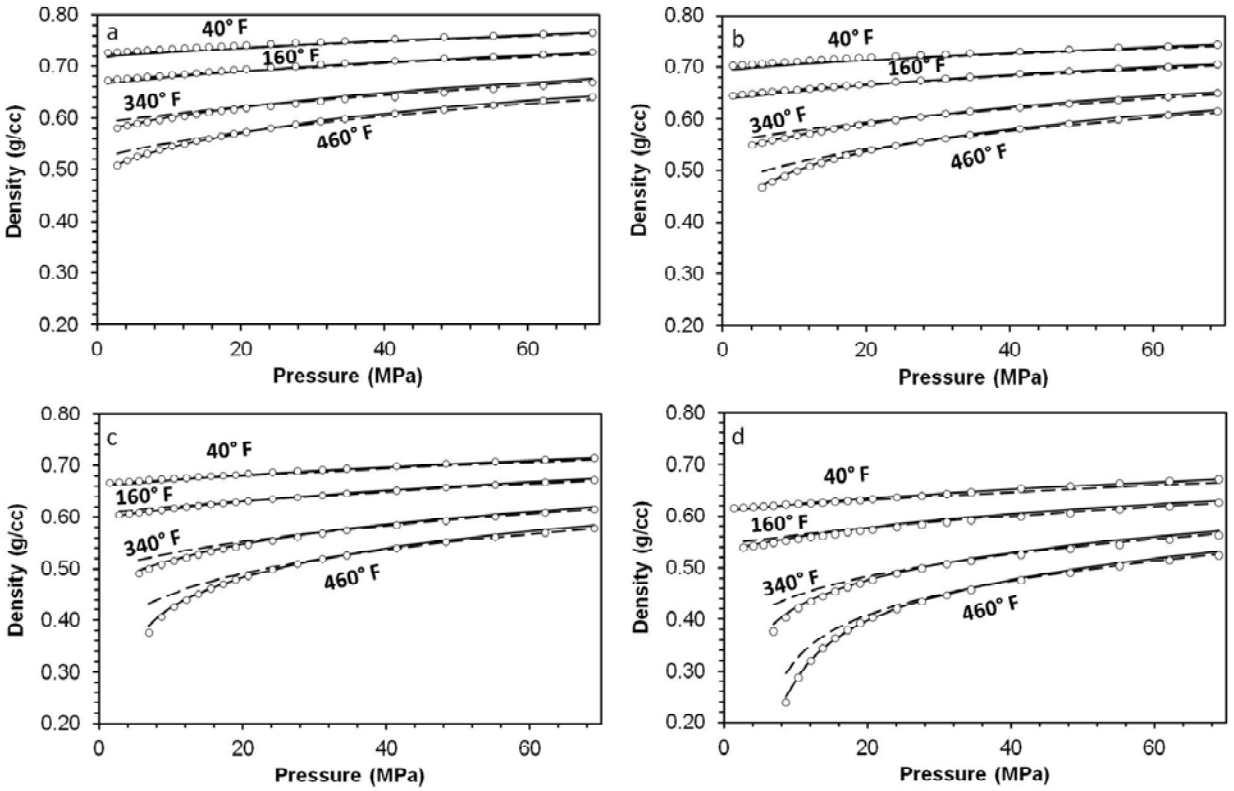

Figure 36: Hybrid PC-SAFT predictions are superior to HTHP PC-SAFT predictions for propane-n-decane mixtures of composition (a) 0.2:0.8, (b) 0.4:0.6, (c) 0.6:0.4, and (d) 0.8:0.2. k_{12} = 0. (——) Hybrid PC-SAFT (- - -) HTHP PC-SAFT (o) Reamer and Sage [78].

Figure 37 [79] and Figure 38 [80] show that hybrid PC-SAFT predictions are in agreement with the experimental density data for the n-hexane/n-hexadecane mixture and n-hexane/toluene mixtures in the HTHP region.

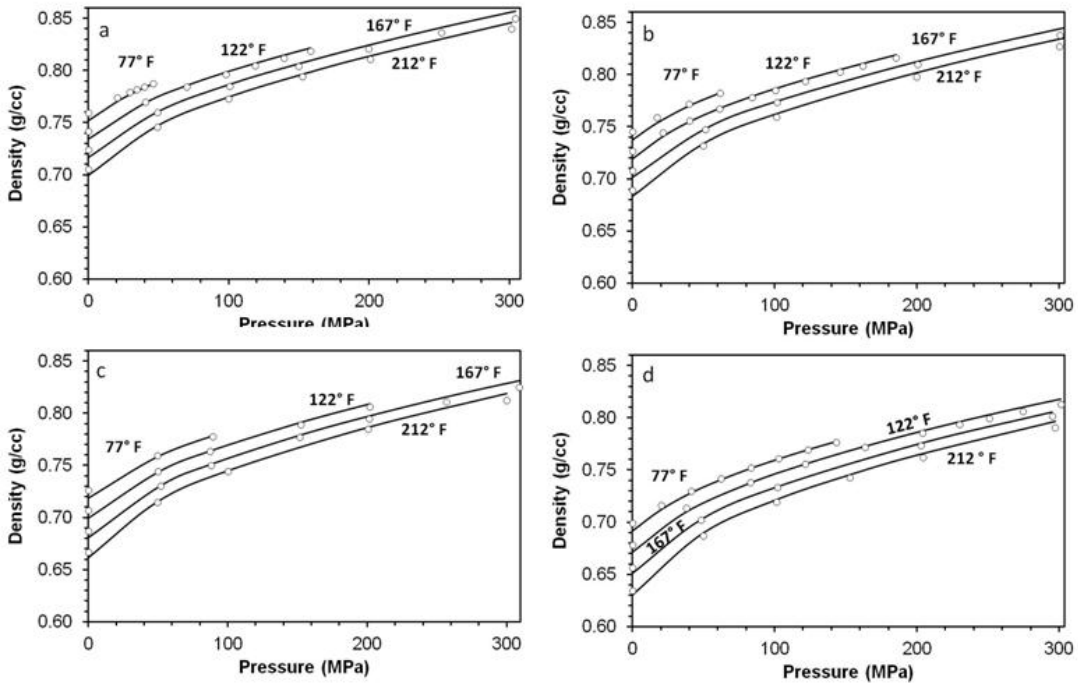

Figure 37: Hybrid PC-SAFT density predictions for n-hexane-n-hexadecane mixtures containing (a) 0.2, (b) 0.4, (c) 0.6, and (d) 0.8 mole fraction n-hexane. $k_{12} = 0$ (o) Dymond et al. [79].

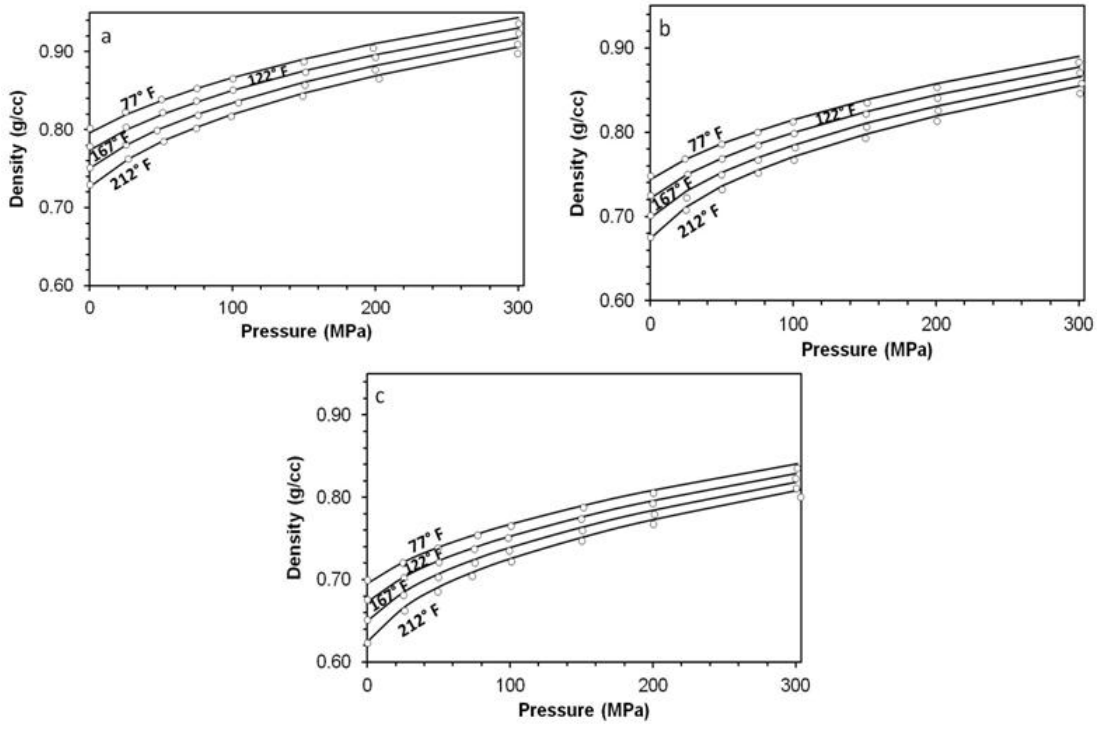

Figure 38: Hybrid PC-SAFT density predictions for n-hexane-toluene binary mixtures containing (a) 0.25, (b) 0.50, and (c) 0.75 mole fraction n-hexane. $k_{12} = 0$ (o) Dymond et al. [80].

8.2.3 Hybrid PC-SAFT Phase Equilibrium Predictions

The HTHP PC-SAFT did not predict the phase equilibrium accurately. The ability of the hybrid PC-SAFT model to predict phase equilibrium was evaluated. The binary interaction parameter k_{12} was set equal to zero for all mixtures studied. As shown in Figure 39, the hybrid PC-SAFT phase equilibrium predictions are a great improvement over those of HTHP PC-SAFT for the mixture of propane and n-decane. Most importantly, the critical point pressure is over predicted by no more than 10% by hybrid PC-SAFT.

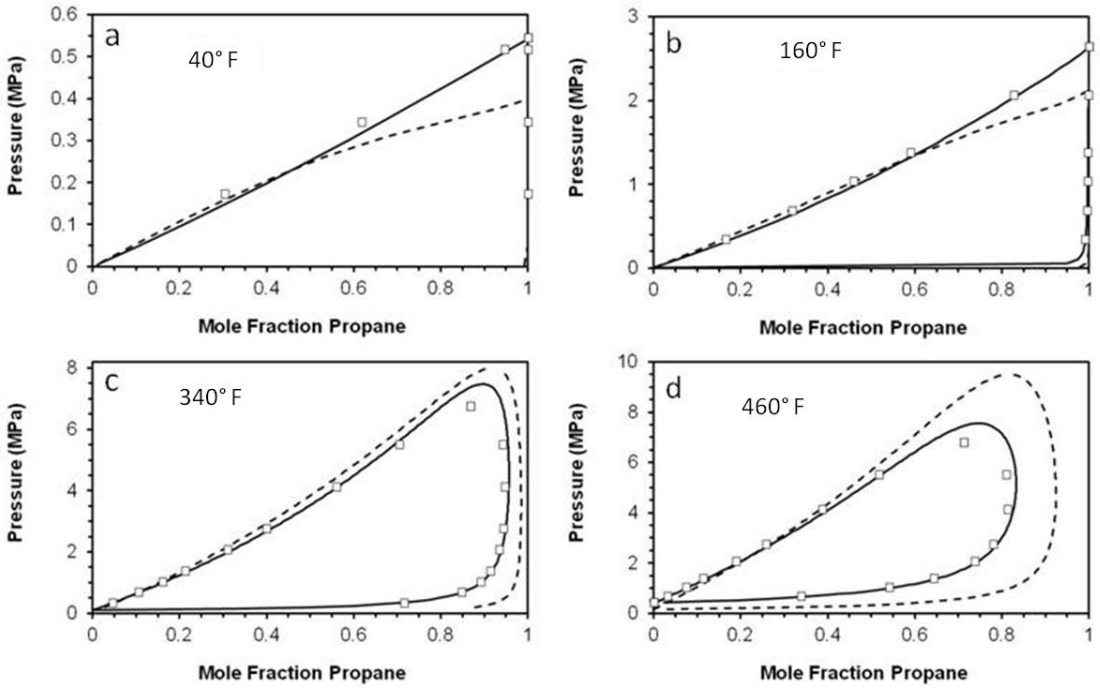

Figure 39: The hybrid PC-SAFT phase compositions for C_3/C_{10} binary predictions are almost identical to those predicted by the G-S PC-SAFT method at (a) 277.6 K, (b) 344.3 K, (c) 444.3 K, and (d) 510.9 K. k_{12} = 0. (──) Hybrid PC-SAFT (- - -) HTHP PC-SAFT (o) Reamer and Sage [78].

Mixtures like methane and decane were evaluated and exhibit two phases well into the HTHP region. Hybrid PC-SAFT was evaluated for its ability to predict phase equilibria within the lower pressure end of the HTHP region. The critical pressure of the methane/n-decane system at 311 K is ~ 35 MPa and the methane/toluene system at 462 K (189°C) is ~ 25 MPa. Results are shown in Figure 40 [81] and Figure 41 [82]. Hybrid PC-SAFT slightly over predicts the density compared to G-S PC-SAFT at these pressures.

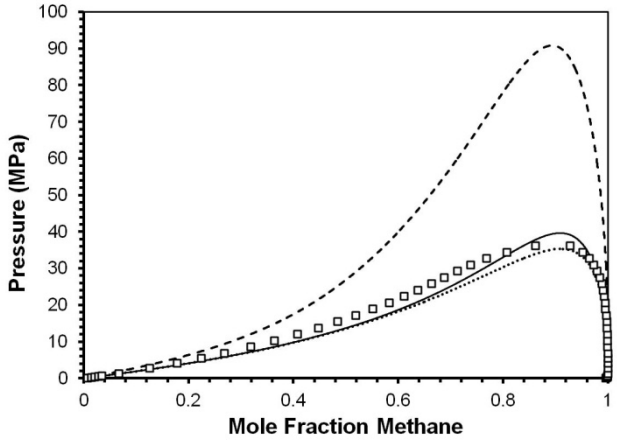

Figure 40: Phase equilibrium predictions by hybrid PC-SAFT exhibit little difference from those of G-S PC-SAFT for a methane/n-decane system at 311 K (38°C). —— Hybrid PC-SAFT ----- HTHP PC-SAFT ..... G-S PC-SAFT □ Exp. [81].

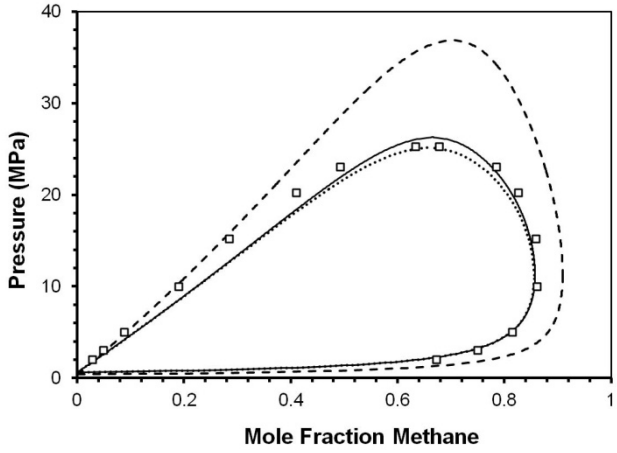

Figure 41: Phase equilibrium predictions by hybrid PC-SAFT exhibit little difference from those of G-S PC-SAFT for a methane/toluene system at 462 K (189°C). —— Hybrid PC-SAFT ----- HTHP PC-SAFT ..... G-S PC-SAFT □ Exp. [82].

Hybrid PC-SAFT was also evaluated for the mixtures containing at least one non-hydrocarbon dioxide and n-decane. For $k_{12} = 0.128$, hybrid PC-SAFT accurately predicts phase equilibrium for a mixture of carbon dioxide and n-decane at temperatures of 310 K and 511 K. A slight adjustment of the k_{12} value to 0.12 optimizes hybrid PC-SAFT phase equilibrium predictions for a mixture of CO_2 and propane. As shown in Figure 42 [83,84], the hybrid PC-SAFT model eliminates the general over prediction of the phase envelope by HTHP PC-SAFT and the hybrid PC-SAFT phase equilibrium predictions are virtually identical to those of G-S PC-SAFT.

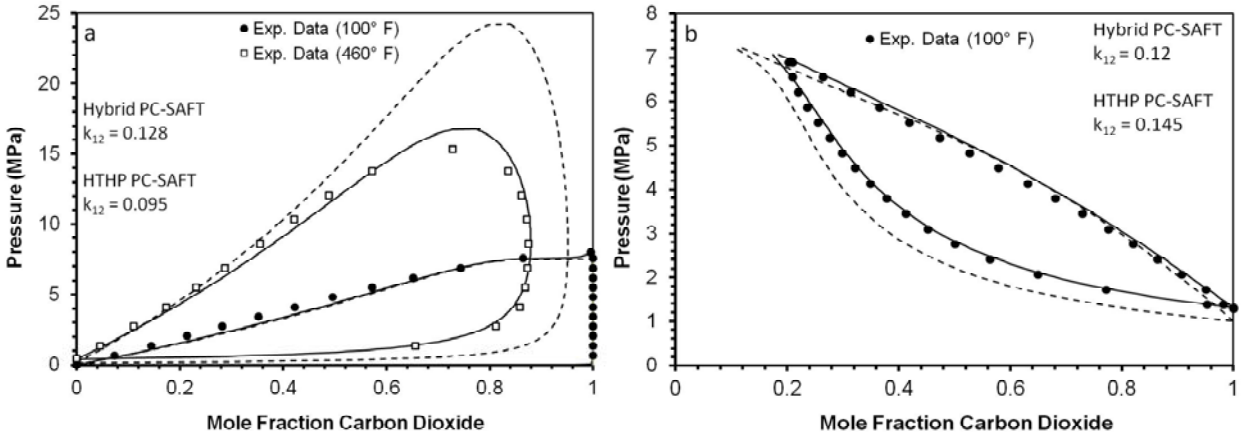

Figure 42: Hybrid PC-SAFT improves greatly on HTHP PC-SAFT, closely mirroring experimental phase equilibrium data for binary mixtures of CO_2 and (a) n-decane [83], (b) propane [84] —— Hybrid PC-SAFT ----- HTHP PC-SAFT.

By correlating the PC-SAFT equation of state to HTHP density data, we have produced a new set of pure-component parameters that, when utilized with the PC-SAFT equation, typically give absolute percent deviations of less than 1% over the full range of temperatures from ambient to 523 K and pressures from 4.2 to 300 MPa. The over prediction of density in the HTHP region by PC-SAFT vanishes when the HTHP parameters are used instead of those put forth by Gross and Sadowski. The HTHP parameters obtained for normal and branched alkanes, toluene, cyclooctane, and carbon dioxide can be used to give $P\rho T$ predictions for both pure components and mixtures that are superior to those provided by the original G-S PC-SAFT equation although the HTHP parameters are not recommended for use at pressures below ~ 20 MPa when within at least 180°F (100°C) of the mixture critical temperature. HTHP PC-SAFT has potential for its use in the petroleum recovery and processing industry where it could be utilized to model petroleum within ultradeep formations and the associated production well. The HTHP PC-SAFT density predictions are also clearly superior, especially at pressures above ~ 200 MPa, to those obtained using a cubic.

In the region of pressures from ~ 0-6.9 MPa, the G-S PC-SAFT parameters give superior predictions for both pure-component $P\rho T$ behavior (especially for the more volatile components) and phase equilibrium. Application of the hybrid PC-SAFT model is limited by the relatively small number of compounds, mostly n-alkanes, for which HTHP PC-SAFT parameters are available. The size of this list is limited by the relative lack of experimental density data over the HTHP range for many compounds of interest to us, especially aromatics and cycloalkanes. Therefore, an ongoing research effort in our laboratory is to obtain such density data for these compounds, so that HTHP PC-SAFT parameters can subsequently be fit.

9. VISCOSITY MODEL DEVELOPMENT

Various modeling approaches have been investigated to reproduce high pressure viscosity values.

Dymond and Brawn [85] proposed a model based on hard-sphere theory to predict the viscosities. Dymond and coworkers [86,87,88,89,90] subsequently utilized their approach to reproduce experimental viscosities for n-alkanes, branched alkanes and aromatics, typically within a tolerance of better than ±2%. However, their model is extremely sensitive to minor perturbations in molar volume, resulting in significant deviations in the predicted viscosity.

Assael and co-workers proposed a model similar to Dymond to determine alkane and aromatic viscosity [91,92] that was less sensitive to molar volume perturbations. However, the model over predicts the viscosity of n-octane at ambient temperature and pressures above 200 MPa, even when used in conjunction with the high temperature, high pressure, perturbed-chain statistical associating fluid theory (HTHP PC-SAFT) equation of state [93],which typically gives molar volume results to within less than ±1% of the experimental value.

The Chung-Lee-Starling (CLS) method [94,95] is another model that has demonstrated success at elevated pressures. While the CLS model yields accurate viscosity predictions up to ~ 50 MPa, these predictions are also sensitive to very small (i. e., < 1%) perturbations in the input density. However, even when density predictions are obtained with the highly accurate HTHP PC-SAFT EoS, the viscosity of n-octane is over-predicted by more than 20% at pressures near 276 MPa.

9.1 FRICTIONAL THEORY (F-THEORY) AND FREE VOLUME THEORY (FV THEORY)

The two theories evaluated in this research that have shown great promise with regard to the accurate modeling of viscosity at both low pressures and HTHP conditions are the frictional theory (f-theory) [96,97] and the free volume theory (FV theory) of viscosity [98,99]. Detailed equations for both theories are provided in Appendix B. In this work, f-theory and FV theory are extended to the full HTHP range of temperatures from ambient to 533 K (260°C) and pressures from 6.9 to 276 MPa. The performances of these models are presented by comparing calculated and experimental viscosities for carbon dioxide, normal and branched alkanes, aromatics, and cycloalkanes.

9.1.1 Friction Theory Evaluation

In f-theory, the viscosity is assumed to be a function of a number of temperature-dependent coefficients, and the attractive and repulsive pressures provided by a suitable EoS, such as the Soave-Redlich-Kwong (SRK), Peng-Robinson (PR) EoS, and PC-SAFT EoS [20]. F-theory gives its best predictions for n-alkane viscosity values at pressures upto 100 MPa when the attractive and repulsive pressure inputs P_a and P_r are obtained using the PC-SAFT equation. However, PC-SAFT-FT begins to under-predict the viscosity pressures greater than ~ 150 MPa.

In order to correct the under-prediction of viscosity by PCSAFT-FT, a viscosity translation (i.e. viscosity correction term) was developed for PCSAFT-FT equations. The viscosity translation term was dependent on the pressure and also component melting temperature, T_m. Equation 28 was able was able to correct the PCSAFT-FT viscosity predictions for n-alkanes to values that are typically within ±2% of the experimental values.

$$c = \left[A\left(T - T_m\right)^n + \frac{B}{\left(T - T_m\right)^n} \right] P^3 \eta_{FT} \tag{28}$$

$$\eta_{corr} = \eta_{FT} + c \tag{29}$$

The constants *A*, *B*, and *n* are pure-component parameters that are obtained by fitting the corrected PCSAFT-FT viscosity predictions to $P\mu T$ data at pressures ranging from ambient to 276 MPa and temperatures ranging from ambient to 533 K (260°C). The value η_{FT} is the viscosity prediction obtained using the PC-SAFT-FT equations defined earlier, while η_{corr} is the corrected, translated viscosity value.

The corrected (viscosity-translated) PCSAFT-FT model (VT PC-SAFT FT) indicates considerable improvement when the correction term is applied, a conclusion graphically supported in Figure 43.

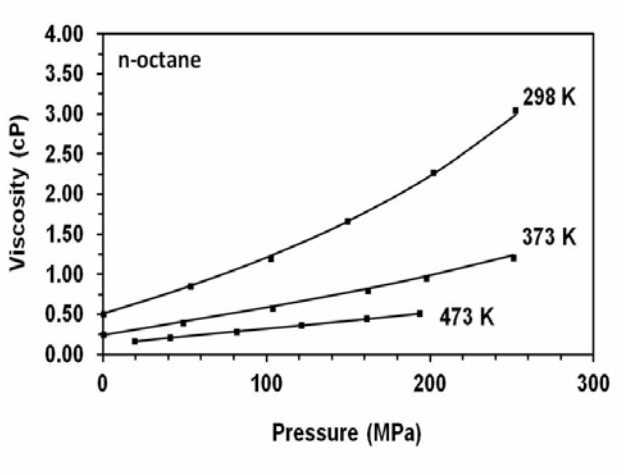

Figure 43: Viscosity results for n-octane yielded by the corrected f-theory VT PC-SAFT FT.

A visual examination of the results in Figure 43 indicates that the viscosity under-prediction for n-octane is all but eliminated when the viscosity correction term is used.

To assessing the predictive capability of the f-theory viscosity translation term, values for the pure-component parameters η_a and η_r had to be obtained for a number of aromatic and naphthenic compounds. These parameters are given in Appendix C. The η_a and η_r parameters were determined by modeling after available $P\mu T$ data. If possible, the full pressure range from 7-276 MPa was covered. Viscosity predictions are shown in Table 14.

9.1.2 Free Volume Theory Evaluation

In FV theory, viscosity is assumed to be dependent on the molecular free-volume fraction, which is expressed as a function of density. Previous workers have used both experimental data [98] and SAFT-based models [99] to obtain the needed density input to FV theory, although the advent of volume-translated cubic EoS [100] that is effective in the HTHP region provides an opportunity to also couple a cubic EoS with FV theory. In general, FV theory over predicts the viscosity at HTHP conditions.

In order to obtain improved HTHP viscosity predictions, new values for the parameters L, α, and B, were determined by fitting experimental $P\mu T$ data at temperatures and pressures to 533 K (260°C) and 276 MPa, respectively. Because pressure effects on the viscosity can vary considerably with respect to temperature, the most accurate set of parameters will only be obtained when experimental data are available over the whole temperature and pressure range of interest. The parameters were obtained for following EOS and are in Appendix C.

FV Theory coupled to G-S PC-SAFT density model (denoted as PCSAFT-FVT)

FV Theory coupled to HTHP PC-SAFT density predictions denoted as HTHP PCSAFT-FVT

FV Theory coupled to HTHP-VT-SRK density predictions denoted as HTHP-VT-SRK-FVT

FV Theory coupled to HTHP-VT-PR density predictions denoted as HTHP-VT-PR-FVT

9.1.3 Comparison of Viscosity Results

The performances of two f-theory models, PCSAFT-FT, and VT- PCSAFT-FT, and four FV theory models, PCSAFT-FVT, HTHP PC-SAFT FVT, HTHP-VT-SRK-FVT, and HTHP-VT-PR-FVT were compared by predicting the viscosity values for 17 hydrocarbons and carbon dioxide.

Table 14: Comparison of MAPDs of viscosity predictions made by predictive models studied for 19 compounds of interest to the petrochemicals industry.

	PCSAFT-FT	Corrected PCSAFT-FT	PCSAFT-FVT	HTHP PCSAFT-FVT	HTHP VT-SRK FVT	HTHP VT-PR FVT
Methane	2.84	9.13	2.53	3.34	2.86	2.52
n-C_6H_{14}	4.26	1.26	0.67	1.93	1.77	1.63
n-C_8H_{18}	3.19	1.41	2.06	3.35	4.14	3.98
n-C_9H_{20}	3.57	2.00	1.54	1.94	2.18	2.03
n-$C_{10}H_{22}$	3.64	1.77	1.67	2.22	2.10	2.15
n-$C_{12}H_{26}$	7.73	4.33	2.61	3.75	2.68	3.16
n-$C_{15}H_{32}$	5.24	1.59	1.73	3.19	2.30	2.83
n-$C_{16}H_{34}$	4.67	2.13	1.34	3.75	2.54	3.65
n-$C_{18}H_{38}$	3.74	2.81	1.60	3.37	2.50	2.94
benzene	9.94	5.66	0.80		2.31	1.48
toluene	5.44	2.55	1.99	2.56	2.75	2.28
m-xylene	1.42	1.56	0.88		1.70	1.08
tetralin	11.95	10.54	3.23		4.36	3.77
1-methyl-naphthalene	14.52	13.60	6.04		7.16	6.43
iso-C_6H_{14}	4.32	2.29	1.14	2.92	1.71	1.74
iso-C_8H_{18}	17.29	7.82	2.67	4.15	3.24	4.00
Cyclohexane	5.48	5.3	1.54		2.25	1.65
CO_2	3.81	4.35	0.67	3.00	2.14	0.88

The uncorrected and corrected f-theory viscosity predictions given for n-decane and isooctane indicate that while the addition of the correction term to f-theory yields excellent results for n-decane viscosity, it is not universally applicable. A subsequent study indicates that the term works well for n-alkanes, lightly branched alkanes, and some aromatics such as toluene and m-xylene. While corrected PCSAFT-FT fails to give accurate viscosity predictions for isooctane; isooctane viscosity predictions are much improved when any one of the FV theory-based models is used. These models also predict n-decane viscosity to within ±2%. Of all models studied, the PCSAFT-FVT consistently gives the lowest MAPDs from reference value for the compounds examined in this work (see Table 14). Notably, it can be employed to successfully predict viscosities for normal and branched alkanes, aromatics, and cycloalkanes, while the predictive power of the corrected PCSAFT-FT is sufficient only in the case of normal alkanes.

10. VISCOSITY STANDARD: KRYTOX OIL VISCOSITY

10.1 INTRODUCTION

On June 19, 2009, the International Association of Transport Properties (IATP) held its 9th meeting in Boulder Colorado and decided to identify a short term and long term high temperature, high pressure viscosity standard (HTHPVS). The short term target was to identify a fluid that would have a dynamic viscosity of 200 MPa s at 200°C (473.15 K) and 173 MPa (25,000 psia) with an uncertainty of ± 2%. The long term standard of 200 mPa s at 300°C (573.15 K) and 241 MPa (35000 psia) with an uncertainty of ± 1% was more demanding with respect to temperature, pressure, and uncertainty. Subsequently, during the HTHP Workshop initiated by Schlumberger and Cambridge Viscosity on January 22, 2010, these specifications were changed to reflect interest in two types of petroleum targets, which have increasing importance as the search for domestic energy sources in increasingly harsh conditions escalates. These include light oils found in ultradeep formations that are typically accessed via offshore platforms in the deep waters of the Gulf of Mexico (Deepwater Standard), and heavy oils produced from bitumen reserves found in shallow oil sands (Heavy Oil Standard). The targeted Deepwater Standard has a dynamic viscosity of 20 MPa s at 260°C (533.15 K) and 241 MPa (35000 psia), while the Heavy Oil Standard is to have a dynamic viscosity of 1000 mPa s at 200°C and 10.34 MPa (1500 psia). The desired uncertainty for both standards was set at 5-10%. One of the conclusions of this meeting was that candidates for these standards should be assessed at multiple labs using multiple experimental techniques. For example, it was anticipated that oscillating piston, rolling ball, falling object, torsional crystal, vibrating cylinder, oscillating disk, vibrating crystal, and capillary viscometers could be used to evaluate the HTHP viscosity standard candidates. A review of current viscometry laboratories indicated, however, that these Deepwater Standard conditions of 260°C and 241 MPa would be particularly challenging and would require modifications to existing viscometry equipment. The U.S. Department of Energy's NETL recently worked with Chandler Engineering to design a HTHP Couette viscometer rated to 316°C and 276.0 MPa (40000 psia) [101]. This apparatus, which is located at NETL's Morgantown site, was designed to measure the viscosity of drilling fluids with viscosity values of 3–300 mPa s employed for ultradeep drilling. This apparatus was selected for this study of the Deepwater HTHPVS.

The desirable characteristics of a HTHP viscosity standard include thermal stability, inertness, insensitivity to UV radiation, and ready availability throughout the world at a specified purity. Further, the candidate should be safe to use in the laboratory and environmentally benign. Scientists at NIST, Georgia Tech, the University of Pittsburgh, and NETL independently concluded that perfluoropolyether oils were excellent candidates for the Deepwater Standard.

10.2 MATERIAL: KRYTOX® OILS

The full Krytox® GPL 100 series of fluorinated lubricating oils was obtained from DuPont. Molecular weight estimates (there is some batch-to-batch variation) for the members of this series, provided to us by DuPont Performance Lubricants, are given in Table 15. These oils have a "fairly broad" molecular weight distribution. Krytox GPL 100-107 oils are nonreactive, nonflammable materials that possess chemical resistance, including protection against oxidation. They contain no additives. Thus, they are typically used in general purpose applications, to lubricate bearings that come into contact with chemicals and oxygen.

Table 15: Number average molecular weight estimates provided by DuPont for the Krytox 100 series of perfluoropolyethers.

Krytox GPL	Number Average Molecular Weight(g/mol)
100	960
101	1180
102	1720
103	2275
104	3150
105	4730
106	5940
107	7475

10.3 ANALYTICAL INSTRUMENTS

10.3.1 Couette Viscometer

The couette viscometer [101] is used to measure viscosities. It is rated for pressures of up to 40,000 psig (276 MPa), temperatures up to 600°F (316°C), and can be operated at shear rates of up to 1022 s^{-1}. A more detailed description of the development and testing of this apparatus is referenced [101] along with illustrations.

Briefly, Couette flow describes drag-induced laminar flow in a thin slit. The viscometer consists of two coaxial cylinders. The outer cylinder (the rotor) rotates, causing the fluid to flow and also exerting a torque on the inner cylinder. Under conditions of fully developed, isothermal, unidirectional laminar flow in the θ direction, the flow inside the viscometer can be defined as Couette flow if the ratio of the bob and rotor radii is near unity, and if gravity-induced flow can be neglected. This is convenient, as Couette flow is well understood and viscosity can be easily determined by measuring variables such as the shear rate and the torque exerted by the fluid.

10.3.2 Viscosity Results

Viscosity of Krytox 107, Krytox 104, Krytox 102, and Krytox 101 was determined at 35,000 psi (241 MPa) and 260°C. Krytox 107 reached the viscosity of 20 cP at 260°C and pressure of 5,000 psi only. At 35,000 psi the viscosity was in the range of 150-250 cP depending on shear rate.

Krytox 104, a lighter oil (molecular weight 3150 g/mol), was expected to possess a lower viscosity than Krytox 107. Krytox 104 indicates that this compound is an improvement over Krytox 107 because its flow is Newtonian at shear rates higher than ~ 600 s^{-1}. However, at these conditions it has a viscosity of about 60 cP and would be necessary to lower the pressure to 20,000 psi at the experimental temperature of 260°C in order to measure the desired viscosity of 20 cP.

The viscosity was obtained for two light oils, Krytox 101 and 102 (molecular weights 1180 and 1720 g/mol). The viscosity results shown in Figure 44 for Krytox 102 and Krytox 101 are 26 cP and 17 cp at 260°C and 35,000 psi respectively. For both fluids, above a shear rate of ~ 600/s flow is approximately Newtonian and hysteresis is observed. Krytox 101 and 102 reach the target viscosity of 20 cP at 40,000 psi and 30,000 psi.

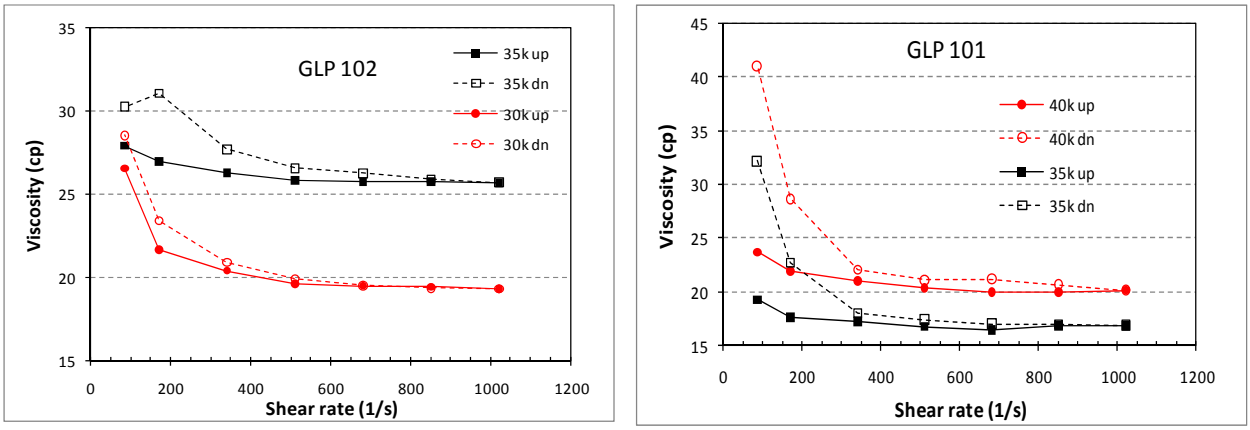

Figure 44: Viscosities of (a) Krytox GPL 102 and (b) Krytox GPL 101 at 260°C and 35000 psi.

10.3.3 Rolling Ball Viscometer

The rolling ball viscometer has been described in previous sections of this report. To measure the viscosity of Krytox oil, the viscometer was calibrated with bis(2-ethylhexyl)phthalate, also known as dioctyl phthalate (DOP). The calibration results for three isotherms with high viscous fluid are presented in Figure 45.

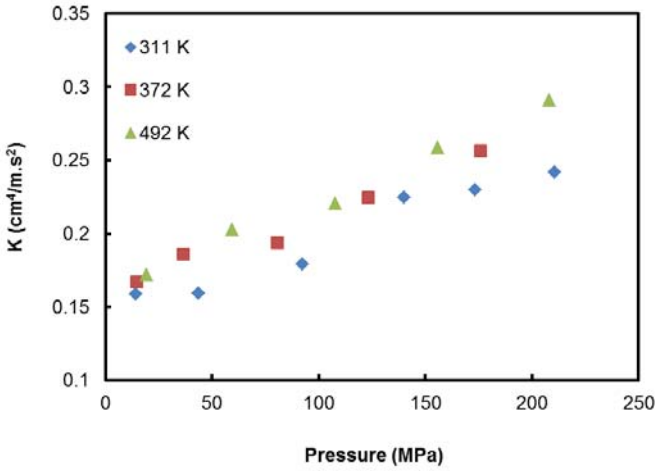

Figure 45: Viscometer constant, K, measured with DOP for 0.995 ratio at different temperatures as a function in pressure.

The calibration results are then used to determine the viscosity of Krytox® GPL 102 oil at 311, 372, and 533K. Krytox oils are a viable candidate for Deepwater Viscosity Standard. Krytox oils are chemically inert liquids over a wide temperature range They are odorless, colorless, and have extreme temperature stability, with operating ranges from below 200 K and upto 620 K (347°C). The desired Deepwater viscosity standard is a fluid that exhibits a viscosity of 20 cP at 500°F (533K or 260°C) and 35,000 psia (241 MPa).

Figure 46 shows the viscosity of Krytox oil 102 at 533K. The results of this isotherm were obtained by extrapolating the linear correlations of the viscometer constant determined with DOP at 311, 372, and 533K. Considering there are no published viscosity data of Krytox oil 102 at HTHP conditions, the viscosity of Krytox oil 102 measured with the rolling ball viscometer is compared with results obtained with a Couette viscometer.

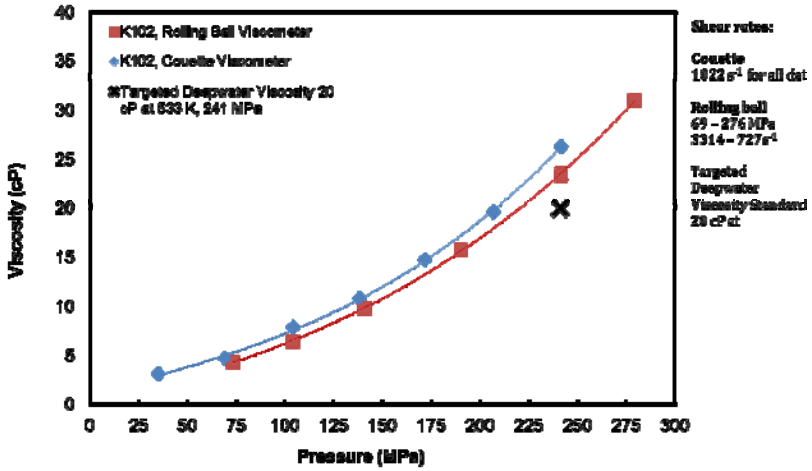

Figure 46: Viscosity of Krytox oil 102 at 533 K (260°C).

11. APPENDIX A: DENSITY DATA FOR ALL COMPOUNDS

Table 16: Density of n-pentane at 52.6, 149.9, and 247.3°C obtained in this study. MAPD is the average absolute percent deviation in density for n data points relative to those calculated at the NIST website for a maximum density of 0.762 g/ml or a pressure of 100 MPa [7].

52.6 ± 0.2°C MAPD = 0.5, n = 9		149.9 ± 0.1°C MAPD = 0.5, n = 4		247.3 ± 0.3°C MAPD = 0.5, n = 4	
P (MPa)	Density (g/ml)	P (MPa)	Density (g/ml)	P (MPa)	Density (g/ml)
1.8	0.595	28.6	0.553	28.5	0.472
3.6	0.598	43.7	0.570	43.1	0.507
7.0	0.603	56.8	0.592	54.9	0.526
13.8	0.613	85.5	0.621	87.1	0.562
28.9	0.630	112.8	0.645	112.7	0.584
43.3	0.643	137.0	0.658	141.2	0.603
55.3	0.653	171.9	0.676	174.7	0.622
70.9	0.664	209.4	0.692	209.6	0.639
84.1	0.672	241.0	0.702	241.1	0.652
110.2	0.686	276.6	0.712	273.5	0.665
137.8	0.700				
171.0	0.714				
206.2	0.727				
239.5	0.739				
275.5	0.750				

Table 17: Density of n-octane at 48.7, 150.2, and 248.4°C obtained in this study. MAPD is the average absolute percent deviation in density for n data points relative to data of Caudwell, et al. [6], to a maximum pressure of 200 MPa, a temperature of 200°C, and densities calculated at the NIST website to a maximum density of 0.764 g/ml or a pressure of 100 MPa [7].

48.7 ± 0.1°C MAPD = 0.5, n = 10		150.2 ± 0.2°C MAPD = 0.5, n = 9		248.4 ± 0.3°C MAPD = 0.3, n = 4	
P (MPa)	Density (g/ml)	P (MPa)	Density (g/ml)	P (MPa)	Density (g/ml)
14.3	0.688	28.7	0.628	15.4	0.538
28.5	0.702	56.1	0.659	28.0	0.571
56.3	0.721	84.2	0.681	55.9	0.614
84.0	0.735	111.2	0.699	82.9	0.636
111.3	0.748	139.0	0.714	112.0	0.655
139.9	0.760	172.9	0.730	140.5	0.672
172.5	0.771	207.5	0.744	174.6	0.689
207.6	0.783	240.6	0.756	208.7	0.704
241.0	0.792	275.7	0.768	242.7	0.718
274.4	0.802			276.9	0.730

Table 18: Density of cyclooctane at 51.3, 151.7, and 250.7°C obtained in this study. At 51.3°C cyclooctane solidifies at pressures greater than 85 MPa. No attempt is made to determine the exact pressure of solidification at this temperature.

51.3 ± 0.1°C No MAPD		151.7 ± 0.2°C No MAPD		250.7 ± 0.1°C No MAPD	
P (MPa)	Density (g/ml)	P (MPa)	Density (g/ml)	P (MPa)	Density (g/ml)
14.0	0.830	28.1	0.745	14.8	0.675
28.8	0.841	55.8	0.777	28.0	0.699
42.9	0.850	84.0	0.798	43.1	0.718
56.4	0.857	111.0	0.814	56.8	0.732
70.8	0.865	138.3	0.828	69.3	0.742
84.5	0.872	172.1	0.844	84.1	0.754
		206.7	0.859	97.0	0.763
		240.5	0.872	111.0	0.772
		274.0	0.885	125.1	0.781
				138.3	0.788
				172.9	0.805
				205.9	0.820
				240.2	0.834
				275.7	0.848

Table 19: Density of 2,2,4-trimethylpentane at 50.9, 149.5, and 247.1°C obtained in this study. MAPD is the average absolute percent deviation in density for n data points relative to data of Malhotra and Woolf [5, 102] for densities to a maximum pressure of 280 MPa at 50.9°C.

50.9 ± 0.1°C MAPD = 0.05, n = 16		149.5 ± 0.1°C No MAPD		247.1 ± 0.2°C No MAPD	
P (MPa)	Density (g/ml)	P (MPa)	Density (g/ml)	P (MPa)	Density (g/ml)
4.2	0.671	28.0	0.621	14.5	0.524
6.5	0.674	55.9	0.660	28.3	0.567
9.1	0.677	83.0	0.684	55.7	0.611
11.5	0.679	110.2	0.701	85.1	0.639
14.4	0.683	137.6	0.717	112.3	0.659
29.1	0.697	172.8	0.735	139.4	0.676
42.3	0.708	206.4	0.750	172.8	0.694
55.7	0.718	240.8	0.764	208.2	0.710
70.8	0.727	275.6	0.776	242.4	0.724
84.3	0.734			276.3	0.736
112.3	0.749				
143.3	0.762				
178.4	0.777				
211.5	0.789				
246.7	0.799				
281.1	0.808				

Table 20: Density of n-decane at 51.3, 149.7, and 247.0°C obtained in this study. MAPD is the average absolute percent deviation in density for n data points relative to data of Caudwell, et al. [6] for a maximum pressure of 200 MPa, a temperature of 200°C, and to densities calculated at the NIST website to a maximum density of 0.770 g/ml [7].

51.3 ± 0.2°C MAPD = 0.8, n = 7		149.7 ± 0.3°C MAPD = 0.1, n = 8		247.0 ± 0.3°C MAPD = 0.2, n = 10	
P (MPa)	Density (g/ml)	P (MPa)	Density (g/ml)	P (MPa)	Density (g/ml)
14.6	0.714	15.0	0.648	15.3	0.580
29.3	0.724	28.0	0.667	28.4	0.605
56.6	0.741	56.8	0.692	55.5	0.639
82.7	0.754	83.1	0.710	85.7	0.666
111.4	0.767	113.5	0.727	112.8	0.685
144.2	0.780	141.9	0.741	140.5	0.701
173.2	0.790	174.9	0.756	174.5	0.719
207.0	0.801	204.8	0.767	209.5	0.734
241.2	0.811			245.4	0.749
274.5	0.820			278.8	0.762

Table 21: Density of toluene at 49.7, 149.1, and 251.9°C obtained in this study. MAPD is the average absolute percent deviation in density for n data points relative to densities calculated at the NIST website to a maximum density of 0.975 g/ml [7].

49.7 ± 0.1°C MAPD = 0.4, n = 8		149.1 ± 0.2°C MAPD = 0.7, n = 9		251.9 ± 0.1°C MAPD = 0.4, n = 9	
P (MPa)	Density (g/ml)	P (MPa)	Density (g/ml)	P (MPa)	Density (g/ml)
54.1	0.882	28.6	0.780	39.6	0.713
83.2	0.899	55.5	0.811	56.3	0.738
110.8	0.912	82.5	0.836	82.7	0.767
137.8	0.925	109.6	0.857	109.8	0.791
172.2	0.937	137.9	0.872	137.7	0.811
206.7	0.952	173.4	0.887	173.5	0.836
239.6	0.961	206.5	0.899	204.8	0.849
274.9	0.973	240.3	0.913	239.5	0.865
		274.6	0.928	274.4	0.881

Table 22: Density data of n-hexadecane at 50.5, 149.7, and 249.4°C obtained in this study. The MAPD = 0.02% for n = 101 using the data of Outcalt, et al.[103], to a maximum pressure of 110 MPa and temperatures between 50 and 150°C.

P	Density	P	Density	P	Density
(MPa)	(g/ml)	(MPa)	(g/ml)	(MPa)	(g/ml)
50.5 ± 0.1°C		149.7 ± 0.1°C		249.4 ± 0.2°C	
14.9	0.758	14.1	0.700	15.1	0.643
27.9	0.769	27.9	0.713	27.1	0.660
41.5	0.779	41.2	0.724	42.0	0.675
55.5	0.787	55.5	0.734	55.4	0.687
69.4	0.792	69.8	0.743	69.1	0.698
81.3	0.799	82.8	0.750	82.1	0.707
109.7	0.807	108.8	0.765	107.9	0.723
		136.9	0.778	135.8	0.738
		170.7	0.792	170.1	0.755
		204.3	0.804	203.3	0.769
		236.5	0.815	235.8	0.782
		262.3	0.823	255.0	0.788

Table 23: Density data of n-octadecane at 51.1, 149.6, and 249.4°C obtained in this study. The MAPD = 0.11% for n = 42 using the data of Caudwell, et al.[65], to a maximum pressure of 90 MPa and temperatures between 50 and 150°C.

P (MPa)	Density (g/ml)	P (MPa)	Density (g/ml)	P (MPa)	Density (g/ml)
51.1 ± 0.1°C		149.6 ± 0.2°C		249.4 ± 0.1°C	
7.0	0.764	7.7	0.702	15.3	0.651
14.4	0.769	15.1	0.711	29.4	0.668
28.3	0.778	29.4	0.724	43.2	0.681
42.2	0.788	42.5	0.732	56.4	0.692
55.6	0.797	56.1	0.741	70.8	0.703
68.9	0.800	73.2	0.752	84.4	0.712
		84.5	0.761	110.0	0.727
		110.0	0.774	137.8	0.742
		138.5	0.787	170.4	0.757
		171.7	0.801	205.3	0.771
		206.1	0.813	235.7	0.782
		235.5	0.823	257.0	0.790
		255.9	0.829		

Table 24: Density data of n-eicosane at 50.4, 149.6, and 248.1°C obtained in this study. The MAPD=0.03% for n=113 using the data of Dutour, et al.[104] to a maximum pressure of 50 MPa and temperatures between 50 and 120°C and the MAPD=0.15% for n=44 using the data of Doolittle [55] to a maximum pressure of 260 MPa and temperatures between 50 and 250°C.

P (MPa)	Density (g/ml)	P (MPa)	Density (g/ml)	P (MPa)	Density (g/ml)
50.4 ± 0.1°C		149.6 ± 0.2°C		248.1 ± 0.1°C	
7.3	0.771	7.4	0.711	16.4	0.661
14.9	0.777	14.3	0.719	28.3	0.676
21.4	0.784	20.6	0.723	41.9	0.691
27.4	0.787	27.9	0.730	55.5	0.706
34.2	0.789	34.6	0.735	69.6	0.719
		54.2	0.748	82.5	0.727
		81.6	0.765	109.2	0.744
		109.2	0.781	138.2	0.763
		136.1	0.792	173.1	0.777
		169.5	0.806	204.7	0.791
		203.1	0.818	239.8	0.805
		235.5	0.829	258.0	0.810
		260.0	0.837		

Table 25 lists the available literature data n-pentane, n-octane, cyclooctane, 2,2,4-trimethylpentane, n-decane, and toluene.

Table 25: Literature references for n-pentane, n-octane, cyclooctane, 2,2,4-trimethylpentane, n-decane, and toluene density data. The last column lists the approximate temperatures and pressures for the density measurements of the present study that differ from those in each of these literature references.

Literature	Literature Temperature Range (°C)	Literature Maximum Pressure (MPa)	Literature Data Points	Temperatures and Pressures for Density Data Obtained in the Present Study that Differ From Available Literature Data
n-Pentane				
Audonnet and Padua [105]	30 to 110	100	40	50°C: 100 < P (MPa) < 280 150°C: P (MPa) < 280 250°C: P (MPa) < 280
Byun, et al. [11]	50 to 150	240	84	50°C: 240 < P (MPa) < 280 150°C: 240 < P (MPa) < 280 250°C: P (MPa) < 280
Oliveira and Wakeham [69]	30 to 50	250	29	50°C: 250 < P (MPa) < 280 150°C: P (MPa) < 280 250°C: P (MPa) < 280
Kiran and Sen [106]	45 to 170	70	139	50°C: 70 < P (MPa) < 280 150°C: 70 < P (MPa) < 280 250°C: P (MPa) < 280
Palavra, et al. [107]	33 to 69	283	68	150°C: P (MPa) < 280 250°C: P (MPa) < 280
Lee and Ellington [108]	38 to 238	54	286	50°C: 54 < P (MPa) < 280 150°C: 54 < P (MPa) < 280 250°C: P (MPa) < 280
Gehrig and Lentz [109]	40 to 400	236	not used	50°C: 120 < P (MPa) < 280 150°C: 205 < P (MPa) < 280 250°C: 236 < P (MPa) < 280
Easteal and Woolf [10]	5 to 65	280	not used	150°C: P (MPa) < 280 250°C: P (MPa) < 280

Literature	Literature Temperature Range (°C)	Literature Maximum Pressure (MPa)	Literature Data Points	Temperatures and Pressures for Density Data Obtained in the Present Study that Differ From Available Literature Data
n-Octane				
Caudwell, et al. [6]	25 to 200	200	67	50°C: 200 < P (MPa) < 280 150°C: 200 < P (MPa) < 280 250°C: P (MPa) < 280
Moravkova, et al. [110]	25 to 55	40	92	50°C: 40 (MPa) < P < 280 150°C: P (MPa) < 280 250°C: P (MPa) < 280
Goodwin, et al. [111]	50 to 150	68	92	50°C: 68 (MPa) < P < 280 150°C: 68 < P (MPa) < 280 250°C: P (MPa) < 280
2,2,4-Trimethylpentane				
Padua, et al. [112,113]	– 75 to 75	100	33	50°C: 100 < P (MPa) < 280 150°C: P (MPa) < 280 250°C: P (MPa) < 280
Malhotra and Woolf [5,102]	5 to 80	400	89	150°C: P (MPa) < 280 250°C: P (MPa) < 280
Dymond, et al. [114]	25 to 100	540	not used	150°C: P (MPa) < 280 250°C: P (MPa) < 280
n-Decane				
Caudwell, et al. [6]	25 to 100	192	19	50°C: 192 < P (MPa) < 275 150°C: P (MPa) < 205 250°C: P (MPa) < 280
Audonnet and Padua [115]	30 to 120	76	40	50°C: 76 < P (MPa) < 275 150°C: P (MPa) < 205 250°C: P (MPa) < 280
Oliveira and Wakeham [69]	30 to 75	254	46	50°C: 254 < P (MPa) < 275 150°C: P (MPa) < 205 250°C: P (MPa) < 280
Lee and Ellington [116]	38 to 238	54	140	50°C: 54 < P (MPa) < 275 150°C: 54 < P (MPa) < 205 250°C: P (MPa) < 280
Gehrig and Lentz [117]	25 to 400	300	not used	50°C: 50 < P (MPa) < 275 150°C: 140 < P (MPa) < 205 250°C: 225 < P (MPa) < 280
Dymond, et al. [118]	25 to 100	500	not used	150°C: 54 < P (MPa) < 205 250°C: P (MPa) < 280

Literature	Literature Temperature Range (°C)	Literature Maximum Pressure (MPa)	Literature Data Points	Temperatures and Pressures for Density Data Obtained in the Present Study that Differ From Available Literature Data
Toluene				
Glen and Johns [119]	20 to 100	30	48	50°C: 30 < P (MPa) < 275 150°C: P (MPa) < 275 250°C: P (MPa) < 275
Harris, et al. [120]	25 to 50	373	22	150°C: P (MPa) < 275 250°C: P (MPa) < 275
Pölhler and Kiran [121]	50 to 150	65	69	50°C: 65 < P (MPa) < 275 150°C: 65 < P (MPa) < 275 250°C: P (MPa) < 275
Dymond, et al. [122]	26 to 50	492	17	150°C: P (MPa) < 275 250°C: P (MPa) < 275
Et-Tahir, et al. [123]	25 to 90	40	45	50°C: 40 < P (MPa) < 275 150°C: P (MPa) < 275 250°C: P (MPa) < 275
Assael, et al. [124]	30 to 50	71	30	50°C: 71 < P (MPa) < 275 150°C: P (MPa) < 275 250°C: P (MPa) < 275
Franck, et al. [70]	50 to 400	300	not used	
Kashiwagi, et al. [125]	0 to 100	250	not used	50°C: 225 < P (MPa) < 280 150°C: P (MPa) < 280 250°C: P (MPa) < 280

Literature	Literature Temperature Range (°C)	Literature Maximum Pressure (MPa)	Literature Data Points	Temperatures and Pressures for Density Data Obtained in the Present Study that Differ From Available Literature Data
N-Hexadecane				
Amorim, et al. [126]	45 to 140	62	54	50°C: 62 < P < 110 150°C: P < 265 250°C: P < 255
Banipal, et al. [127]	40 to 100	10	72	50°C: 10 < P < 110 150°C: P < 265 250°C: P < 255
Chang, et al. [128]	60 to 140	30	21	50°C: P < 110 150°C: P < 265 250°C: P < 255
Dymond, et al. [79]	25 to 100	451	27	150°C: P < 265 250°C: P < 255
Glaser, et al. [129]	30 to 87	18	63	50°C: 18 < P < 110 150°C: P < 265 250°C: P < 255
Gouel [130]	40 to 120	40	75	50°C: 40 < P < 110 150°C: P < 265 250°C: P < 255
Matthews, et al. [131]	50 to 290	4	10	50°C: 4 < P < 110 150°C: 4 < P < 265 250°C: 4 < P < 255
Outcalt, et al. [103]	40 to 190	51	101	50°C: 51 < P < 110 150°C: 51 P < 265 250°C: P < 255
Snyder, et al. [132]	25 to 85	290	93	150°C: 51 P < 265 250°C: P < 255
Tanaka, et al. [68]	25 to 75	151	16	150°C: P < 265 250°C: P < 255

Literature	Literature Temperature Range (°C)	Literature Maximum Pressure (MPa)	Literature Data Points	Temperatures and Pressures for Density Data Obtained in the Present Study that Differ From Available Literature Data
n-Octadecane				
Caudwell, et al. [65,133]	50 to 200	92	49	150°C: 92 < P < 265 250°C: P < 260
Cutler, et al. [134]	60 to 135	551	53	50°C: P < 70 150°C: P < 260 250°C: P < 260
Dutour, et al. [73]	40 to110	150	111	50°C: P < 70 150°C: P < 260 250°C: P < 260
n-Eicosane				
Doolittle [55]	100 to 303	500	55	50°C: P < 40
Dutour, et al. [104]	100 to 120	150	113	150°C: P < 260 250°C: P < 260
Rodden, et al. [135]	100 to 533.15	1.4	5	50°C: P < 70 150°C: 1.4 < P < 260 250°C: 1.4 < P < 260

Table 26: Experimental density data for Krytox® GPL 102 obtained at VCU.

P (MPa)	Density (g/ml)	P (MPa)	Density (g/ml)	P (MPa)	Density (g/ml)	P (MPa)	Density (g/ml)
24.9 °C ± 0.1°C		50.1°C ± 0.1°C		80.1 ± 0.1°C		130.9 ± 0.1°C	
1.2	1.850	3.0	1.810	1.7	1.777	1.8	1.696
3.3	1.856	4.1	1.814	2.9	1.783	3.8	1.711
10.8	1.879	6.9	1.824	10.2	1.815	11.1	1.752
27.5	1.925	14.0	1.851	27.3	1.864	27.7	1.809
55.0	1.973	41.5	1.923	54.8	1.912	49.0	1.856
97.7	2.022	64.1	1.959	81.2	1.948	78.4	1.905
151.1	2.076	103.5	2.006	110.8	1.983	111.2	1.948
208.2	2.121	140.2	2.043	139.4	2.013	141.1	1.982
272.9	2.164	172.0	2.070	174.3	2.046	170.0	2.006
		207.7	2.098	205.0	2.067	208.2	2.042
		240.0	2.121	238.7	2.095	240.0	2.067
		274.0	2.136	272.1	2.120	274.4	2.094

P (MPa)	Density (g/ml)	P (MPa)	Density (g/ml)	P (MPa)	Density (g/ml)
200.0± 0.1°C		230.0± 0.1°C		259.9± 0.1°C	
5.1	1.566	6.9	1.528	31.6	1.622
14.7	1.627	15.4	1.585	41.9	1.662
29.1	1.688	29.5	1.654	43.2	1.663
42.2	1.735	42.6	1.698	55.1	1.701
55.9	1.771	56.2	1.736	55.2	1.698
83.3	1.828	56.5	1.740	83.2	1.772
103.8	1.862	72.7	1.773	111.8	1.821
110.8	1.867	81.2	1.795	111.9	1.822
136.1	1.907	109.1	1.844	137.1	1.861
172.6	1.937	135.8	1.883	172.2	1.909
201.8	1.979	171.7	1.922	205.3	1.948
237.1	2.010	203.9	1.961	240.0	1.984
238.9	2.009	234.6	1.989	240.1	1.984
268.9	2.038	269.3	2.021	269.4	2.012

12. APPENDIX B. FRICTION-THEORY AND FREE-VOLUME THEORY EQUATIONS

For both f-theory and FV theory, the fluid viscosity η can be expressed as the summation of two terms (Equation 30).

$$\eta = \eta_0 + \Delta\eta \tag{30}$$

In Eq. 30, η_0 is the fluid viscosity in the dilute gas limit, while the $\Delta\eta$ term dominates at liquid-like densities. The term $\Delta\eta$, which is dependent on the viscosity model, is pressure-dependent and vanishes at the dilute gas limit. This dilute gas model was proposed by Chung et al. [94,95,136]. It is derived mainly from the Chapman-Enskog kinetic theory of gases, reproducing gas viscosity within an average of 1.5% of the experimental value for both non-interacting and strongly interacting compounds.

$$\eta_0 = \frac{40.785\sqrt{M_w T}}{v_c^{2/3}\Omega^*} F_c \tag{31}$$

In Equation 31:

η_0 = dilute gas viscosity term, cP

M_w = molecular weight g/mol

T = temperature, K

v_c = critical volume, cm^3/mol

An empirical expression for the collision integral Ω^* was first defined by Neufeld, et al. [137].

Finally, for nonpolar species, $F_c = 1 - 0.2756\omega$, where ω is Pitzer's acentric factor.

Frictional theory of viscosity (f-theory)

In f-theory, shear-induced fluid flow is modeled as two sliding surfaces under a shear stress. From the friction laws, the "shear force" of friction is proportional to the normal forces on the surfaces. Therefore, the shear stress of friction must be proportional to the normal stresses on the surfaces. The normal stress is assumed to be equivalent to the system pressure, which is separated into the attractive and repulsive pressure terms P_a and P_r ,which are calculated using an equation of state. Newton's law of viscosity defines a relationship between shear stress and viscosity. Thus, the high-pressure viscosity term $\Delta\eta$ is derived:

$$\Delta\eta = \kappa_a P_a + \kappa_{aa} P_a^2 + \kappa_r P_r + \kappa_{rr} P_r^2 \tag{32}$$

Previous work [96,97] has indicated f-theory gives accurate viscosity predictions at pressures up to 100 MPa when the friction coefficients κ_a, κ_{aa}, κ_r, and κ_{rr} are defined as exponential functions of reduced temperature. F-theory has been successfully used when the P_a and P_r inputs to Equation 32 is calculated using the PR, SRK, and PC-SAFT equations. However, it is necessary to define separate sets of equations for κ_a, κ_{aa}, κ_r, and κ_{rr} each time a different EoS is used to

determine P_a and P_r. The set of equations defined for use with the PC-SAFT equation yields the best results for n-alkanes, typically modeling their viscosity to within better than 1.5% of the experimental value. In this case, the frictional coefficients κ_a, κ_{aa}, κ_r, and κ_{rr}, as defined as indicated in Equations 33-36.

$$\kappa_a = \eta_a \frac{\tilde{\kappa}_a}{P_c} \tag{33}$$

$$\kappa_{aa} = \eta_a \frac{\tilde{\kappa}_{aa}}{P_c^2} \tag{34}$$

$$\kappa_r = \eta_r \frac{\tilde{\kappa}_r}{P_c} \tag{35}$$

$$\kappa_{rr} = \eta_r \frac{\tilde{\kappa}_{rr}}{P_c^2} \tag{36}$$

In Equations 33-36:

η_a = attractive viscosity parameter

η_r = repulsive viscosity parameter

P_c = component critical pressure of a component as calculated using the PC-SAFT equation (not the literature value)

$\tilde{\kappa}_a$, $\tilde{\kappa}_r$, $\tilde{\kappa}_{aa}$ and $\tilde{\kappa}_{rr}$ = temperature-dependent friction parameters that are also dependent on segment number *m*

Collectively, the friction parameters given in Equations 33-37 are a function of 38 model constants, which are obtained by modeling after smoothed experimental viscosity values for normal alkanes ranging in carbon number from 1 to 18. The interested reader is referred to the literature for their definition [97].

Free volume equations

Doolittle [138] proposed that $\Delta\eta$ is proportional to the fluid free volume fraction f_v, which is a measure of the space within a system that is not occupied by molecules. Thus, viscosity is correlated to molecular structure via the empirical relationship:

$$\Delta\eta = e^{B/f_v} \tag{37}$$

Allal and coworkers [98] hold that f_v is a function of PM_w/ρ, the energy required to form vacant vacuums required for diffusion, and $\alpha\rho$, a barrier energy that a molecule must surpass for diffusion to occur. Their final equation, Equation 38, is relatively simple and requires the molecular weight M_w, $P\rho T$ values, and the three pure-component parameters L, α, and B as inputs only. One advantage of using free volume theory is that unlike f-theory, an equation of state is not necessary if experimental $P\rho T$ data points are available.

$$\Delta\eta = \frac{\rho L\left(\alpha\rho + \dfrac{PM_w}{\rho}\right)}{\sqrt{3RTM_w}} e^{\left[B\left(\dfrac{\alpha\rho + \dfrac{PM_w}{\rho}}{RT}\right)^{1.5}\right]} \tag{38}$$

In Equation 38:

M_w = molecular weight, kg/mol

ρ = density, kg/m^3

T = absolute temperature, K

R = gas constant, 8.3145 J/mol*K

P = pressure, MPa

L = length parameter, Å

α = diffusion energy parameter, m^3/mol*s^2

B = unitless parameter

13. APPENDIX C. F-THEORY AND FV-THEORY PARAMETERS

Table 27: Values of ηa and ηr for selected alkanes, aromatics, and naphthenics.

Compound	η_a	η_r	T_m (K)	Reference
Methane	11	40.5	90	
n-pentane	-6.42895	75.1365	143.4	69
n-hexane	-17.06	86.3043	178	86
n-octane	-49.7901	112.585	216	87,139
n-nonane	-65.2920	120	220	72
n-decane	-78.6746	133.007	243	69,72
n-dodecane	-94.6198	140.528	263.6	72, 140
n-C15	-102.101	147.090	291	140
n-C16	-93.7225	145.777	291	86
n-C18	-104.067	150.037	302	140
CO_2	-16.1322	118	195	72
2-methylpentane	-17.06	86.3043	119.5	72
isopentane	-6.42895	75.1365	113	141
isooctane	-49.7901	106	166	88
Benzene	-43.5	136	278	90
toluene	-35.9555	112	180	89
m-xylene	-23.4043	93.0517	225	139
o-xylene	-46	119	248	141, 142
p-xylene	-31	98	286	141, 142
Tetralin	-80	160.5	237	139
1-methylnaphthalene	-81	147	251	139
cyclohexane	-154	260	280	143
methylcyclohexane	-63.5	159	147	142

Table 28: FV Theory parameter sets obtained when density inputs are given by PC-SAFT.

		PCSAFT-FVT			
Compound	**Mol Wt**	**L**	**α**	**B**	**Ref.**
	g/mol	**Å**	**$m^5/mol*s^2$**	**x 10^{-3}**	
Methane	16.04	0.2714	100.82	1.0961	72
n-C_2H_6	30.07	0.9579	38.65	9.2750	72
n-C_6H_{14}	86.18	0.8016	103.40	5.3070	86
n-C_8H_{18}*	114.23	0.6652	141.33	4.8357	87
n-C_9H_{20}	128.25	0.5727	173.22	4.1001	72
n-$C_{10}H_{22}$	142.29	0.6423	178.46	4.1173	69,72
n-$C_{12}H_{26}$	170.34	0.5839	231.51	3.3020	72,140
n-$C_{15}H_{32}$	212.42	0.4148	337.93	2.4308	140
n-$C_{16}H_{34}$	226.45	0.3285	394.44	2.1134	86
n-$C_{18}H_{38}$	254.50	0.4201	405.73	1.9871	140
benzene	78.11	0.5024	83.93	9.6945	90
toluene	92.14	0.7904	81.72	7.4175	89
m-xylene	106.17	0.6858	101.16	5.6937	139
tetralin	132.21	0.5136	122.78	7.1461	139
1-methyl-naphthalene	142.2	0.4102	127.08	7.6240	139
iso-C_6H_{14}	86.18	0.7555	101.30	5.6915	72
iso-C_8H_{18}	114.23	0.8961	109.07	6.4693	88
Cyclohexane	84.15	0.5532	92.05	13.432	143, 144
CO_2	44.01	0.5652	21.65	13.546	72

*m, σ, and ε/k for n-octane were used to obtain PC-SAFT density values for isooctane.

Table 29: FV Theory parameter sets obtained when density inputs are given by the HTHP PC-SAFT equation.

		HTHP PCSAFT-FVT			
Compound	Mol Wt	L	α	B	Ref.
	g/mol	Å	$m^5/mol*s^2$	x 10^{-3}	
Methane	16.04	0.5276	34.98	8.0855	72
n-C_2H_6	30.07	1.5589	9.59	14.555	72
n-C_6H_{14}	86.18	0.8625	97.33	5.7780	86
n-C_8H_{18}	114.23	0.7463	132.05	5.2529	87
n-C_9H_{20}	128.25	0.6463	159.36	4.6474	72
n-$C_{10}H_{22}$	142.29	0.7315	160.05	4.8053	69,72
n-$C_{12}H_{26}$	170.34	0.6646	209.07	3.8108	72,140
n-$C_{15}H_{32}$	212.42	0.4623	298.11	2.9491	140
n-$C_{16}H_{34}$	226.45	0.3728	344.39	2.5962	86
n-$C_{18}H_{38}$	254.50	0.3894	388.62	2.2950	140
toluene	92.14	0.8360	75.74	8.1256	89
iso-C_6H_{14}	86.18	0.8404	90.86	6.5592	72
iso-C_8H_{18}	114.23	0.9417	106.06	6.7475	88
CO_2	44.01	0.4279	32.91	6.9894	72

Table 30: FV Theory parameter sets obtained when density inputs are given by the HTHP-VT-SRK equation.

		HTHP-VT-SRK-FVT			
Compound	**Mol Wt**	**L**	**α**	**B**	**Ref.**
	g/mol	**Å**	**$m^5/mol*s^2$**	**x 10^{-3}**	
Methane	16.04	0.2595	117.10	0.3397	72
n-C_6H_{14}	86.18	1.0567	83.54	6.5966	86
n-C_8H_{18}	114.23	0.7818	121.53	6.1441	87
n-C_9H_{20}	128.25	0.7200	139.69	5.5545	72
n-$C_{10}H_{22}$	142.29	0.7841	141.42	5.7510	69,72
n-$C_{12}H_{26}$	170.34	0.7236	176.33	4.7800	72,140
n-$C_{15}H_{32}$	212.42	0.5213	245.52	3.8835	140
n-$C_{16}H_{34}$	226.45	0.4207	272.94	3.5420	86
n-$C_{18}H_{38}$	254.50	0.3885	329.53	3.0730	140
benzene	78.11	0.6902	65.57	12.144	90
toluene	92.14	0.9380	67.00	9.3330	89
m-xylene	106.17	0.8391	85.03	6.9490	139
tetralin	132.21	0.5544	133.58	7.4980	139
1-methyl-naphthalene	142.20	0.4266	118.45	8.9120	139
iso-C_6H_{14}	86.18	0.9610	80.69	7.0740	72
iso-C_8H_{18}	114.23	0.9890	95.42	7.5943	88
Cyclohexane	84.15	0.6868	80.27	14.160	143,144
CO_2	44.01	0.6416	23.21	8.6630	72

Table 31: FV Theory parameter sets obtained when density inputs are given by the HTHP-VT-PR equation.

		HTHP-VT-PR-FVT			
Compound	**Mol Wt**	**L**	**α**	**B**	**Ref.**
	g/mol	**Å**	**$m^5/mol*s^2$**	**x 10^{-3}**	
Methane	16.04	0.3168	85.75	1.8616	72
n-C_6H_{14}	86.18	1.0441	78.99	7.2546	86
n-C_8H_{18}	114.23	0.8322	112.35	6.6129	87
n-C_9H_{20}	128.25	0.7782	125.58	6.2280	72
n-$C_{10}H_{22}$	142.29	0.8227	126.69	6.6474	69,72
n-$C_{12}H_{26}$	170.34	0.7983	161.37	5.2227	72,140
n-$C_{15}H_{32}$	212.42	0.5292	235.17	4.1448	140
n-$C_{16}H_{34}$	226.45	0.4585	251.55	3.9396	86
n-$C_{18}H_{38}$	254.50	0.4038	312.82	3.2885	140
benzene	78.11	0.5714	66.57	13.495	90
toluene	92.14	0.9468	65.37	9.7903	89
m-xylene	106.17	0.8858	77.84	7.9310	139
tetralin	132.21	0.6583	116.07	8.4771	139
1-methyl-naphthalene	142.20	0.4813	108.03	9.6672	139
iso-C_6H_{14}	86.18	0.9833	74.30	8.0467	72
iso-C_8H_{18}	114.23	0.9742	88.74	8.2679	88
Cyclohexane	84.15	0.7538	63.48	20.529	143,144
CO_2	44.01	0.7657	19.07	15.832	72

14. REFERENCES

1. Assessment of Flow Rate Estimates for the Deepwater, Horizon/Macondo Well Oil Spill, U.S
2. Wireline Evaluation Technology in HTHP Wells, Serko Sarian, Arthur Gibson, Schlumberger Oilfield Services, SPE 97571
3. http://www.theoildrum.com/node/6135
4. http://www.theoildrum.com/files/Deepwater%20GOM%20Wilcox%20Map_1.jpg
5. Malhotra, R. and L.A. Woolf, Thermodynamic properties of 2.2.4-trimethylpentane. International Journal of Thermophysics, 1990. 11(6): p. 1153-1172.
6. Caudwell, D.R., et al., Viscosity and density of five hydrocarbon liquids at pressures up to 200 MPa and temperatures up to 473 K. Journal of Chemical and Engineering Data, 2009. 54: p. 359-366.
7. NIST. Thermophysical Properties of Fluid Systems. 2008; Available from: http://webbook.nist.gov/chemistry/fluid/.
8. Span, R., Multiparameter equations of sate - An accurate source of thermodynamic property data, 2000. Berlin: Springer.
9. Span, R. and W. Wagner. Equations of state for technical applications. II. Results for nonpolar fluids. International Journal of Thermophysics, 2003. 24: p. 41-109.
10. Easteal, A.J. and L.A. Woolf. Volume ratios for n-pentane in the temperature range 278-338 K and at pressures up to 280 MPa. International Journal of Thermophysics, 1987. 8: p. 231-238.
11. Byun, H.S., T.P. DiNoia, and M.A. McHugh. High pressure density of ethane, pentane, deuterated pentane, 25.5 wt% ethane in deuterated pentane, 2.4 wt% deuterated poly(ethylene-co-butene) (PEB) in ethane, 5.3 wt% hydrogenated PEB in pentane, 5.1 wt% hydrogenated PEB in deuterated pentane, and 4.9 wt% hydrogenated PEB in deuterated pentane + 23.1 wt% ethane. Journal of Chemical and Engineering Data, 2000. 45: p. 810-814.
12. Caudwell, D.R., Martin Trusler, J.P., Vesovic, V., Wakeham, W.A., J. Chem Eng. Data, 54, 2099, p. 359.
13. Y. Wu, B. Bamgbade, K. Liu, M. A. McHugh, H. Baled, R. M. Enick, W. A. Burgess, D. Tapriyal, B. D. Morreale. Fluid Phase Equilib. 311 (2011) 17-24.
14. H. O. Baled, R. M. Enick, W. A. Burgess, D. Tapriyal, B. D. Morreale, Y. Wu, M. A. McHugh, Monthly DOE report, July 2011.
15. H. Baled, R. M. Enick, Y. Wu, M. A. McHugh, W. Burgess, D. Tapriyal, B. D. Morreale. Fluid Phase Equilib., (2012) DOI: 10.1016/j.fluid.2011.12.027.
16. W.G. Chapman, K.E. Gubbins, G. Jackson, M. Radosz. Ind. Eng. Chem. Res., 29 (1990) 1709-1721.
17. W.G. Chapman, G. Jackson, K.E. Gubbins. Mol. Phys., 65 (1988) 1057-1079.
18. S.H. Huang, M. Radosz. Ind. Eng. Chem. Res., 29 (1990) 2284-2294.
19. S.H. Huang, M. Radosz. Ind. Eng. Chem. Res., 30 (1991) 1994-2005.
20. J. Gross, G. Sadowski. Ind. Eng. Chem. Res., 40 (2001) 1244-1260.

21. P. D. Ting, P. C. Joyce, P. K. Jog, W. G. Chapman, M. C. Thies. Fluid Phase Equilib., 206 (2003) 267-286.

22. J. M. Lasarte, L. Martín, E. Langa, J. S. Urieta, A. M. Mainar. J. Chem. Eng. Data, 53 (2008) 1393-1400.

23. K. Liu, Y. Wu, M.A. McHugh, H. Baled, R.M. Enick, B.D. Morreale, Journal of Supercritical Fluids, 55 (2010) 701-711.

24. G. Soave. Equilibrium Constants from a Modified Redlich-Kwong Equation of State, Chemical Engineering Science, 27 (1972) 1197-1203.

25. D.Y. Peng, D.B. Robinson. A new two-constant equation of state, Industrial & Engineering Chemistry Fundamentals, 15 (1976) 59-64.

26. G. Schmidt, H. Wenzel. A Modified van der Waals Type Equation of State, Chemical Engineering Science, 35 (1980) 1503-1512.

27. W.G. Chapman, G. Jackson, K.E. Gubbins. Phase equilibria of associating fluids. Chain molecules with multiple bonding sites., Molecular Physics, 65 (1988) 1057-1079.

28. W.G. Chapman, K.E. Gubbins, G. Jackson, M. Radosz. New reference equation of state for associating liquids., Ind. Eng. Chem. Res., 29 (1990) 1709-1721.

29. I. Polishuk. Hybridizing SAFT and cubic EOS: What can be achieved? Industrial & Engineering Chemistry Research, 50 (2011) 4183-4198.

30. G.M. Kontogeorgis, E.C. Voutsas, I.V. Yakoumis, D.P. Tassios. An equation of state for associating fluids, Ind. Eng. Chem. Res., 35 (1996) 4310-4318.

31. G.M. Kontogeorgis, I.V. Yakoumis, H. Meijer, E. Hendriks, T. Moorwood. Multicomponent phase equilibrium calculations for water–methanol–alkane mixtures, Fluid Phase Equilibria, 158–160 (1999) 201–209.

32. G.M. Kontogeorgis, M.L. Michelsen, G.K. Folas, S. Derawi, N.V. Solms, E.H. Stenby. Ten years with the CPA (Cubic-Plus-Association) equation of state. Part 1. Pure compounds and self-associating systems, Ind. Eng. Chem. Res., 45 (2006) 4855-4868.

33. M.J. Pratas, M.B. Oliveira, M.J. Pastoriza-Gallego, A.J. Queimada, M.M. Piñeiro, J.A.P. Coutinho. High-pressure biodiesel density: Experimental measurements, correlation, and Cubic-Plus-Association Equation of State (CPA EoS) modeling, ACS, 25 (2011) 3806-3814.

34. A.J. Queimada, C. Miqueu, I.M. Marrucho, G.M. Kontogeorgis, J.A.P. Coutinho. Modeling vapor–liquid interfaces with the gradient theory in combination with the CPA equation of state, Fluid Phase Equilibria, 228–229 (2005) 479–485.

35. I. Polishuk. Till which pressures the fluid phase EOS models might stay reliable? J. of Supercritical Fluids, 58 (2011) 204-215.

36. R. Span. Multiparameter equations of state: An accurate source of thermodynamic property data, 1 edition ed., Springer, Berlin, 2000.

37. G. Scalabrin, L. Bettio, P. Marchi, L. Piazza, D. Richon. An extended equation of state modeling method I. pure fluids, International Journal of Thermophysics, 27 (2006) 1281-1318.

38. G. Scalabrin, L. Bettio, P. Marchi, P. Stringari. A fundamental equation of state for sulfur hexafluoride (SF6) in extended equation of state format, J. Phys. Chem. Ref. Data, 36 (2007) 617-662.

39. RPSEA, http://www.rpsea.org/

40. A. Peneloux, E. Rauzy. A consistent correction for Redlich-Kwong-Soave volumes, Fluid Phase Equilibria, 8 (1982) 7-23.

41. W.R. Ji, D.A. Lempe. Density improvement of the SRK equation of state, Fluid Phase Equilibria, 130 (1997) 49-63.

42. L.S. Wang, J. Gmehling. Improvement of the SRK equation of state for representing volumetric properties of petroleum fluids using Dortmund Data Bank, Chemical Engineering Science, 54 (1999) 3885-3892.

43. K. Magoulas, D.P. Tassios. Thermophysical properties of n-alkanes from C1 to C20 and their prediction for higher ones, Fluid Phase Equilibria 56 (1990) 119-140.

44. P. Ungerer, C. Batut Prédiction des propriétés volumétriques des hydrocarbures par une translation de volume améliorée, Revue de l'Institut Francais du Petrole 52 (1997) 609-623.

45. P. Ungerer, C. Batut, G. Moracchini, J. Sanchez, H.B. de Sant'Ana, J. Carrier, D.M. Jensen. Measurement and prediction of volumetric and transport properties of reservoir fluids at high pressure, Revue de l'Institut Francais du Petrole 53 (1998) 265-281.

46. P. Ungerer, H.B. De Sant'Ana. Reply to the letter to the editor by O. Pfohl about the paper "Evaluation of an improved volume translation for the prediction of hydrocarbon volumetric properties" [FPE 154, 193-204 (1999)], Fluid Phase Equilibria, 163 (1999) 161-162.

47. H.B. de Sant'Ana, P. Ungerer, J.C. de Hemptinne. Evaluation of an improved volume translation for the prediction of hydrocarbon volumetric properties, Fluid Phase Equilibria, 154 (1999) 193-204.

48. J.C. de Hemptinne, P. Ungerer. Accuracy of the volumetric predictions of some important equations of state for hydrocarbons, including a modified version of the Lee-Kesler method, Fluid Phase Equilibria 106 (1995) 81-109.

49. O. Pfohl. Letter to the editor ''Evaluation of an improved volume translation for the prediction of hydrocarbon volumetric properties'', Fluid Phase Equilibria 163 (1999) 157-159.

50. K. Frey. Improving thermodynamic property estimation through volume translation, in, Massachusetts Institute of Technology, 2010.

51. P.M. Mathias, T. Naheiri, E.M. Oh. A Density Correction for the Peng-Robinson Equation of State, Fluid Phase Equilibria, 47 (1989) 77-87.

52. J. Tester, K. Frey, C. Augustine, R.P. Ciccolini, S. Paap, M. Modell. Volume translation in equations of state as a means of accurate property estimation, Fluid Phase Equilibria, 260 (2007) 316-325.

53. J. Tester, K. Frey, M. Modell. Density-and-temperature-dependent volume translation for the SRK EOS: 1. Pure fluids, Fluid Phase Equilibria, 279 (2009) 56-63.

54. H.H. Reamer, B.H. Sage. Volumetric behavior of cyclohexane, Industrial & Engineering Chemistry, 2 (1957) 9-12.

55. A.K. Doolittle. Specific volumes of n-alkanes, Journal of Chemical and Engineering Data 9(1964) 275-279.

56. NIST Thermophysical Properties of Fluid Systems, (http://webbook.nist.gov/ chemistry/fluid/).

57. U. Setzmann, W. Wagner. A New Equation of State and Tables of Thermodynamic Properties for Methane Covering the Range from the Melting Line to 625-K at Pressures up to 1000-Mpa, Journal of Physical and Chemical Reference Data, 20 (1991) 1061-1155.

58. H. Miyamoto, M. Uematsu. Measurements of vapor pressures from 280 to 369 K and (p, rho, T) properties from 340 to 400 K at pressures to 200 MPa for propane, International Journal of Thermophysics, 27 (2006) 1052-1060.

59. S.R.R. Deul, E.U. Franck. The dielectric constant and density of benzene to 400°C and 3000 bar, Berichte der Bunsengesellschaft für Physikalische Chemie, 95 (1991) 515-519.

60. F.J. Vieira dos Santos, C.A. Nieyo de Castro. Viscosity of toluene and benzene under high pressure, International Journal of Thermopgysics, 18 (1997) 367-378.

61. S. Stamataki, D. tassios. Performance of cubic EoS at high pressures, Revue de l'Institut Francais du Petrole, 53 (1998) 367-377.

62. G. Soave, S. Gamba, L.A. Pellegrini. SRK equation of state: Predicting binary interaction parameters of hydrocarbons and related compounds, Fluid Phase Equilibria 299 (2010) 285-293.

63. P. Dauge´, A. Baylaucq, L. Marlin, C. Boned. Development of an isobaric transfer viscometer operating up to 140 MPa. Application to a methane + decane system, Journal of Chemical and Engineering Data, 46 (2001) 823-830.

64. J.M. Beaudon, J.P. Kohn. Multiphase and volumetric equilibria of the methane-+decane binary system at temperatures between -36o and 15OoC, Journal of Chemical and Engineering Data, 12 (1967) 189-191.

65. D.R. Caudwell, J.P.M. Trusler, V. Vesovic, W.A. Wakeham, Int. J. Thermophys., 25 (2004) 1339-1352.

66. P. J. Linstrom, W. G. Mallard, Eds., NIST Chemistry WebBook, NIST Standard Reference Database Number 69, June 2005, National Institute of Standards and Technology, Gaithersburg MD, 20899 (http://webbook.nist.gov/chemistry/fluid/)

67. Y. Wu, B. Bamgbade. M. A. McHugh, To be submitted for publication

68. Y. Tanaka, H. Hosokawa, H. Kubota, T. Makita. Int. J. Thermophys., 12 (1991), 245-264.

69. C. M. B. P. Oliveira, W. A. Wakeham. Int. J. Thermophys., 13 (1992), 773-790.

70. E. U. Franck, S. Kerschbaum, G. Wiegand. Ber. Bunsenges. Phys. Chem., 102 (1998), 1794-1797.

71. H.-S. Byun, T. P. DiNoia, M. A. McHugh. J. Chem. Eng. Data, 45 (2000), 810-814.

72. P. J. Linstrom, W. G. Mallard. Eds., NIST Chemistry WebBook, NIST Standard Reference Database Number 69, June 2005, National Institute of Standards and Technology, Gaithersburg MD, 20899 (http://webbook.nist.gov/chemistry/fluid/)

73. S. Dutour, J. L. Daridon, B. Lagourette. Int. J. Thermophys., 21 (2000), 173-184.

74. P. J. Linstrom, W. G. Mallard. Eds., NIST Chemistry WebBook, NIST Standard Reference Database Number 69, June 2005, National Institute of Standards and Technology, Gaithersburg MD, 20899 (http://webbook.nist.gov/chemistry/fluid/)

75. Y. Wu, B. Bamgbade, M. A. McHugh, W. A. Burgess, D. Tapriyal, B. D. Morreale, H. O. Baled, R. M. Enick, unpublished data.

76. A. K. Doolittle. J. Chem. Eng. Data, 9 (1964) 275-279.

77. D.R. Caudwell, J.P.M. Trusler, V. Vesovic, W.A. Wakeham. Int. J. Thermophys., 25 (2004) 1339-1352

78. H. H. Reamer, B. H. Sage. J. Chem. Eng. Data, 11 (1966) 17-24.

79. J. H. Dymond, K. J. Young, J. D. Isdale. J. Chem. Thermodynamics, 11 (1979) 887-895.

80. J. H. Dymond, M. A. Awan, N. F. Glen, J. D. Isdale. Int. J. Thermophys., 12 (1991) 275-287.

81. H. H. Reamer, R. H. Olds, B. H. Sage, W. N. Lacey. Ind. Eng. Chem., 34 (1942) 1526-1531.

82. H.-M. Lin, H. M. Sebastian, J. J. Simnick, K.-C. Chao. J. Chem. Eng. Data, 24 (1979) 146-149.

83. H. H. Reamer, B. H. Sage. J. Chem. Eng. Data, 8 (1963) 508-513.

84. H. H. Reamer, B. H. Sage, W. N. Lacey. Ind. Eng. Chem., 43 (1951) 2515-2520.

85. Dymond, J. H.; Brawn, T. A. Proc. 7th Symp. Thermophys. Prop.(Am. Soc. Mech. Engrs., New York, 1977), p. 660.

86. J. H. Dymond, K. J. Young, J. D. Isdale. Int. J. Thermophys. 1 (1980), 345-373.

87. J. H. Dymond, J. Robertson, J. D. Isdale. Int. J. Thermophys. 2 (1981), 133-154.

88. J. H. Dymond, N. F. Glen, J. D. Isdale. Int. J. Thermophys. 6 (1985), 233-250.

89. J. H. Dymond, M. A. Awan, N. F. Glen, J. D. Isdale. Int. J. Thermophys. 12 (1991), 275-287.

90. J. H. Dymond, J. Robertson, J. D. Isdale. Int. J. Thermophys. 2 (1981), 223-236.

91. M. J. Assael, J. H. Dymond, M. Papadaki, P. M. Patterson. Int. J. Thermophys. 13 (1992), 269-281.

92. M. J. Assael, J. H. Dymond, M. Papadaki, P. M. Patterson. Int. J. Thermophys. 13 (1992), 895-905.

93. W. A. Burgess, D. Tapriyal, B. D. Morreale, Y. Wu, M. A. McHugh, H. O. Baled, R. M. Enick. Submitted for publication to Fluid Phase Equilib.

94. T.-H. Chung, M. Ajlan, L. L. Lee, K. E. Starling. Ind. Eng. Chem. Res. 27 (1988), 671-679.

95. M. E. Brulé, K. E. Starling. Ind. Eng. Chem. Process Des. Dev. 23 (1984), 833-845.

96. S. E. Quiñones-Cisneros, C. K. Zéberg-Mikkelsen, E. H. Stenby. Fluid Phase Equilib. 178 (2001), 1-16.

97. S. E. Quiñones-Cisneros, C. K. Zéberg-Mikkelsen, J. Fernández, J. García. AIChE Journal 52 (2006) 1600-1610.

98. A. Allal, C. Boned, Q. Baylaucq. Phys. Rev. E 64 (2001), 011203.

99. S. P. Tan, H. Adidharma, B. F. Towler, M. Radosz. Ind. Eng. Chem. Res. 44 (2005), 8409-8418.

100. H. Baled, R. M. Enick, Y. Wu, M. A. McHugh, W. Burgess, D. Tapriyal, B. D. Morreale. Fluid Phase Equilib., 317 (2012) 65-76.

101. Gussler, W.; Pless, M.; Maxey, J.; Grover, P.; Perez, J.; Moon, J.; Boaz, T. A New Extreme HP/HT Viscometer for New Drilling-Fluid Challenges, " paper SPE 99009 first presented at the 2006 IADC/SPE Drilling Conference, Miami, Florida, Feb 21-23, 2006; SPE Drilling and Completion, June 2007, 81- 89

102. Malhotra, R. and L.A. Woolf. Volumetric measurements under pressure for 2.2.4-trimethylpentane at temperatures up to 353.15 K and for benzene and three of their mixtures at temperatures up to 348.15 K. International Journal of Thermophysics, 1993. 14(6): p. 1153-1172.

103. Outcalt, S., A. Laesecke, and T.J. Fortin. Density and speed of sound measurements of hexadecane. Journal of Chemical Thermodynamics, 2010. 42(6): p. 700-706.

104. Dutour, S., J.L. Daridon, and B. Lagourette. Speed of sound, density, and compressibilities of liquid eicosane and docosane at various temperatures and pressures. High Temperatures-High Pressures, 2001. 33(3): p. 371-378.

105. Audonnet, F. and A.A.H. Padua. Simultaneous measurement of density and viscosity of n-pentane from 298 to 383 K and up to 100 MPa using a vibrating-wire instrument. Fluid Phase Equilibria, 2001. 181: p. 147–161

106. Kiran, E. and Y.L. Sen. High-pressure viscosity and density of n-alkanes. International Journal of Thermophysics, 1992. 13: p. 411-442.

107. Palavra, M.F., W.A. Wakeham, and M. Zalaf. Thermal conductivity of normal pentane in the temperature range 306-360 K at pressures up to 0.5 GPa. International Journal of Thermophysics, 1987. 8: p. 305-318.

108. Lee, A. and R.T. Ellington. Viscosity of n-pentane. Journal of Chemical and Engineering Data, 1965. 10: p. 101-104.

109. Gehrig, M. and H. Lentz. Values of p(V,T) for n-pentane in the range 5 to 250 MPa and 313 to 643 K. Journal of Chemical Thermodynamics, 1979. 11: p. 291-300

110. Moravkova, L., et al., (P,Vm,T) measurements of (octane + 1-chlorohexane) at temperatures from 298.15 K to 328.15 K and at pressures up to 40 MPa. J. Chemical Thermodynamics, 2006. 38: p. 861–870

111. Goodwin, A.R.H., et al. A vibrating edge supported plate, fabricated by the methods of micro electro mechanical system for the simultaneous measurement of density and viscosity: results for methylbenzene and octane at temperatures between (323 and 423) K and pressures in the range (0.1 to 68) MPa. Journal of Chemical and Engineering Data, 2006. 51: p. 190-208.

112. Padua, A.A.H., et al. Density and viscosity measurements of 2,2,4-trimethylpentane (isooctane) from 198 K to 348 K and up to 100 MPa. Journal of Chemical and Engineering Data, 1996. 41: p. 1488-1494.

113. Padua, A.A.H., et al. Validation of an accurate vibrating-wire densimeter: Density and viscosity of liquids over wide ranges of temperature and pressure. International Journal of Thermophysics, 1996. 17(4): p. 781-802.

114. Dymond, J.H., J.D. Isdale, and N.F. Glen. Density measurement at high pressure. Fluid Phase Equilibria, 1985. 20: p. 305-314.

115. Audonnet, F. and A.A.H. Padua. Viscosity and density of mixtures of methane and n-decane from 298 to 393 K and up to 75 MPa. Fluid Phase Equilibria, 2004. 216: p. 235-244

116. Lee, A. and R.T. Ellington. Viscosity of n-decane in the liquid phase. Journal of Chemical and Engineering Data, 1965. 10: p. 346-348.

117. Gehrig, M. and H. Lentz. Values of p(V,T) for n-decane up to 300 MPa and 673 K. Journal of Chemical Thermodynamics, 1983. 15: p. 1159-1167.

118. Dymond, J.H., J. Robertson, and J.D. Isdale. (p, p, T) of some pure n-alkanes and binary mixtures of n-atkanes in the range 298 to 373 K and 0.1 to 500 MPa. Journal of Chemical Thermodynamics, 1982. 20: p. 305-314.

119. Glen, N.F. and A.I. Johns. Determination of the density of toluene in the range from (293 to 373) K and from (0.1 to 30) MPa. Journal of Chemical and Engineering Data, 2009. 54: p. 2538-2545.

120. Harris, K.R., R. Malhotra, and L.A. Woolf, Temperature and density dependence of the viscosity of octane and toluene. Journal of Chemical and Engineering Data, 1997. 42: p. 1254-1260.

121. Pölhler, H. and E. Kiran. Volumetric properties of carbon dioxide + toluene at high pressures. Journal of Chemical and Engineering Data, 1996. 41: p. 482-486.

122. Dymond, J.H., et al. The viscosity of liquid toluene at elevated pressures. International Journal of Thermophysics, 1995. 16: p. 877-882.

123. Et-Tahir, A., et al. Determination of the viscosity of various hydrocarbons and mixtures of hydrocarbons versus temperature and pressure. International Journal of Thermophysics, 1995. 16: p. 1309-1334.

124. Assael, M.J., M. Papadaki, and W.A. Wakeham. Measurements of the viscosity of benzene, toluene, and m-xylene at pressure up to 80 MPa. International Journal of Thermophysics, 1991. 12: p. 449-457.

125. Kashiwagi, H., et al. Conductivity and density of toluene in the temperature range 273-373 K at pressures up to 250 MPa. International Journal of Thermophysics, 1982. 3: p. 201-215.

126. Amorim, J.A., et al. High-pressure density measurements for the binary system cyclohexane plus n-hexadecane in the temperature range of (318.15 to 413.15) K. Journal of Chemical and Engineering Data, 2007. 52(2): p. 613-618.

127. Banipal, T.S., S.K. Garg, and J.C. Ahluwalia. Heat-capacities and densities of liquid normal-octane, normal-nonane, normal-decane, and normal-hexadecane at temperatures from 318.15 K to 373.15 K and at pressures up to 10 MPa. Journal of Chemical Thermodynamics, 1991. 23(10): p. 923-931.

128. Chang, J.S., M.J. Lee, and H.M. Lin. Densities of binary mixtures of hexadecane with m-xylene and tetralin from 333 K to 413 K and pressures up to 30 MPa. Journal of Chemical and Engineering Data, 1998. 43(2): p. 233-237.

129. Glaser, M., et al. Phase-equilibria of (methane + n-hexadecane) and (P, Vm, T) of n-hexadecane. Journal of Chemical Thermodynamics, 1985. 17(9): p. 803-815.

130. Gouel, P. Specific volume of cycloalkanes and alkylbenzenes (C6-C16). Bull. Cent. Rech. Explor.-Prod. Elf-Aquitaine, 1978. 2: p. 211-225.

131. Matthews, M.A., J.B. Rodden, and A. Akgerman. High-temperature diffusion, viscosity, and density-measurements in n-hexadecane. Journal of Chemical and Engineering Data, 1987. 32(3): p. 317-319.

132. Snyder, P.S. and J. Winnick. The pressure, volume and temperature properties of liquid n-alkanes at elevated pressures. Proceedings of the Symposium on Thermophysical Properties, 1970. 5: p. 115-129.

133. Caudwell, D.R. Viscosity of dense fluid mixtures, 2004, Imperial College: London.

134. Cutler, W.G., et al. Study of the compressions of several high molecular weight hydrocarbons. The Journal of Chemical Physics, 1958. 29(4): p. 727-740.

135. Rodden, J.B., C. Erkey, and A. Akgerman, High-temperature diffusion, viscosity, and density-measurements in normal-eicosane. Journal of Chemical and Engineering Data, 1988. 33(3): p. 344-347.

136. T. H. Chung, L. L. Lee, K. E. Starling. Ind. Eng. Chem. Fundam. 23 (1984) 8-13.

137. P. D. Neufeld, A. R. Janzen, R. A. Aziz. J. Chem. Phys. 57 (1972), 1100.

138. A. K. Doolittle. J. Appl. Phys. 22 (1951), 1471.

139. D. R. Caudwell, J. P. Martin Trusler, V. Vesovic, W. A. Wakeham. J. Chem. Eng. Data 54 (2009), 359-366.

140. D. L. Hogenboom, W. Webb, J. A. Dixon. J. Chem. Phys. 46 (1967), 2586-2598.

141. P. W. Bridgman. Proc. Amer. Acad. Arts Sci. 61 (1926), 57-99.

142. A. Et-Tahir, C. Boned, B. Lagourette, P. Xans. Int. J. Thermophys. 16 (1995), 1309-1334.

143. Y. Tanaka, H. Hosokawa, H. Kubota, T. Makita. Int. J. Thermophys. 12 (1991), 245-264.

144 . M. A. Hernandez-Galván, F. García-Sánchez, B. E. García-Flores, J. Castro-Arellano. J. Chem. Eng. Data 54 (2009), 2831-2838.

John Duda
Director
Strategic Center for Natural Gas and Oil
National Energy Technology Laboratory
U.S. Department of Energy

Maria Vargas
Deputy Director
Strategic Center for Natural Gas and Oil
National Energy Technology Laboratory
U.S. Department of Energy

Roy Long
Technology Manager
Strategic Center for Natural Gas and Oil
National Energy Technology Laboratory
U.S. Department of Energy

Elena Melchert
Program Manager
Oil & Gas Production
Office of Fossil Energy
U.S. Department of Energy

Cynthia Powell
Director
Office of Research and Development
National Energy Technology Laboratory
U.S. Department of Energy

Timothy McNulty
Associate Vice-President for
Government Relations
Carnegie Mellon University

Henry Foley
Vice President for Research
The Pennsylvania State University

George Klinzing
Vice Provost for Research
University of Pittsburgh

Robert Walters
Vice President for Research
Virginia Tech

Fred King
Vice President for Research and
Economic Development
West Virginia University

Terri Marts
RES Program Manager
URS Corporation

NETL Technical Report Series